Assessing Critical Metal Incorporation in Ca-Carbonate Minerals Using Cyanobacteria: Application to Mine Site Environments

by

Benjamin Lei

A thesis
presented to the University of Waterloo
in fulfillment of the
thesis requirement for the degree of
Master of Science
in
Earth Sciences

Waterloo, Ontario, Canada, 2025

© Benjamin Lei 2025

Author’s declaration

This thesis consists of material all of which I authored or co-authored: see Statement of Contributions included in the thesis. This is a true copy of the thesis, including any required final revisions, as accepted by my examiners. I understand that my thesis may be made electronically available to the public.

Statement of contributions:

Chapters 2 and 3 of this thesis may be submitted as journal manuscripts after revision. As the first author of both chapters, I contributed to the experimental design, execution, data collection, analysis and writing. These articles will be co-authored by myself, my supervisor – Dr. Jenine McCutcheon, Dr. Brian Kendall, Natasha Bell and others who have contributed to the publication. The design of both chapters, figures, writing and interpretation was under the guidance of Jenine McCutcheon. Brian Kendall and Natasha Bell conducted the data collection from the ICP-MS. Joy Hu conducted the data collection for the IC. Dr. Rodney Smith provided access to the Raman instrument as well as the Origin software and provided guidance in the Raman data processing.

Abstract:

Meeting the current global market demand for critical metals will require an increase in the number of mining operations in Canada. While mining will generate mine tailings, which can be an environmental concern, tailings also present an opportunity for carbon sequestration and metal recovery. Carbon sequestration in mine tailings can be implemented by using divalent cations from the tailings to form stable carbonate minerals. Ultramafic mine tailings typically contain an abundance of divalent cations, including various transition metals, that can be incorporated into carbonate minerals. During this process, critical metal enrichments are possible, and thus tailings may become valuable sources of metals as high-grade ore deposits continually become less accessible for mining. Microorganisms, including cyanobacteria, can contribute to carbonate mineral precipitation, however, this process is understudied with respect to transition metal incorporation into biogenic carbonate minerals. This thesis explores the application of these processes to ultramafic mine sites through two laboratory experiments using a pure culture of cyanobacteria, *Synechococcus leopoliensis*. In the first experiment, a biosorption study explores the metal sorption abilities of *S. leopoliensis* in a nutrient limited environment. The second experiment examines the incorporation of transition metals into precipitates during microbial mineral carbonation.

In Chapter 2, the ability of *S. leopoliensis* to remove Co^{2+} and Ni^{2+} from solution via biosorption in a nutrient limited environment what tested in a lab experiment. Comparison between nutrient enriched conditions and a nutrient deficient condition (simulating an ultramafic mine site solution) was conducted in mono-metal and di-metal systems. The results revealed that measured nickel and cobalt concentrations were lowest in the first 3 days of the experiment, which indicates a fast metal removal rate. The biosorption of nickel and cobalt was upwards of 34.2–49.4% removal of metal from solution. Imposing nutrient limitations caused increased production of extracellular polymeric substances (EPS), which can increase metal sorption, and resulted in a decrease in measured nickel concentrations in solution in the di-metal system. The findings from this experiment indicate that inducing additional stress through metal exposure and nutrient limitations can increase the metal biosorption capacity of *S. leopoliensis*.

In Chapter 3, a microbially induced carbonate precipitation experiment was conducted to test the incorporation of nickel and cobalt into biogenic calcium carbonate mineral precipitates. These results are preliminary due to an experimental failure that occurred. Nevertheless, the

measured concentrations of dissolved cobalt and nickel in solution indicated metal(s) removal success of up to 89.5% and 94.5% in the first day after metal addition. Observation of the biofilms using scanning electron microscopy (SEM) revealed nanometer-scale amorphous calcium carbonate (ACC) precipitates. This preliminary result suggests that inducing calcium carbonate precipitation may remove dissolved metals solution.

The results from Chapter 2 and Chapter 3 together reveal that *S. leopoliensis* can quickly remove metals from solution, which could be applied to both metal recovery and remediation projects. Data from this research could be applied to the development of photobioreactors at ultramafic mine sites. The outcomes suggest that inducing nutrient limitation can enhance metal removal by increasing metal binding through enhanced EPS production. The research presented in this thesis will contribute to the development of sustainable mine operations, with the aim of recovering metals from tailings, and lowering CO_2 emissions, thereby working towards net-neutral mining operations.

Acknowledgments

I would like to thank my supervisor, Dr. Jenine McCutcheon, for her continual guidance, wisdom, support throughout these last two years. She has been patient and kind throughout the challenging times during my MSc. training and teaching me to become a better scientist. Her continuous assurance makes me thankful. I am grateful to Dr. Rodney Smith for providing the use of the Raman instruments and offering guidance as an early career researcher. Having you on my committee is something I am incredibly thankful for. I would like to Dr. Philippe Van Capellen, for providing guidance in my experimental design and feedback on my results. The completion of this thesis and the passion for science are very much owed to both my supervisor and my two committee members. I hope that one day I can become a future collaborator and work on projects with all three of you.

Thank you to Heather Roshon for providing the cyanobacteria used in this thesis and helping investigate why my cyanobacteria struggled with adapting to the lab. Thank you to Natasha Bell and Dr. Brian Kendall for conducting my ICP-MS measurements. I would like to thank Nina Heinig for training me to use the SEM and for providing guidance.

I am fortunate and thankful to be surrounded by wonderful lab mates, which include Sana Ahmad, Lisa Yu and Decla McParland. Our lively chats about life and internet drama and, eating meals together will be missed. I appreciate both Sana and Decla to be my safety buddy during the after-hours during my experiments. Your guys' encouragement and constant reassurance are something that I will miss. Chicago and Sudbury were some of the most amazing that I got to share memories with you guys. Hopefully, we can go on more journeys and have dinner as we all continue our academic journey.

I would like to be thankful to a cohort of friends during these last 3 years, which includes Stephen Wang, Myles Schulz, Nicole Sos, Paul Sherk, and Hailey Jack. I am going to miss the random banters and the watching movies, karaoke or relaxing together. To Myles, I will miss going on morning runs while discussing lab experiments and what we have been writing to our supervisor during this summer with you. I am beyond grateful to both Nicole and Hailey. Your constant reassurance and cheering me up during my lowest moments will be memories I cherish dearly. I would like to thank Hang Nguyen for checking up on me and the constructive criticism.

To Paul, although our time together was short, it has been amazing to always talk with you during our quarterly meetings.

I would also like to thank you for my little support system. I would like to thank “the Boys”, which includes Tony, Sangho and Abraham. Throughout these last two years, I do not think I would have stayed sane with your constant support. I would like to thank to Spencer Kwok and Philip Lu for everything. Without your friendship and constant reminders, I would not be the individual I am today. Your advice and suggestions to continue my Msc. means everything. I would like to thank Evon Choi and Evelyn Liu for the constant calls and check ups throughout these last two years.

This research would have not been possible without the support from the Natural Sciences and Engineering Research Council of Canada (NSERC) Discovery Grant.

Finally, I would like to thank my parents and sisters for their unconditional love and support in life. I am sad that numerous members of my extended family that cannot see my success anymore, but I hope I am continually making you proud. Finally, I dedicate this thesis to my grandfather's wishes.

Dedication:

For everyone who stood by me through the challenging times that I faced while completing this thesis

Table of contents

List of Figures ..... ***xi***

List of Tables ..... ***xiii***

List of Abbreviations ..... ***xiv***

Chapter 1 Introduction ***1***

1.1 Thesis organization *1*

1.2 Background *1*

1.2.1 Carbon sequestration in an ultramafic mine operation 1

1.2.2 Bioremediation in ultramafic mine sites 2

1.3 The importance of cyanobacteria in ultramafic mine operations *2*

1.4 Research objectives *3*

Chapter 2 Biosorption of Critical Metals in a Simulated Ultramafic Mine site ***4***

2.1 Introduction *4*

2.1 Research objectives *6*

2.2 Methods *7*

2.2.1 Bacterial strain and culture conditions 7

2.2.2 Cell counting 8

2.2.3 Water Chemistry Analyses 8

2.2.4 EPS Extraction 9

2.2.5 Scanning electron spectroscopy- energy dispersive spectroscopy 9

2.2.6 Raman Spectroscopy 10

2.2.7 Data analysis 10

2.3 Results *10*

2.3.1 Cell counting 10

2.3.2 Water chemistry analyses: 11

2.3.3 Electron microscopy 18

2.3.4 Raman spectroscopy: 24

2.4 Discussion *28*

2.4.1 Biosorption of cobalt and nickel by *S. leopoliensis* 28

2.4.2 Impact of low nutrient environments 32

2.4.3 Implication for ultramafic mine operations 33

2.5 Conclusions *33*

Chapter 3 Preliminary Investigation of Critical Metal Incorporation during Biotic Carbonate Mineral Precipitation..... 35

3.1 Introduction:.....35

3.2 Research objective.....38

3.3 Methods:.....38

3.3.1 Bacterial Strain and culture conditions:.....38

3.3.2 Water Chemistry analyses:.....39

3.3.3 Scanning Electron microscopy (SEM):.....40

3.3.4 Raman spectroscopy:.....40

3.3.5 Data analysis:.....40

3.4 Results:.....40

3.4.1 Water Chemistry analyses:.....40

3.5 Scanning electron microscopy-energy dispersive spectroscopy:.....44

3.5.1 Raman Spectroscopy:.....47

3.6 Discussion.....49

3.6.1 Biogenic calcium carbonate mineral precipitation:.....49

3.6.2 Implications of ultramafic mine environment:.....50

3.7 Conclusion:.....51

4.1 Summary of Findings:.....52

4.2 Summary of Findings:.....54

References:..... 55

Appendix:..... 75

List of Figures

Figure 2.1. Cell densities of *S. leopoliensis* in nutrient enriched (H) and nutrient deficient (L) flasks over the 30-day experiment. Cell counts plotted versus time for the control groups (A), nickel doped (B), cobalt doped (C), and di-metal (D) treatments. 11
Figure 2.2. Evolution of pH over the 30-day biosorption experiments for the control groups (A) nickel doped (B), cobalt doped (C), and di-metal (D) treatments. 12
Figure 2.3. Dissolved oxygen measured in the nutrient enriched and nutrient deficient treatments for the control groups (A), Ni (B), Co (C), and the di-metal treatments (D)..... 13
Figure 2.4. Conductivity measured in the nutrient enriched (A) and nutrient deficient (B) treatments throughout the 30-day experiment. 14
Figure 2.5. Concentrations of nitrate (A, B), phosphate (C, D), and phosphorus (E, F) in the nutrient depleted (A, C, E) and nutrient enriched (B, D, F) flasks throughout the 30-day experiment..... 15
Figure 2.6. Cobalt (A) and nickel (b) concentrations decreased and then increased, followed by minor fluctuations throughout the remainder of the experiment. 17
Figure 2.7. Scanning electron micrographs showing *S. leopoliensis* cells on day 1 of the experiment in the nutrient enriched control (A), cobalt (B), nickel (C), and di-metal (D) flasks. 19
Figure 2.8. Scanning electron micrographs showing *S. leopoliensis* cells on day 12 of the experiment in the nutrient enriched control (A), cobalt (B), nickel (C), and di-metal (D) flasks. 20
Figure 2.9. Scanning electron micrographs showing *S. leopoliensis* cells on day 1 of the experiment in the nutrient deficient control group (A), cobalt (B), nickel (C), and di-metal (D) flasks. 21
Figure 2.10. Scanning electron micrographs showing *S. leopoliensis* cells on day 12 of the experiment in the nutrient deficient control group (A), cobalt (B), nickel (C), and di-metal (D) flasks. 22
Figure 2.11. Raman spectra showing vibration bands from *S. leopoliensis* cells and EPS exposed to both nutrient enriched and nutrient deficient environments on day 12 of the experiment. 25
Figure 2.12. Raman spectra showing surface functional groups on the cells and EPS in the mono-metal systems when exposed to Ni (A) and Co (B) from day 12. While there are some similarities, most of the peaks were different. The di-metal system (C) exhibits a combination of cobalt and nickel peaks present..... 28
Figure 2.13. Plots showing 30 simulated curves compiled with the maximum metal removal and maximum metal release on a given day based on the measured concentration of nickel in mono-metal nutrient enriched (A) and nutrient deficient (B) systems, and di-metal nutrient enriched (C) and nutrient deficient (D) systems. 30
Figure 2.14. Plots showing 30 simulated curves compiled with its maximum metal removal and maximum metal release as boundaries based on measured cobalt concentrations. The filled areas indicate the potential concentration in mono-metal nutrient enriched (A), mono metal and nutrient deficient (B) systems, and di-metal nutrient enriched (C) and nutrient deficient (D) systems. 31
Figure 3.1. Evolution of pH (A), dissolved oxygen (B), and conductivity (C) throughout the 3 day experiment. Each enviorment condition include abiotic control (AC), biotic control (BC),Ni-doped system, Co-doped systsem (Co), and di-metal system(2M). 41
Figure 3.2. Nitrate (A) and Phosphorus (B) concentrations measured in mg/L throughout the experiment..... 42

Figure 3.3. Alkalinity concentrations reported as mg/L $CaCO_3$, and Ca concentrations (mg/L) over the 3-day experiment in the abiotic (A), biotic (B), nickel (C), cobalt (D), and di-metal systems (E). 43
Figure 3.4. SEM micrographs of precipitation products in each condition including abiotic control group (A,B), biotic control group (C,D), nickel (E,F), cobalt (G,H) and both metals present (I,J). For each treatment, the displayed micrographs show samples collected on day 1(A, C, E, G, I), and day 3 (B, D, F, H). 46
Figure 3.5. Raman spectroscopy spectra of precipitates in the abiotic (A) and biotic (B) control groups on day 1 of the experiment. Both the abiotic and biotic control group exhibit similar spectra shape to one another. 48
Figure 3.6. Raman spectra of the biotic control samples comprising cells, EPS, and associated precipitates on day 1 (A) and day 3 (B). 48
Figure 3.7 Raman spectra collected on day 3 in the Ni (A), Co (B) and di-metal (C) samples that contain cells, EPS and the precipitates. Peaks are labeled to indicate vaterite peaks and notable functional groups identified in the spectra. 49

List of Tables

Table 2.1: Quantities of ingredients added to BG-11 growth medium used in the biosorption experiment, adjusting for dilution. Values for $NaNO_3$ and K_2HPO_4 correspond to the high and low nutrient treatments, respectively. BG-11 medium and trace metal mix recipe from Rippka et al. 1979..... 8
Table 2.2. Maximum cobalt and nickel removal by *S. leopoliensis* during the 30-day experiment based on dissolved metal concentrations measured using ICP-MS..... 17
Table 2.3. Average atomic abundance (%) detected by energy dispersive spectroscopy on cyanobacteria and EPS material observed using SEM. 23
Table 2.4. Raman peak assignments in both control groups containing whole cells of *S. leopoliensis* under nutrient enriched and nutrient deficient environments on day 12. 25
Table 2.5. Raman peak assignments in samples of *S. leopoliensis* cells collected from the nutrient deficient metal systems on day 12 of the experiment..... 26
Table 3.1. Quantities of ingredients in the BG-11 growth medium used in the biogenic calcite precipitation experiment. Flasks were prepared by combining 5 mL of the metal solution, 10–15 mL of cyanobacteria inoculum, and 45–50 mL BG-11 medium for the total final volume of 65 mL per flask. BG-11 medium and trace metal mix recipe from Rippka et al. 1979..... 39
Table 3.2. Co and Ni removal efficiency in the 24 hours after metal addition. Metals were added on day 2 of the experiment, with the dissolved metal concentrations measured on day 3 used to calculate removal (%). 44
Table 3.3. The average elemental composition (atomic%) of samples observed using SE-SEM, as measured using EDS..... 44

List of Abbreviations

AC	Abiotic Control group
ACC	Amorphous calcium carbonate
Al	Aluminum
At%	Atomic percent
A.U	Arbitrary Unit
BC	Biotic control group
°C	Degree Celsius
C	Carbon
Ca	Calcium
$CaCl_2 \cdot 2H_2O$	Calcium chloride dihydrate
$CaCO_3$	Calcium carbonate
CG-L	Control group in nutrient deficient condition
CG-H	Control group in nutrient enriched condition
cm	Centimeter
cm^{-1}	Wavenumber
CPCC	Canadian Phycological Culture Center
Co	Cobalt
Co-O	Cobalt-oxygen bond
CO_2	Carbon dioxide
CO_3^{2-}	Carbonate anion
$CoCl_2 \cdot 6H_2O$	Cobalt (II) chloride hexahydrate
Co-H	Cobalt doped group in nutrient enriched condition
Co-L	Cobalt doped group in nutrient deficient condition
$CoNO_3 \cdot 6H_2O$	Cobalt (II) nitrate hexahydrate
$CuSO_4 \cdot 5H_2O$	Copper (II) sulfate pentahydrate
DO	Dissolved oxygen
DOM	Dissolved organic matter
EDS	Energy dispersive spectroscopy
EPS	Extracellular polymeric substances
EWM	Enhanced weathering and mineralization
GCS	Geological carbon sequestration
h	Hour
HBO_3	Metaboric acid
H_2CO_3	Carbonic acid
HCO_3^-	Bicarbonate
HMDS	Hexamethyldisilane
IC	Ion chromatography
ICP-MS	Inductively coupled plasma-mass spectrometry
L	Liter
lux	Unit for illuminance
Mg	Magnesium
mg	Milligram
mL	Milliliter

mm	Millimeter
$MnCl_2 \cdot 4H_2O$	Manganese(II) chloride tetrahydrate
M-O	Metal-oxygen bond
mS	Millisiemens
N	Nitrogen
NaCl	Sodium chloride
Na_2CO_3	Sodium carbonate
$Na_2MoO_4 \cdot 2H_2O$	Sodium molybdate dihydrate
$NiCl_2 \cdot 6H_2O$	Nickel (II) chloride hexahydrate
Ni-H	Nickel doped group in nutrient enriched condition
Ni-L	Nickel doped group in nutrient deficient condition
Ni-O	Nickel-oxygen bond
nm	Nanometer
PES	Polyether sulfone
PTFE	Polytetrafluoroethylene
rpm	Revolution per minute
SE	Secondary electron
SEM	Scanning-electron microscopy
Si	Silicon
v/v	Volume per volume
Zn	Zinc
$ZnSO_4 \cdot 7H_2O$	Zinc sulfate heptahydrate
2M-L	Nickel and cobalt doped group in nutrient deficient condition
2M-H	Nickel and cobalt doped group in nutrient enriched condition
μg	Microgram
μL	Microliter
μm	Micrometer

Chapter 1 Introduction

1.1 Thesis organization

This thesis is organized in four chapters, starting with an introduction of the research topic. The second chapter presents an experiment studying the biosorption capacity of cyanobacteria in a simulated ultramafic mining environment, primarily investigating changes in the microbial extracellular polymeric substances (EPS) and the associated water chemistry. The third chapter is a preliminary study that investigates the fate of critical metals during microbially induced carbonate mineral precipitation. The forth and final chapter discusses and summarizes both research chapters, and implications for future research and implementation for ultramafic mining operations.

1.2 Background

Critical metals are an essential component of a wide range of technologies in the renewable green energy industry. The demand for metals is increasing because of the transition from fossil fuels to more sustainable alternatives to reduce carbon dioxide (CO_2) emissions (Ministry of Natural Resources and Ministry of Science 2023; McCutcheon and Power 2023). Therefore, the extent of mining operations within Canada will need to increase to meet global market demands, resulting in a substantial increase in associated CO_2 emissions (Ministry of Natural Resources and Ministry of Science 2023; McCutcheon and Power 2023). A challenge various mines face is in mitigating anthropogenic CO_2 emissions while improving metal recovery from tailings and waste rock. Implementing mineral carbonation for critical metal recovery is attractive alternative solution for mines to addresses both challenges simultaneously (Wilson and Hamilton 2022).

1.2.1 Carbon sequestration in an ultramafic mine operation

Carbon sequestration is a method for reducing anthropogenic CO_2 emissions by capturing and storing CO_2 using carbon capture systems, direct air capture, or even enhanced weathering reactions (Power et al. 2013; Smith et al. 2016). These technologies can be applied at mine sites, and Canada intends to lower its CO_2 emissions by applying these technologies at suitable mine sites (Natural Resources Canada 2023). Enhanced weathering can occur in mine tailings, the waste milled rock remaining after mining, during which atmospheric CO_2 can react with the weathered minerals to form secondary minerals (Wilson et al. 2009; McCutcheon et al. 2014,

Bullock et al. 2021). The estimated removal of atmospheric CO_2 by implementing carbon dioxide removal technology in ultramafic-mafic tailings is 93–465 Mt of CO_2 annually (Bullock et al. 2022). Critical metals within these tailings can be immobilized as the mineral carbonation is occurring (Kandji et al. 2017; Hamilton et al. 2020; Bullock et al. 2021; Wilson and Hamilton 2022,). Integrating biogeochemical processes paired with mineral carbonation in tailing materials can remove upwards of 5 Gt of CO_2 annually (Bullock et al. 2021, Wilson and Hamilton 2022, McCutcheon & Power 2023). Thus, ultramafic mine operations can use carbon sequestration as a method of critical metal recovery.

1.2.2 Bioremediation in ultramafic mine sites

Bioremediation utilizes biological processes to aid the remediation of contaminants in any environment (e.g., ultramafic mines) (Mani and Kumar 2014). Bioremediation by microorganisms can aid the removal of contaminants, including metals, from solution (Kalita et al. 2023, Ciani et al. 2024). Thus, bioremediation provides a solution for immobilizing critical metals by using the microbial communities in ultramafic mine sites. McCutcheon et al. demonstrated the application of bioremediation by binding asbestos fibers in Mg-carbonate minerals from ultramafic mine tailings (2017). The secondary cements formed from ultramafic tailings immobilized metals from the primary serpentinite minerals in the tailings (Hamilton et al. 2018). The generation of carbonate minerals can be an incentive for mining operations to transition towards a carbon neutral approach (Power et al. 2013; Power et al. 2024). The tailings can be leached to enhance metal recovery by bioleaching while reducing remediation costs and carbon emissions (Power et al. 2010). Therefore, interest in applying bioremediation and biotechnology in mining operations is attractive as it can be a potential pathway to reach carbon neutral mining (Power et al. 2014). Although much research has focused on ureolytic and cyanobacteria in reducing metals, there is a lack of studies that focus on metal recovery combined with carbon sequestration.

1.3 The importance of cyanobacteria in ultramafic mine operations

Cyanobacteria are a great candidate for both the sequestration of CO2 in carbonate minerals, and sorbing different metals from solution to the extracellular polymeric substances EPS they exude to their cell exteriors (McCutcheon et al. 2019; Selim and Haffner 2020, Carreira et al. 2023; Smječanin et al. 2023). The production, structure, and composition of cyanobacteria EPS can be altered when cells are exposed to nutrient limitations (Qian et al. 2022;

Duan et al. 2023). This in turn can affect the cyanobacteria's capacity to bind metal. Ultramafic environments often contain less nitrogen and phosphate than media used in biosorption studies (Carreira et al. 2023; Paulo et al. 2023). Limited nitrogen and phosphate availability in the ultramafic mine environments can result in additional EPS production by cyanobacteria, which has implications for mineral weathering and carbonation reactions (Bundelava et al. 2014, McCutcheon et al. 2014). Involving biological processes can be used in a low maintenance, cost effective methods of recovering metals from waste materials (Asghari et al. 2013; McCutcheon and Power 2023). Therefore, recent developments have increased interest in biotic mineral weathering as a precursor to carbonate mineral precipitation in association with mining operations. However, there is little published research on critical metal mobility associated with biotic weathering of minerals in tailings and waste rock in relation to how these dissolution reactions apply to carbon sequestration. For example, Hamilton et al. (2018) and Scullet-Dean et al. (2023) restricted their research on critical metal enrichment by abiotic weathering and dissolution, with little research examining the mobilization of critical metals with microbial involvement. Furthermore, previous biosorption experiments provide optimal nitrate and phosphate concentration for biosorption experiments, with little research focusing on impacts of nitrate and phosphate limitations to metal binding (Paulo et al. 2018; Selim and Haffner 2020; Carreira et al. 2023). As a result, it is important to understand the role of biogeochemical processes during carbonate mineral precipitation and the fate of critical metals.

1.4 Research objectives

This thesis will examine how nutrient limitation impacts the production of EPS and the binding of critical metals to cyanobacteria EPS. This research focuses on the potential incorporation of these critical metals during secondary carbonate mineral precipitation in association with cyanobacteria in a simulated ultramafic environment. Solid-state characterization techniques are used to assess metal binding to EPS and incorporation into mineral precipitates. These characterization techniques include scanning-electron microscopy (SEM) and Raman spectroscopy. Water chemistry analyses are used to document changes to the cyanobacteria growth environment as the metals are immobilized during the experiments. The results of both research chapters are discussed in the final chapter in the context of broader applications of bioremediation and carbon sequestration at ultramafic mine operations.

Chapter 2 Biosorption of Critical Metals in a Simulated Ultramafic Mine site

2.1 Introduction

Carbon sequestration within mining operations is of particular of interest as Canada needs to lower its CO_2 emissions while continuing to become a global economic supplier of critical metals (Ministry of Natural Resources and Ministry of Science 2023; Natural Resources Canada 2023). Application of carbon sequestration in ultramafic environments is possible and can provide opportunities to reduce CO_2 emission rates from mining operations, thereby contributing to lowering overall emissions within Canada (Wilson et al. 2009; Gras et al. 2020). Therefore, opportunities for sustainable mining operations are available to lower the global CO_2 emissions.

Ultramafic mining operations often produce tailings and waste rock that can contain trace amounts of toxic metals (e.g., Cr^{6+}), which can pose a potential risk to both the environment and human health if they are leached from their host minerals and contaminate the soil and groundwater (Hamilton et al. 2018; Kierczak et al. 2021). Chromium is a known carcinogen often co-existent with other metals including nickel and cobalt, which all have economic value (Hausladen et al. 2018; Hamilton et al. 2018, Ministry of Natural Resources and Ministry of Science 2023). Although Ni^{2+} and Co^{2+} are both not as dangerous in comparison to Cr^{6+}, observations have indicated a serious decline in human health when exposed to these metals in elevated concentrations (Kierczak et al. 2021). Elevated cobalt concentrations in the range of 300–700 mg/L can result in symptoms impacting the cardiovascular, neurological, and endocrine systems in a human (Leyssenes et al. 2017). Nickel is a known carcinogen and has shown to impact the respiratory system when inhaled by people in concentrations of 0.15–34 mg/L over an extended period (Buxton et al. 2019; Begum et al. 2022). In addition to direct impacts on human health, these toxic metals can affect entire communities by contaminating the groundwater. Thus, proper remediation strategies limiting metal mobilization are necessary to prevent potential negative impacts of critical metals on the environment.

Mining operations will need to factor in economic viability when considering mine closure and remediation strategies. Traditional remediation strategies in mine operations can include permeable reactive barriers, chemical oxidation, and phytoremediation (Karaca et al. 2018).

Bioremediation and the involvement of bacteria can be an alternative solution to traditional remediation strategies as it is often cost effective, low maintenance and requires less labour (Gavrilescu 2022). McCutcheon et al. utilized cyanobacteria to immobilize asbestos fibers with successful deployment in an experimental microbial mineral carbonation field experiment (2016, 2017). Hence, mine site bioremediation strategies would benefit from optimizing microorganism activity in ultramafic (i.e., chromite, kimberlite, serpentinite) mine environments.

Cyanobacteria are Gram-negative photoautotrophs that are a prominent phylum in a diverse range of environments including hypersaline and ultramafic wetlands and mine environments (Castenholz 1989; McCutcheon et al. 2014; Gupta and Diwan 2017; Al-Amin et al. 2021; Diloreto et al. 2023). Furthermore, recent evidence suggests that cyanobacteria are a versatile bacterium and can remove a wide range of contaminates in a variety of environments (soils, wastewater, mines), including sorbing various metals to functional groups and binding sites within bacterial extracellular polymeric substances (EPS) (Pereira et al. 2011; Rueda et al. 2020, Blanco-Vietes et al. 2023; Nejidat et al. 2023). In the context of bioremediation, cyanobacteria require trace amounts of essential nutrients in comparison to traditional remediation methods (Gavrilescu 2022). Therefore, development of a cyanobacteria strain adjusted to nutrient limited conditions is extremely attractive for industrial bioremediation purposes.

The two most important mechanisms for the uptake of metals by cyanobacteria include bioaccumulation (active) and biosorption (passive), both of which can reduce the metal concentration in solution and create potential nucleation sites for mineral precipitation (Gupta and Diwan 2017). Both mechanisms require the use of the cellular wall and EPS to reduce the concentration of metals in a solution (Gupta and Diwan 2017; Al-Amin et al. 2021). The biosorption mechanism can be described by kinetics and adsorption isotherms (Dixit and Singh 2013; Bishop et al. 2019; Smječanin et al. 2023). Biosorption is a passive process that occurs when microbial EPS interacts with the surrounding environment. EPS's composition often comprises polysaccharides, proteins, DNA, and lipids that are excreted out of the cell (Costa et al. 2018). Often, EPS also serves an important role in protecting cyanobacteria and plays an important role in biosorption by allowing available functional groups (e.g., carboxyl) to act as binding sites, resulting in lower metal concentrations in solution (Pereira et al. 2011). The cell-metal interaction can impact the production of the EPS and is often dictated by several factors including the ionic

potential, preferential ligand spacing, ligand type, temperature, pH, and covalent bonding (Konhauser 2007; Pereira et al. 2011; Zeng al. 2020a; Zeng et al. 2020b; Huang et al. 2022; Rezaei et al. 2022). Therefore, EPS can also be influenced and change its structure in response to both physiochemical and biogeochemical parameters, including nutrient limitations (Nicolaus, 1999; Liu et al. 2016; Mathivanan et al.2021).

Extensive research has focused on the biosorption capacity of different cyanobacteria species in combination with various metals (Gardea-Torresdey et al. 1998; Michelleti et al. 2008, Pereira et al. 2011; Mota et al. 2015). Previous research focused only on the impact of nitrogen or phosphorus in its relationship to binding metals including calcium, iron, molybdenum, nickel, which can impact biomineralization (Zerkle et al. 2006; Paulo et al. 2018; Selim and Haffner 2020; Qian et al. 2022). However, there is little published data surrounding transition metal binding in nutrient depleted environments, which is important for application of this process to ultramafic mine sites. While some experiments have been conducted on nutrient deficient environments, there are few studies that consider the combination of biosorption and nutrient availability and examine the impact on EPS. The chemical and physical modifications in the EPS from both nutrient limitations (C:N:P ratio) and presence of metals ions (Co^{2+}, Ni^{2+}) require investigation to better understand the biosorption capacity of cyanobacteria in ultramafic mine site environments. Understanding the kinetics and mechanisms of metal binding in a nutrient-limited environment can further determine the limitations and capabilities of cyanobacteria for bioremediation application in mine sites.

2.1 Research objectives

To address these research gaps, a strain of *Synechococcus leopoliensis* was assessed for its biosorption capabilities in a simulated ultramafic mine environment. The assessment of the metal sorption and growth curves of *S. leopoliensis* provided insight into how cyanobacteria can reduce elevated metal concentrations in its growth environment. *S. leopoliensis* was grown in varying metal concentrations in nutrient enriched and deficient environments. Cyanobacteria growth and metal sorption in single and di-metal solutions was assessed. The metals, Co^{2+} and Ni^{2+}, were selected due to their abundance in ultramafic mine tailings (Hamilton et al. 2018). The biomass was characterized using Raman spectroscopy and scanning electron microscopy (SEM). The

expectation was that biosorption of di-metals systems would be higher in the nutrient-deficient environment in comparison to the nutrient enriched environments. Furthermore, it was expected that preferential binding and changes within the EPS will dictate the abundance of favoured metals bound to EPS.

2.2 Methods

2.2.1 Bacterial strain and culture conditions

A cyanobacterial strain, *S. leopoliensis* (CPCC-102) was acquired from the Canadian Phycological Culture Center (CPCC) for this biosorption experiment. The experiment consisted of growing the cyanobacteria in modified BG-11 medium for one month and characterizing the change in microbial growth and water chemistry. The final volume of each treatment flask was 65 mL with each flask containing 10 mL of inoculum. The control group flasks contained 55 mL of BG-11 medium, the Ni-doped and Co-doped flasks contained 50 mL of BG-11 medium and 5 mL of the respective metal solution, and the di-metal flasks contained 45 mL of BG-11 medium and 5 mL of each metal solution (**Table *2.1***). Ultramafic mine environments are typically nutrient deficient with low concentrations of phosphate (0.0274–2.22 mg/L) and nitrate (0.0012–50 mg/L) present in associated mine pit waters (Nawab et al. 2016, McCutcheon et al. 2017, Paulo et al. 2023). Concentrations of nitrate (1.65 mg/L) and phosphate (13.2 mg/L) were selected to be representative of the nutrient deficient environments. The trace metal solution contained HBO_3, $MnCl_2{\cdot}4H_2O$, $ZnSO_4{\cdot}7H_2O$, $Na_2MoO_4{\cdot}2H_2O$, $CuSO_4{\cdot}5H_2O$, which were added to aid in the growth of the cyanobacteria (Rippka et al. 1979). The addition of $CoNO_3{\cdot}6H_2O$ was excluded from the trace metal mix because controlling the concentrations of cobalt and nitrate was necessary for this experiment.

Cobalt and nickel were selected as target metals in the interest of the Canadian critical metal strategy (Ministry of Natural Resources and Ministry of Science 2023) and because they have been observed to be incorporation into secondary carbonate precipitates found at mine sites. Mine impacted ultramafic groundwater contained trace amounts of nickel and cobalt (0.030–0.359 mg/L, 0.006–0.693 mg/L, respectively) (Nawab et al. 2016). Certain cyanobacteria may face toxicity at concentrations as lowest as 3 mg/L (Selim and Haffner 2020; Fawzy et al. 2020). However, different cyanobacteria have different toxicity levels; Ni and Co were added to the experiment at concentrations of 10 mg/L, added as $NiCl_2{\cdot}6H_2O$ and $CoCl_2{\cdot}6H_2O$, respectively.

The metals were added after Rippka et al.'s BG-11 medium recipe (**Error! Not a valid bookmark self-reference.**), with phosphate and nitrate added in lower concentrations in some flasks to reflect of ultramafic environments (1979).

Table 2.1: Quantities of ingredients added to BG-11 growth medium used in the biosorption experiment, adjusting for dilution. Values for $NaNO_3$ and K_2HPO_4 correspond to the high and low nutrient treatments, respectively. BG-11 medium and trace metal mix recipe from Rippka et al. 1979.

Ingredient	**Quantity**
$NaNO_3$	1.95 / 0.0235 g
K_2HPO_4	0.052 / 0.0039 g
$MgSO_4 \cdot 6H_2O$	0.0975 g
$CaCl_2 \cdot 2H_2O$	0.046 g
citric acid	0.0078 g
ferric ammonium citrate	0.0078 g
EDTA	0.0013 g
Na_2CO_3	0.026 g
Trace metal mix	1.3 mL
$CoCl\text{-}6H_2O$ (10 mg/L)	5.0 mL
$NiCl\text{-}6H_2O$ (10mg/L)	5.0 mL
Milli-Q water	1L

The cyanobacteria were grown for 35 days in standard BG-11 medium prior to the start of the experiment. The biosorption experiment was conducted in 125 mL Erlenmeyer flasks housed inside a Conviron GEN1000 growth chamber at a light intensity of 600 lux in a 12 hr day/night cycle. Sampling occurred on days 0, 1, 3, 6, 12, 20, and 30, with one flask per treatment sampled on each day for water chemistry analyses, cell counting, and EPS extraction.

2.2.2 Cell counting

Cell counting was conducted by loading 10 µL of sample into a haemocytometer for counting using a Leica DM750 light microscope. A cell count was conducted for each environmental condition on each of the sampling days.

2.2.3 Water Chemistry Analyses

The chemistry of the water in the flasks was characterized on each sampling day during the biosorption experiment. Water samples collected from each flask were filtered using 0.45 µm polyethersulfone (PES) syringe filters into 15 mL centrifuge tubes and stored at 4°C until analyzed. Anions were measured using ion chromatography (IC; Dionex 600-IC-CO3) and cations were measured in filtered samples acidified to pH <2 with trace metal grade nitric acid

using inductively coupled plasma-mass spectrometry (ICP-MS; NuPLasma II multi-collector inductively coupled plasma mass spectrometer)**.** The pH, dissolved oxygen (DO), and conductivity were measured on sampling days using a Thermo Scientific Orion Star A 329 Multiparameter Meter.

2.2.4 EPS Extraction

A modified version of Zeng et al.'s EPS extraction protocol, which is a NaCl centrifugation EPS extraction procedure, was conducted to assess its suitability for use on *S. leopoliensis* (2019). A 10 mL aliquot of sample was allocated for EPS extraction from each treatment on each sampling day. In brief, this method consisted of centrifugation (Sorval X1R Pro MD), removal of the supernatant, and addition of a phosphate buffered saline solution. All centrifugation was conducted at 8000 rpm for 10 minutes at 4°C. An initial centrifugation was conducted with the supernatant being discarded. Subsequently, 10 mL of phosphate buffered saline was added and the sample was centrifuged three times. Each time the centrifugation process occurred; the supernatant was discarded. After the third centrifugation, the addition of 10 mL of phosphate buffered saline and 10 mL of 1.0 M NaCl was added to the falcon tube. This step was centrifuged at 300 rpm for 1 hr. After the 1 hr, it was recentrifuged at 8000 rpm for 10 minutes where the remaining supernatant was collected. Modifications to this method included: adding a rinse of DI water to reduce NaCl recrystallization after the final filtration for the supernatant, weighing the filters to determine the amount of EPS and organics deposited onto the filter paper, and collecting 1 mL of the supernatant after the final filtration to avoid interference from the 0.2 mm Polytetrafluoroethylene (PTFE) filter. Following the extraction, samples were analyzed using Raman spectroscopy as described below.

2.2.5 Scanning electron spectroscopy- energy dispersive spectroscopy

The following procedure was used to prepare samples for SEM by McCutcheon and Southam (2018). The biomass was fixed using 2.5% (v/v) glutaraldehyde for 1 hr. The biomass underwent ethanol dehydration with the following concentrations: 25%, 50%, 75%, 100%, 100%, 100% in 15-minute intervals. This was followed by chemical drying using hexamethyldisilane (HMDS) solution of 50%, 100%, 100% for 15-minute intervals. The samples were be mounted on a aluminum stubs and coated with gold using a Denton Desk II gold sputter. Morphological changes before and after the addition of metals (Co, Ni,) were observed using

UltraPlus FE-SEM in secondary electron (SE)-SEM operated at 2.0 kV and 5.0 mm working distance. Furthermore, the UltraPlus FE-SEM conducted energy dispersive spectroscopy (EDS) measurements, which determined the chemical composition of any precipitates, and any metals mobilized within the EPS.

2.2.6 Raman Spectroscopy

Raman spectroscopy was used to identify the functional groups present in the EPS. Raman spectra were measured using a Renishaw InVia Reflex Raman microscope using a 532 nm Renishaw HeNe Laser along with a 2400 lines/mm diffraction grating. The EPS was analyzed at the fingerprint region (300–2000 cm^{-1}). The Renishaw WiRE 5.5 software was used to acquire measurements and processed the data. Initially, the Raman data underwent processing by removing cosmic rays and redefining the baseline through polynomial subtraction. Three types of spectra were collected, including the whole culture, EPS before filtering, and after deposition of supernatant on the filter paper to determine the change in the functional group composition and whether the extraction methods were successful in isolating the EPS.

2.2.7 Data analysis

Water chemistry data were analyzed and plotted over time using Origin 2020 software version 9.7.0.188. Functional groups were identified in the Raman spectra by comparing peak locations to reference spectra in the literature. A NaCl signal was prevalent throughout most of the Raman spectra collected, and therefore, a background signal of NaCl was collected, peak fitted and normalized. Raman spectra from experimental EPS were normalized and NaCl background signal subtracted. Additional statistical analysis was performed by generating simulated curves to examine the variability of Ni and Co concentration by applying transformations onto the curve.

2.3 Results

2.3.1 Cell counting

The growth of *S. leopoliensis* over the 30-day experiment was assessed using cell counting. The cyanobacteria in the nutrient enriched and depleted control groups showed similar cell densities of 3.13×10^6 and 3.57×10^6 cells/mL, respectively (**Figure 2.1A)**. In flasks containing metals, cell densities were lower, and the rates of cell density increase were slower than the control groups (**Figure 2.1B-D**). The maximum cell density for the various metal

treatments occurred on different days, for instance, the highest cell counts for Ni-H and Co-H occurred on day 6 and day 20 at 1.79×10^6 and 1.81×10^6 cells/mL, respectively. Overall, cell counts were higher in the 2 mono-metal systems compared to the di-metal systems in most of the sampling days.

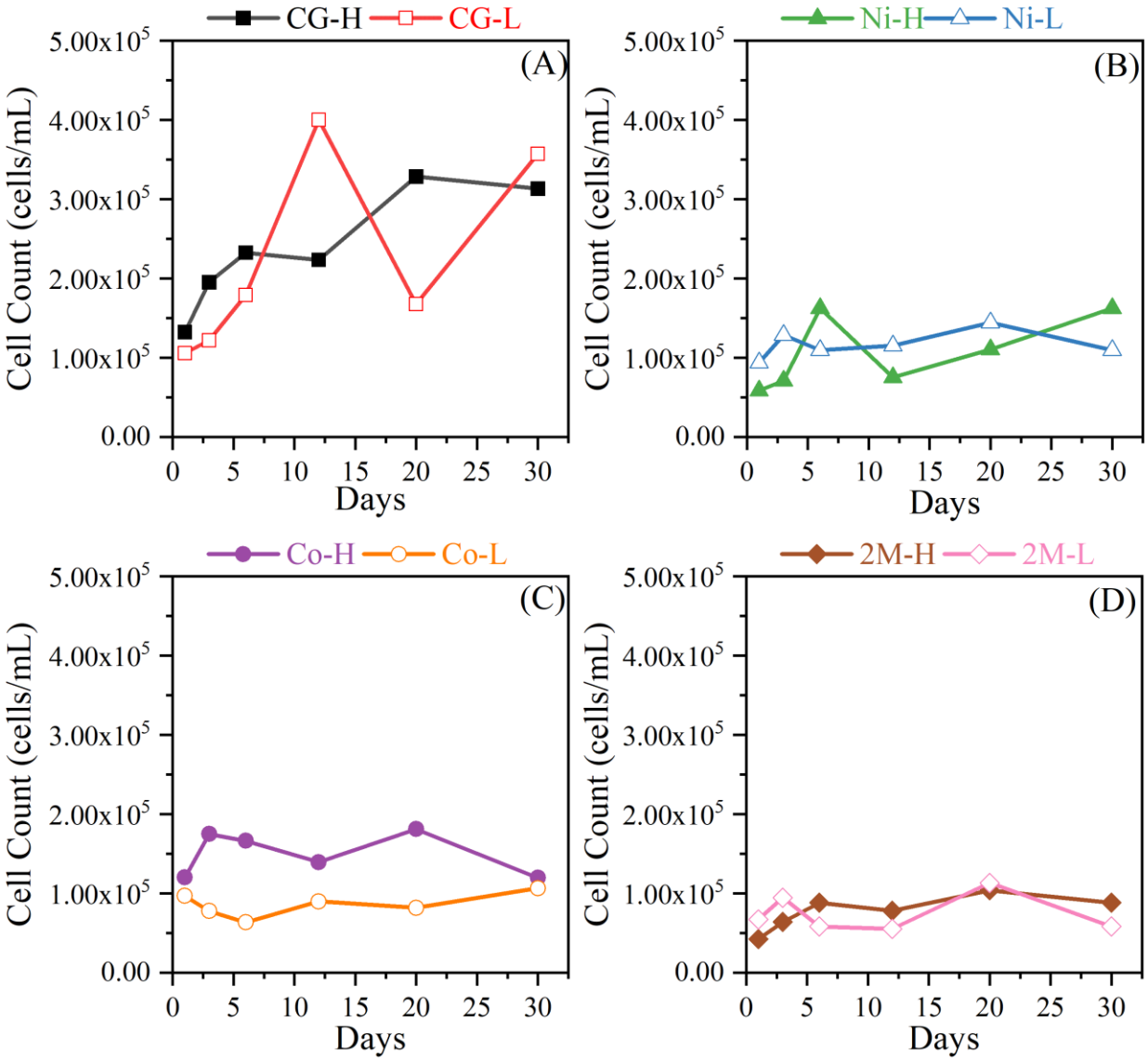


Figure 2.1. Cell densities of *S. leopoliensis* in nutrient enriched (H) and nutrient deficient (L) flasks over the 30-day experiment. Cell counts plotted versus time for the control groups (A), nickel doped (B), cobalt doped (C), and di-metal (D) treatments.

2.3.2 Water chemistry analyses:

Over the 30-day period, pH changed in all control and metal doped flasks (**Figure 2.2**). The change in pH in both nutrient enriched and nutrient depleted control groups was most apparent, with both controls having pH values of ~9.5 near the start of the experiment and

decreasing to ~5 on day 12 and 20, respectively (**Figure 2.2A**). The pH decrease in the control groups may have been due to contamination of the flasks by another organism, possibly a fermentative bacterium based on the high concentrations of acetate measured in these solutions starting on day 12 of the experiment (**Table A-1**). The metal doped flasks did not exhibit the decrease in pH observed in the control group's flasks (**Figure 2.2B-D**). Rather, the pH of all metal doped solutions stabilized at pH values of 7.7–8.0 after an initial fluctuation in pH during the first 6 days of the experiment. Nutrient depleted flasks had slightly higher pH values compared to nutrient enriched flasks by the end of the experiment.

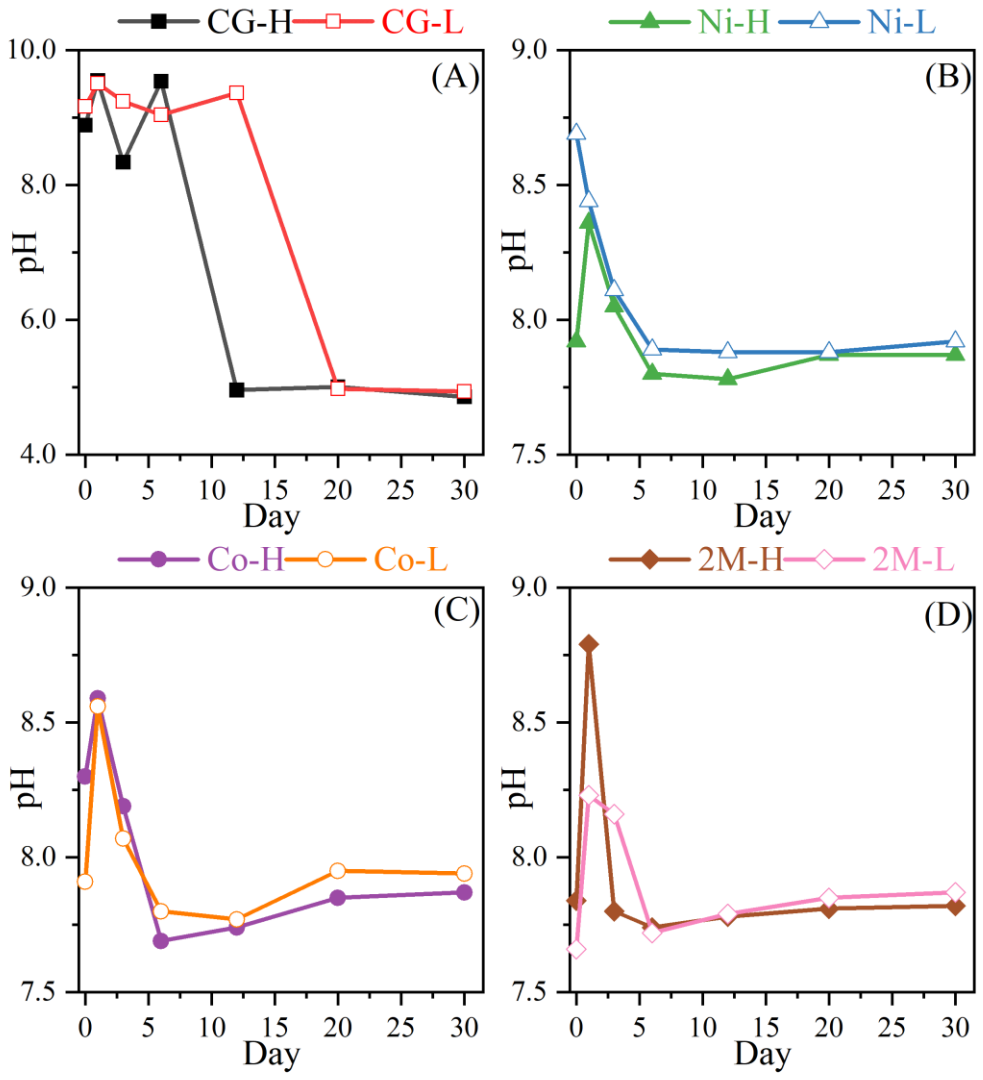


Figure 2.2. Evolution of pH over the 30-day biosorption experiments for the control groups (A) nickel doped (B), cobalt doped (C), and di-metal (D) treatments.

The DO measured in the nutrient enriched and nutrient deficient treatments showed comparable overall trends (**Figure 2.3**). The DO increased for the first 6 days, followed by a gradual decrease over the remainder of the 30-day experiment (**Figure 2.3**). The DO in the nutrient enriched and nutrient-deficient control groups decreased from 8.01 to 7.61 mg/L and 8.09 to 7.39 mg/L, respectively (**Figure 2.3A**). The DO measured in the Co treatments showed a consistent, gradual decrease (**Figure 2.3C**), while the DO measured in the Ni and di-metal treatments showed more fluctuation (**Figure 2.3B, D**). By the end of the experiment, the DO in all the flasks stabilized between 7.4–7.6 mg/L.

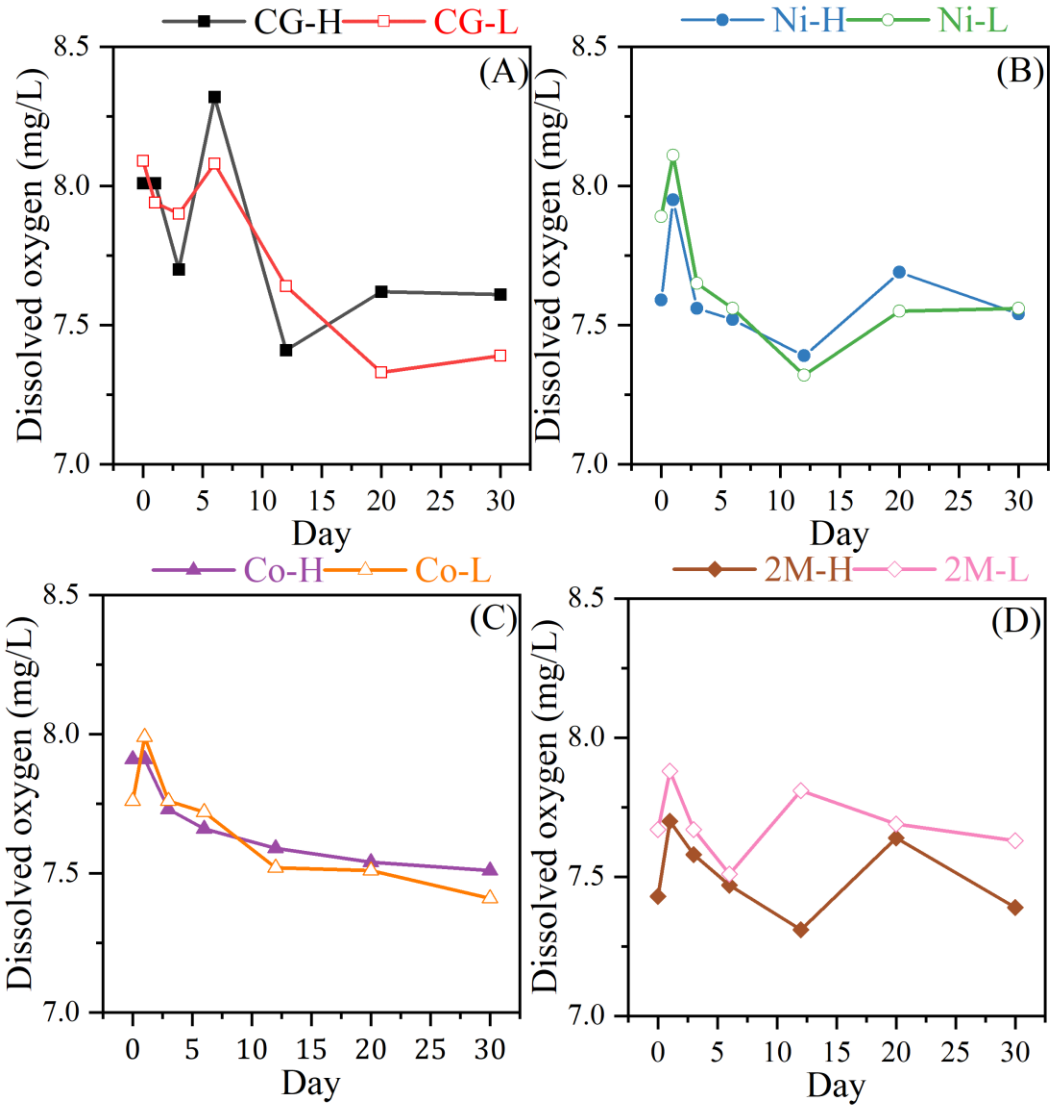


Figure 2.3. Dissolved oxygen measured in the nutrient enriched and nutrient deficient treatments for the control groups (A), Ni (B), Co (C), and the di-metal treatments (D).

The conductivity increased throughout the 30-day experiment for all treatments (**Figure 2.4**). The conductivity of the nutrient-enriched control group increased by 14.3% (2780.0 to 3153.7 mS/cm) (**Figure 2.4A**). Meanwhile, the conductivity in nutrient-deficient control group only increased by 6.4% (590.1 to 627.6 mS/cm) (**Figure 2.4B**). The nutrient-enriched flasks doped with nickel indicated a consistent increase of 12.5% (2565 to 2887 mS/cm) in conductivity that was similarly observed in the control group (**Figure 2.4A**). However, the nutrient-deficient flasks doped with nickel experienced a greater increase in conductivity compared to its nutrient-enriched counterpart, increasing by 22.4% (577.5 to 706.7 mS/cm) (**Figure 2.4B**). Similar trends were observed for the cobalt doped flasks, with the nutrient-enriched and nutrient-deficient flasks showing conductivity increases of 12.6% (2572.0 to 2883.7 mS/cm) and 21.0% (563.8 to 682.4 mS/cm), respectively (**Figure 2.4**). In the di-metal systems, the conductivity increased by 13.6% (2348.0 to 2668.3 mS/cm) in the nutrient-enriched flasks and by 14.9% (603 mS/cm to 692.6 mS/cm) in the nutrient-deficient flasks.

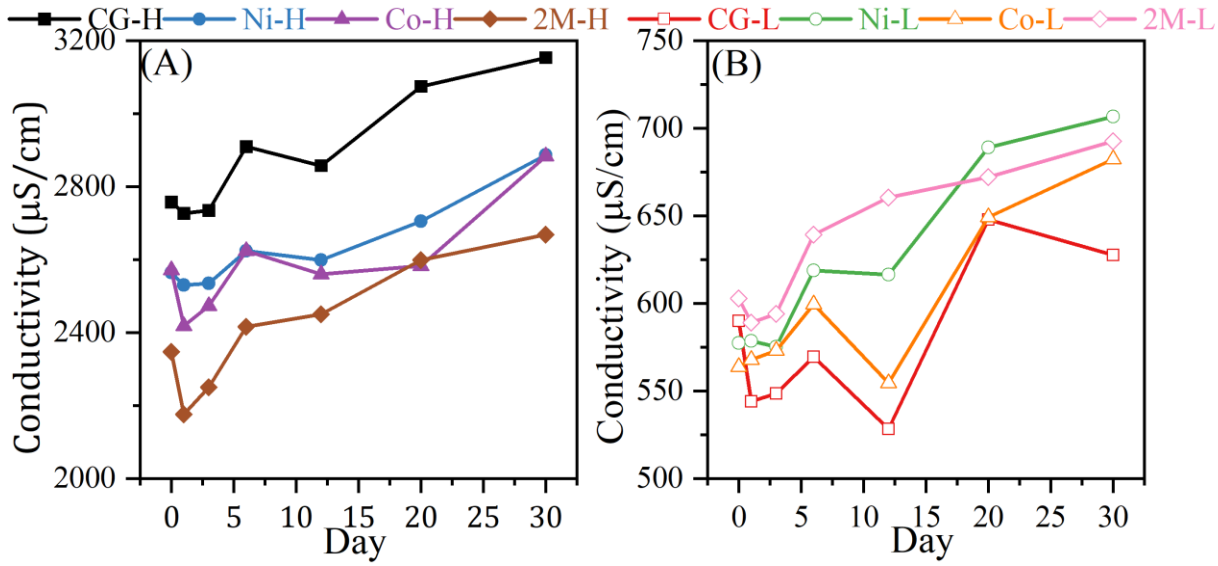


Figure 2.4. Conductivity measured in the nutrient enriched (A) and nutrient deficient (B) treatments throughout the 30-day experiment.

Nitrogen (measured as nitrate) and phosphorus (measured as phosphate and phosphorus) were the key nutrients of interest in the nutrient enriched and depleted treatments. The concentration of nitrate decreased in all flasks between day 1 and day 3 (**Figure 2.5A, B**). After day 3, the measured nitrate concentrations increased slightly throughout the remainder of the experiment in both nutrient deficient and nutrient enriched flasks. The fluctuation in the nutrient deficient control flasks is likely due to the suspected contamination and should be disregarded.

Phosphorus measured as phosphate fluctuated between 0.5 and 3.5 mg/L in the nutrient deficient flasks (**Figure 2.5C**). In the nutrient enriched flasks, the phosphate concentration initially decreased in the first 3 days of the experiment followed with an increase over the next 3 days, followed by consistent or slightly higher concentrations over the remainder of the experiment (**Figure 2.5D**). For phosphorus measured as both phosphate and phosphorus, the nutrient deficient control group was different compared to the rest of the flasks due to possible contamination (**Figure 2.5C, E**).

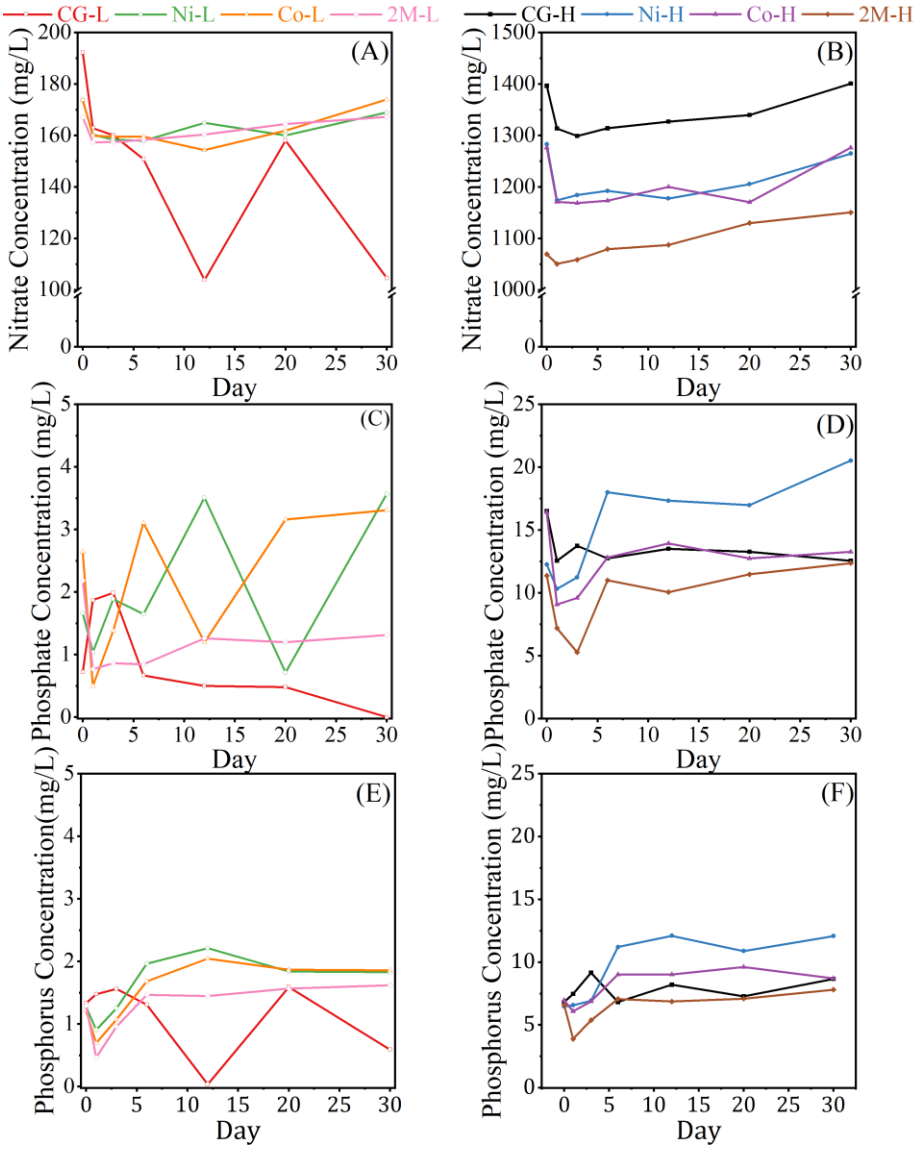


Figure 2.5. Concentrations of nitrate (A, B), phosphate (C, D), and phosphorus (E, F) in the nutrient depleted (A, C, E) and nutrient enriched (B, D, F) flasks throughout the 30-day experiment.

The lowest measured cobalt concentration was predominantly on the first day of the experiment, 24 hours after the addition of metals into the flasks (**Figure 2.6**Error! Reference source not found.**A**). The calculated metal removal in both mono-metal and di-metal systems reached their maximum metal removal capacity on the first day (**Figure 2.6A, Table 2.2).** The removal of cobalt in both a mono-metal and di-metal systems in nutrient enriched conditions achieved approximately 40% removal in the first day. Specifically, both mono-metal and di-metal systems in nutrient enriched conditions removed 4.74 mg/L and 5.19 mg/L worth of cobalt from solution, respectively. However, there were discrepancies between the two metal systems (**Table 2.2**). The di-metal systems in nutrient enriched condition exhibited a delayed effect of reaching their maximum metal removal on day 3 instead of day 1. Once the maximum metal removal was achieved, the cobalt concentration increased steadily, and occurred regardless of mono or di metal system as well as nutrient availability **(Figure 2.6A)**. For example, the cobalt concentration in 1-metal systems on day 3 increased by 40.8% and 33.8% from the measured concentration from day 1 in the nutrient enriched and nutrient deficient environments, respectively. Di-metal systems had similar trends as the cobalt concentration increased after reaching the maximum removal of cobalt in the previous sampling day. The nutrient enriched di-metal system increased its cobalt concentration by day 6, which fluctuated throughout the following 24 days. By the end of the experiment, most of the cobalt remained in the aqueous solution.

The measured dissolved nickel concentration decreased in the first 3 days of the experiment (Error! Reference source not found.**B**). The amount by which nickel decreased was l ess than cobalt in both mono-metal and di-metal systems. However, the amount by which the nickel concentration decreased was typically greater in nutrient-deficient conditions compared to nutrient enriched conditions. The nutrient deficient condition removed up to 43.8% (4.98 mg/L) of nickel within the bulk solution compared to nutrient enriched conditions, which only reached a maximum of 36.0% (3.5 mg/L) of nickel. Similarly, di-metal systems showed nutrient deficient conditions removed more nickel compared to nutrient enriched conditions. The nutrient deficient condition di-metal system showed a decrease in nickel concentration up to 34.2% (3.97 mg/L) in solution from day 1 of the experiment. Meanwhile, the first day in the nutrient enriched di-metal system removed only 18.7% (2.01 mg/L) of nickel. The removal of nickel on day 1 was usually the maximum removal rate of nickel with its concentration increasing afterwards (**Figure 2.6B**).

The increase in the concentration of nickel over time was slower compared to cobalt, as it required 6 days to fully reach almost 93% of its initial nickel concentration. However, the nickel concentration in nutrient deficient 1-metal system increased up to 82%. By the end of the experiment, most of the nickel was released back into solution. The nickel concentration fluctuated but overall increased in the remaining 18 days of the experiment.

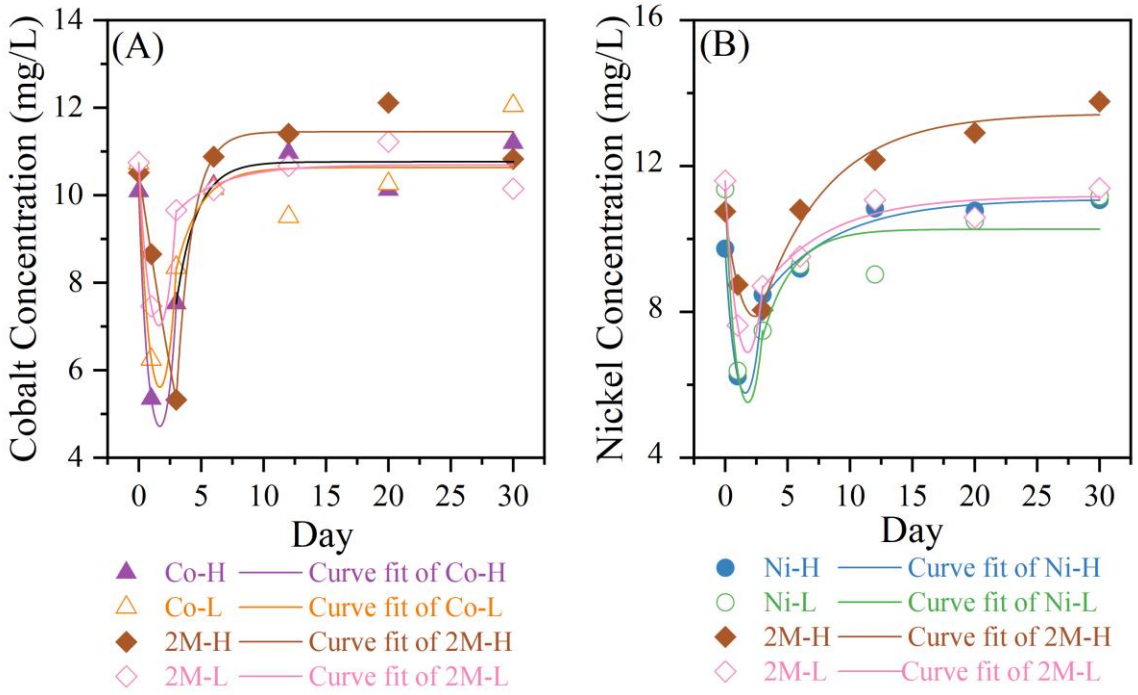


Figure 2.6. Cobalt (A) and nickel (b) concentrations decreased and then increased, followed by minor fluctuations throughout the remainder of the experiment.

Table 2.2. Maximum cobalt and nickel removal by *S. leopoliensis* during the 30-day experiment based on dissolved metal concentrations measured using ICP-MS.

Sample	Metal Removal (%)	Time to reach maximum removal (Days)
Co-H	47.0	1
Co-L	41.8	1
Co in 2M-H	49.4	3
Co in 2M-L	30.6	1
Ni-H	36.0	1
Ni-L	43.8	1

Ni in 2M-H	25.1	3
Ni in 2M-L	34.2	1

2.3.3 Electron microscopy

The cultures were observed using SEM to examine any changes to cell morphology or EPS production during the experiment (**Figure 2.7-Figure 2.10**). No EPS was observed in the nutrient-enriched control sample from day 1 (**Figure 2.7A**). However, small amounts of EPS were observed for the day 1 culture samples from flasks containing cobalt, nickel, and both metals (**Figure 2.7B-D**). EPS production appeared to increase with time and increased metal exposure (**Figure 2.8**). No EPS was observed in the nutrient enriched conditions in the control sample in EPS even by day 12 (**Figure 2.8A**). However, the EPS seemed to have increased within the flask containing metals by day 12 (**Figure 2.8B-D**). All day 1 culture samples from the nutrient-deficient flasks contained EPS material around the cells, including the control group (**Figure 2.9**). The nutrient deficient samples in day 12 contained the highest amount of EPS surrounding the cells (**Figure *2.10***). No precipitates were formed throughout the duration of the experiment.

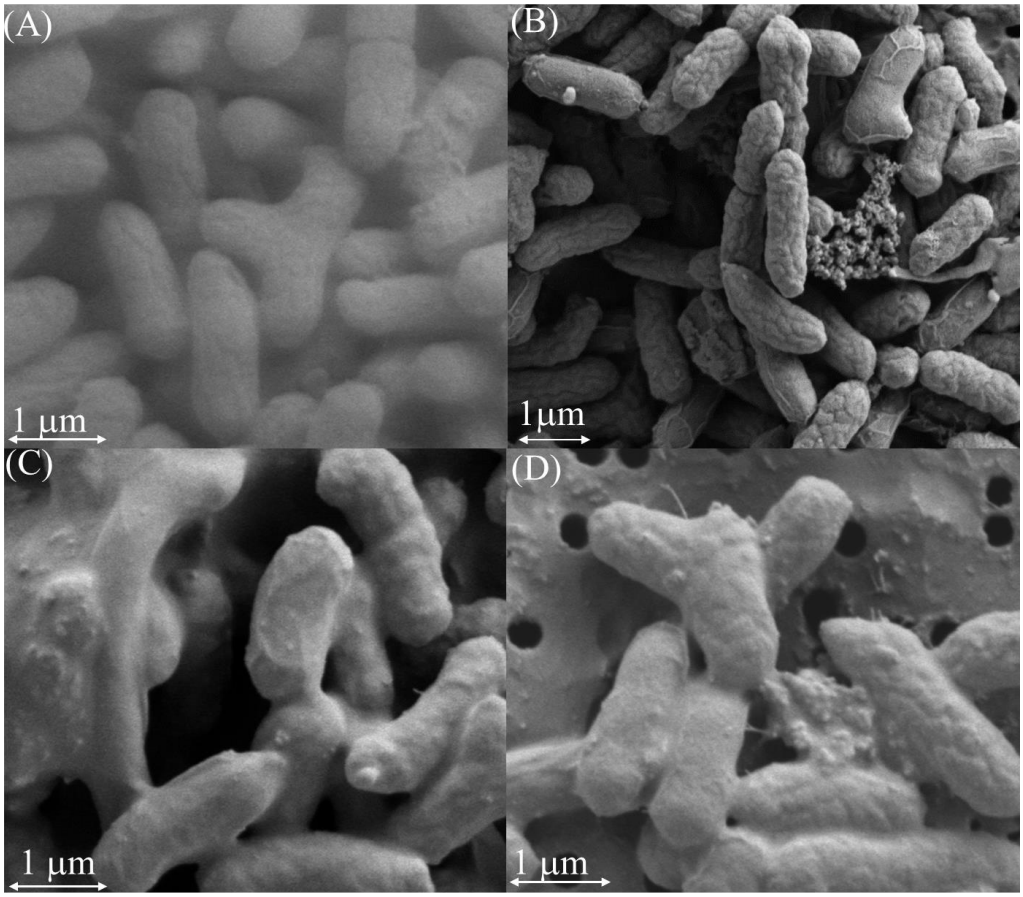


Figure 2.7. Scanning electron micrographs showing *S. leopoliensis* cells on day 1 of the experiment in the nutrient enriched control (A), cobalt (B), nickel (C), and di-metal (D) flasks.

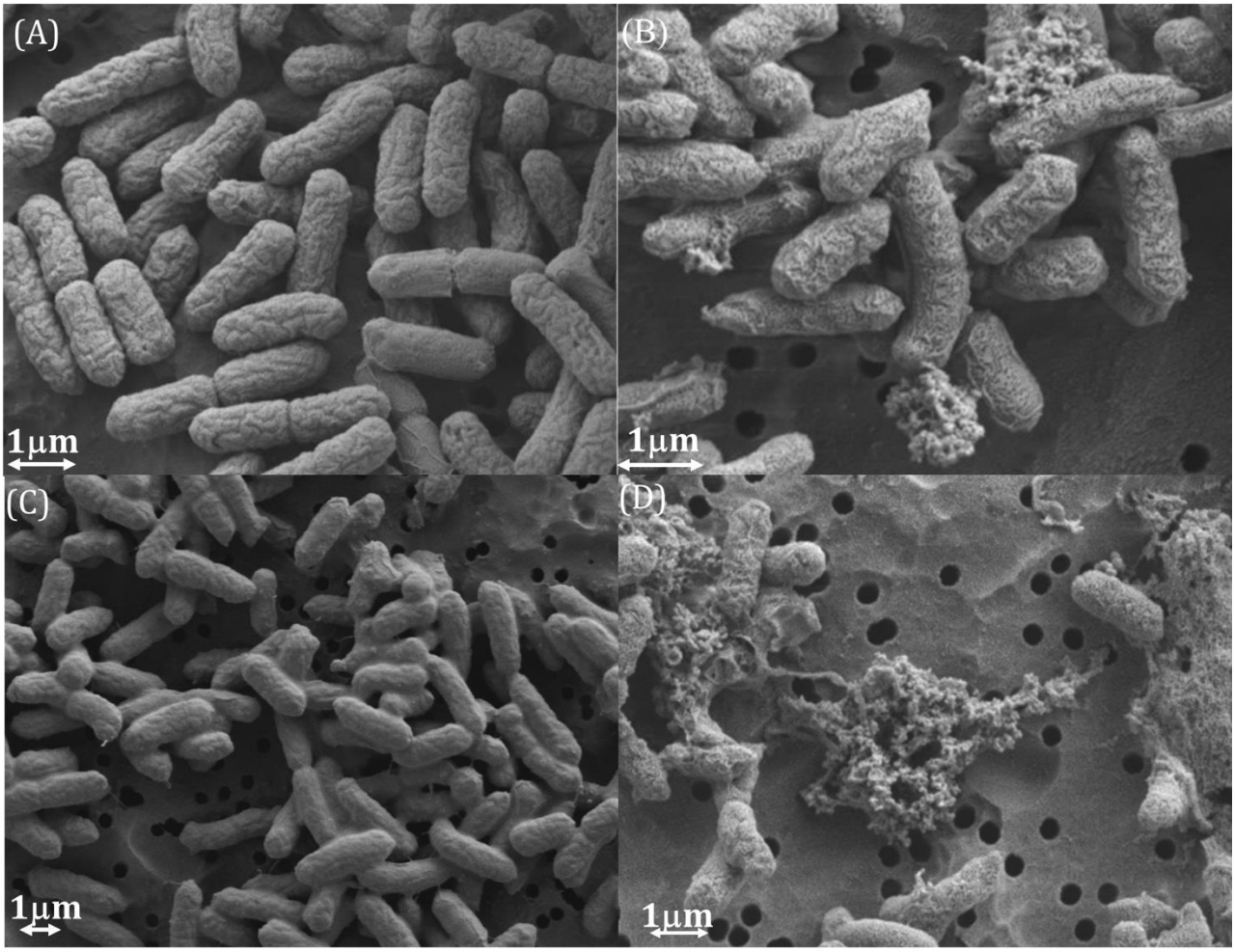


Figure 2.8. Scanning electron micrographs showing *S. leopoliensis* cells on day 12 of the experiment in the nutrient enriched control (A), cobalt (B), nickel (C), and di-metal (D) flasks.

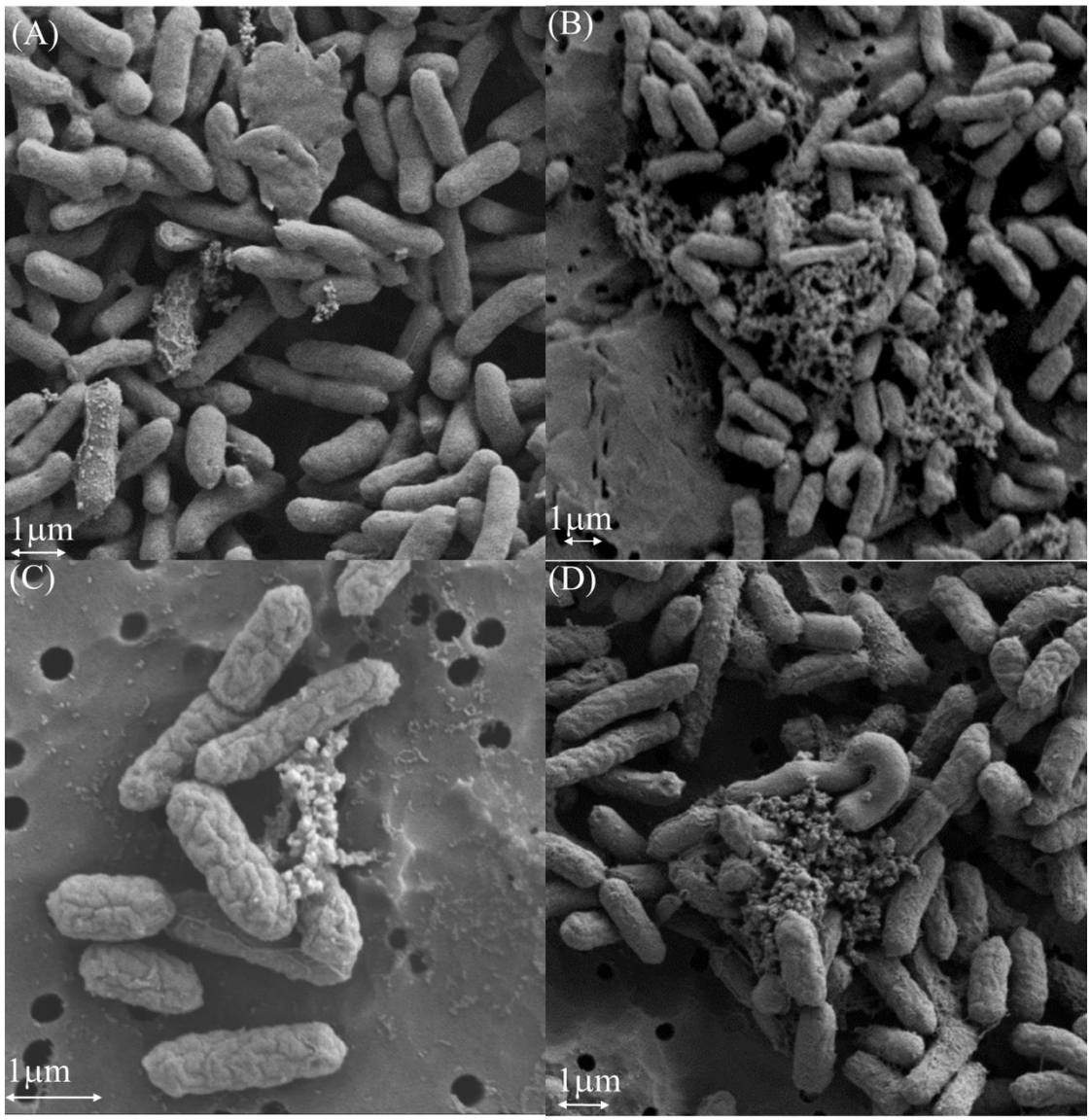


Figure 2.9. Scanning electron micrographs showing *S. leopoliensis* cells on day 1 of the experiment in the nutrient deficient control group (A), cobalt (B), nickel (C), and di-metal (D) flasks.

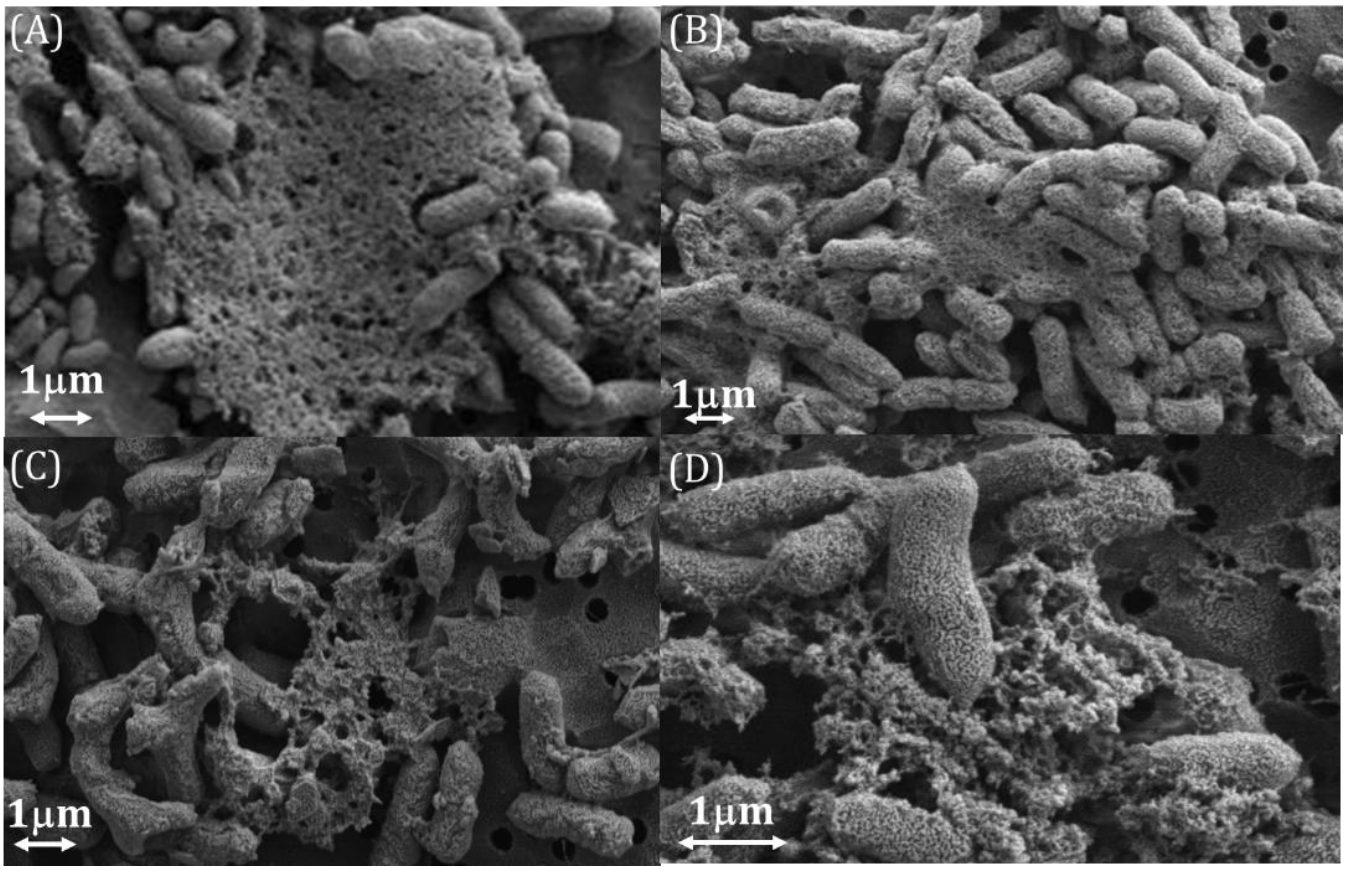


Figure 2.10. Scanning electron micrographs showing *S. leopoliensis* cells on day 12 of the experiment in the nutrient deficient control group (A), cobalt (B), nickel (C), and di-metal (D) flasks.

Energy dispersive spectroscopy (EDS) was used to measure nitrogen, phosphorus, cobalt, and nickel concentrations in the *S. leopoliensis* cultures observed using SEM. The average nitrogen concentrations measured across all treatments were between 8 and 18.5 % (Error! Not a valid bookmark self-reference.). The nitrogen concentration increased slightly between day 1 and 12, with the cobalt doped systems exhibiting greater increases (1–4 %) compared to other metal systems (Error! Not a valid bookmark self-reference.). Nitrogen was higher in the nutrient deficient systems than the nutrient enriched systems, possibly due to the increased production of EPS (Error! Not a valid bookmark self-reference.). Measured phosphorus concentrations were between 0.1 and 1.1 % on day 1. Phosphorus increased slightly in the nutrient enriched conditions by the day 12 (Error! Not a valid bookmark self-reference.). Under nutrient limitations, the phosphorus content increased in the nickel doped system and decreased in the other treatments (Error! Not a valid bookmark self-reference.). Day 1 concentrations of both

cobalt and nickel in a mono-metal and di-metal systems were higher in the nutrient deficient conditions compared to the nutrient enriched conditions (Error! Not a valid bookmark self-reference.). The uptake of cobalt was higher in the di-metal system compared to the mono-metal system on day 1, but the opposite was true by day 12. Nickel content was higher in a mono-metal system compared to the di-metal system on day 1. However, nickel content decreased in both nutrient treatments by day 12 (Error! Not a valid bookmark self-reference.).

Table 2.3. Average atomic abundance (%) detected by energy dispersive spectroscopy on cyanobacteria and EPS material observed using SEM.

		Atomic (%)						
	Day	C	N	O	Si	P	Co	Ni
CG-H (n=2)	1	71.0	10.1	11.5	0.9	0.6		
Co-H (n=3)	1	78.7	9.5	11.2	0.4	0.1	0.1	
Ni-H (n=2)	1	61.7	8.7	24.7	4.6	0.1		0.2
2M-H (n=3)	1	71.3	10.5	16.6	1.4	0.1	0.1	0.1
CG-H (n=3)	12	70.2	14.2	15.2	0.2	0.1		
Co-H (n=4)	12	67.2	16.9	14.7	0.9	0.1	0.2	
Ni-H (n=5)	12	73.3	12.2	13.1	0.9	0.2		0.1
2M-H (n=2)	12	74.0	12.1	13.3	0.2	0.1	0.2	0.1
CG-L (n=4)	1	71.7	15.1	11.9	0.8	0.5		
Co-L (n=4)	1	69.8	16.2	13.0	0.4	0.3	0.3	
Ni-L (n=4)	1	65.8	11.4	20.8	1.6	0.1		0.2
2M-L(n=2)	1	67.5	12.7	18.6	0.5	0.2	0.2	0.1
CG-L (n=3)	12	70.7	11.0	16.9	1.1	0.5		
Co-L (n=4)	12	64.3	18.5	16.3	0.6	0.1	0.1	
Ni-L (n=2)	12	71.8	13.8	13.6	0.4	0.1		0.2
2M-L (n=1)	12	71.4	14.5	13.2	0.6	0.1	0.1	0.1

2.3.4 Raman spectroscopy:

The extraction method was successful in isolating the EPS material. However, the NaCl signal was removed in order detect the signal from the EPS material. Raman data was collected from both cells and extracted EPS material on days 1, 3, and 12. However, the data had a low signal/noise ratio in both day 1 and day 3 samples. Therefore, day 12 samples containing cyanobacteria and the EPS material were selected as the best representative samples despite sodium chloride signal being present. The control groups from nutrient enriched and nutrient deficient environments exhibited both carboxyl and amide collected from Day 12 (**Figure 2.11**, **Table 2.4**). The presence of different metals in the system under nutrient limited environments exhibited specific functional groups, in particular the carboxyl groups (Error! Reference source n ot found., **Table 2.5**). In the presence of nickel, specific vibrations associated to nickel were detected at 421 $cm^{-1}$and 451 cm^{-1}, which have been associated with Ni-N and Ni-O vibrations, respectively (Bell et al. 2003, Alsaç et al. 2022). Vibrations at 481 cm^{-1} and 522 cm^{-1} detected in the cobalt doped sample can be assigned to Co-O vibrations, which have been associated to Co_3O_4 (Gao et al. 2016, Alsaç et al. 2024). In the di-metal system, Ni-O and C-O bonds were observed around 459 cm^{-1} and 532 cm^{-1}, respectively (). In addition, the di-metal systems had vibrations from all three amide bands and carboxyl groups (**Table 2.5)**.

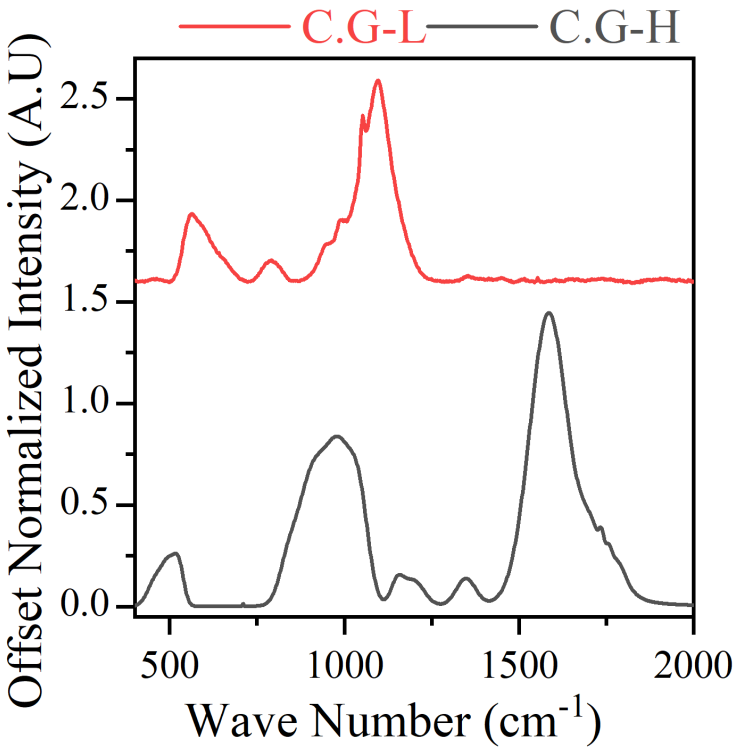


Figure 2.11. Raman spectra showing vibration bands from *S. leopoliensis* cells and EPS exposed to both nutrient enriched and nutrient deficient environments on day 12 of the experiment.

Table 2.4. Raman peak assignments in both control groups containing whole cells of S. leopoliensis under nutrient enriched and nutrient deficient environments on day 12.

Peak Location	**Functional groups In nutrient enriched control group**	**Functional groups In nutrient deficient control group**	**References**
489 cm^{-1}	(δC-C)		Chen et al. 2004
519 cm^{-1}	δCO		
561 cm^{-1}		δC-C	
589 cm^{-1}		δC-O	
790 cm^{-1}		δC-H	
987 cm^{-1}		δCH_3	
980 cm^{-1}	δCNC		Diloreto et al. 2023
990 cm^{-1}	δCH_3		Chen et al. 2004
1050 cm^{-1}	δC–C		Yee et al. 2004; Benning et al. 2004; Dittrich and Sibbler 2006
1095 cm^{-1}		ν C-O/ νP=O	Dittrich and Sibbler 2006; Diloreto et al. 2023
1160 cm^{-1}	H_2PO^{4-}		Dittrich and Sibbler

			2006 ; Braissant et al. 2009
1206 cm^{-1}	δCH and νN-C		Diloreto et al. 2023
1348 cm^{-1}	C-H, CH_3 and CH_2		Yee et al. 2004; Dittrich and Sibbler 2006
1353 cm^{-1}		δCH_3, δC-H, νN-C, and νC-C	Chen et al. 2004; Diloreto et al. 2023
1451 cm^{-1}		Amide band (III)	Dittrich and Sibbler 2006
1517 cm^{-1}		δCH_3, δC-H, νN-C, and νC-C	
1554 cm^{-1}		Amine band (II)	Dittrich and Sibbler 2006
1586 cm^{-1}	Amine band (I)		
1734 cm^{-1}	Ester Bond		Yee et al. 2004

Table 2.5. Raman peak assignments in samples of S. leopoliensis cells collected from the nutrient deficient metal systems on day 12 of the experiment.

Peak Location	**Functional groups in Co-L**	**Functional groups in Ni-L**	**Functional groups in 2M-L**	**References**
421 cm^{-1}		δ Ni-N		Bell et al. 2003
451/59 cm^{1}/		δ Ni-O	δ Ni-O	Alsaç et al. 2022
482 cm-1	δCo-O			Gao et al. 2016, Alsaç et al. 2024
522/32 cm^{-1}	δCo-O		δCo-O	Gao et al. 2016, Alsaç et al. 2024
548 cm^{-1}	(δC-C)	γ C-C		Chen et al. 2004
567 cm^{-1}	δCO	δ/γ C-C		
569 cm^{-1}			γ CO,	
613 cm^{-1}			δ C-C	
683 cm^{-1}		δ C-C=N		
687 cm^{-1}			δ C-C=N	
757 cm^{-1}			γ C-C=N	
858 cm^{-1}	γ CO, δ C-C or δ/γ(C-C=N			
911 cm^{-1}	γ CO, δ C-C or δ/γ(C-C=N			
962 cm^{-1}			δ C-C	(Paulo and

				Dittrich 2014).
980 cm^{-1}	γ CO, δ C-C or δ/γ(C-C=N			(Chen et al. 2004).
983 cm^{-1}			δ C-C	(Paulo and Dittrich 2014).
1003 cm^{-1}	deformation of methyl group and νCO			Diloreto et al. 2023
1030 cm^{-1}		νC-O		Dittrich and Sibler 2006
1032 cm^{-1}	deformation of methyl group and νCO			Diloreto et al. 2023
1085 cm^{-1}		νP=O		Dittrich and Sibbler 2006
1112 cm^{-1}			νC-O-C	Paulo et al. 2021
1114 cm^{-1}	νC-C			Chen et al. 2004,
1128 cm^{-1}	νC-OC, νC-O-P or νP-O-P			Yee et al 2003; Dittrich and Sibbler 2006
1165 cm^{-1}	νC-C			Chen et al. 2004
1172 cm^{-1}	νC-OC, νC-O-P or νP-O-P			Yee et al 2004; Dittrich and Sibbler 2006
1234 cm^{-1}	νP=O			Dittrich and Sibbler 2006
1254 cm^{-1}	νC-O COOH		νP=O the nucleic acids or related to the νC-O	Yee et al. 2004 ; Dittrich and Sibbler 2006 ; Liu et al. 2015
1281 cm^{-}		δCH_3 and νN-C with an aromatic ring; or a simple δCH and νN-C		Chen et al. 2004; Diloreto et al. 2023
1323/1331 cm^{-1}		δC-H, δCH3, δCH2 and νN-C	δC-H, δCH_3, δCH_2 and νN-C	Chen et al.2004; Yee et al. 2004; Diloreto et al. 2023
1368/70 cm^{-1}				
1413/15 cm^{-1}	νP=O		νP=O	Paulo et al. 2018
1451/1462 cm^{-1}	Amide (III)		Amide (III)	Yee et al. 2004; Dittrich and Sibbler 2006; Liu et al. 2015
1538/1554 cm^{-1}		Amide (II) Band/ C=N stretches	Amide (II) Band/ C=N stretches	
1595 cm^{-1}		, δO-H		Yee et al. 2004
1643/1651	Amide(I)		Amide(I)	Yee et al. 2004;

cm^{-1}				Dittrich and Sibbler 2006; Liu et al. 2015
1707/1710 cm^{-1}	δCH and νN-C	C=O,	νC=O	
1732/34/35 cm^{-1}	νC=O	νC=O	νC=O	

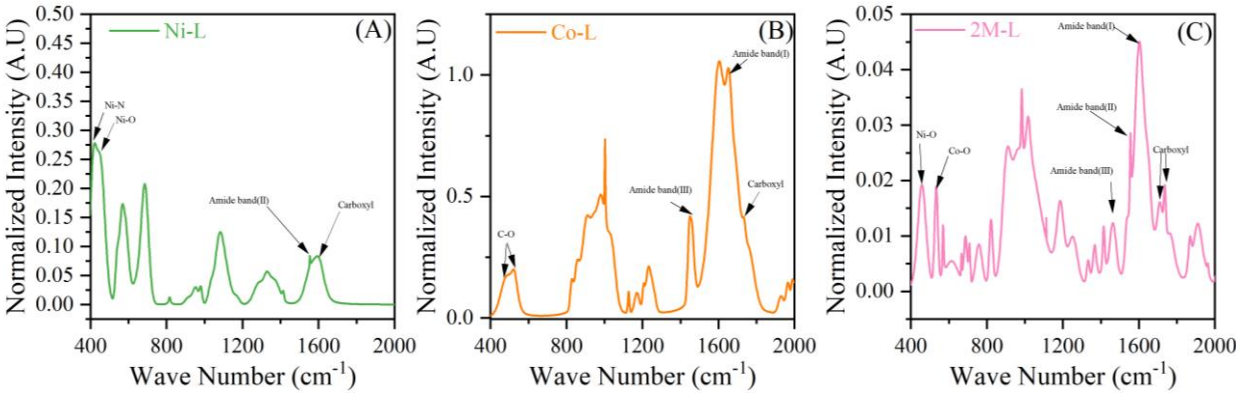


Figure 2.12. Raman spectra showing surface functional groups on the cells and EPS in the mono-metal systems when exposed to Ni (A) and Co (B) from day 12. While there are some similarities, most of the peaks were different. The di-metal system (C) exhibits a combination of cobalt and nickel peaks present.

2.4 Discussion

2.4.1 Biosorption of cobalt and nickel by *S. leopoliensis*

Biosorption is a passive process that can immobilize metals on the surface of bacterial cell walls and EPS by metal adsorption to organic ligands (Gupta and Diwan 2017; Al-Amin et al. 2021). Peaks identified using Raman spectroscopy indicated both Co-O and Ni-O vibrations were present, indicating potential ligands being bound to the metals (Gao et al. 2016; Alsac et al. 2022, Alsaç et al. 2024). Previous research has shown that Ni can form complexes with oxygen that impede photosystem (II), resulting in decreased photosynthesis function (Boisvert et al. 2007; Martínez-Ruiz and Martínez-Jerónimo 2015; Martinez-Ruis and Martinez Jeronimo 2016). The present study detected vibrations similar to Co_3O_4 using the Raman spectroscopy, which was not observed in a previous study of cyanobacteria exposed to cobalt (Fawzy et al. 2020). However, no obvious Co_3O_4 mineral precipitates were observed using SEM. Different metal species that competitively bind to similar ligands in cyanobacterial EPS can result in preferential binding of certain metals (Konhauser 2007, Pereira et al. 2011). The results of this study

indicated that competitive binding may have hindered the metal adsorption in the di-metal system when compared to the mono metal systems.

The measured metal concentrations indicated that desorption occurred over time, a trend which may have been impacted by changes in the pH level within the systems (Gardea-Torresday et al. 1998; Yee et al. 2004; Liu et al. 2015). Another factor that may have limited permanent metal removal from solution is that the metals may have formed complexes with other compounds such as dissolved organic matter (DOM) or dissolved inorganic carbon (DIC) in solution. Typically, DOM and DIC are released into solution during photosynthesis and can form metal complexes (Fallowfield and Daft 1988; Dittrich and Obst 2004; Obst et al. 2009b, Ma et al. 2018, Fan et al. 2021). The release of DOM can also occur during cell lysis after cell death. The excreted compounds become competing ligands to the functional groups found in the EPS and cellular wall, and can reduce metal toxicity by binding to the excess metal in solution (Engel et al. 2004; Bishop et al. 2019, Loudermilk and Dixon 2024). As a result, this process may explain the high dissolved metal concentrations measured in the later stages of the experiment. While this study did not measure DOM or alkalinity produced by *S. leopoliensis*, this would be of interest for understanding the role of these compounds in maximizing metal removal by cyanobacteria.

Maximum biosorption of cobalt and nickel typically occurred in the first 3 days of the experiments in both mono-metal and di-metal systems regardless of nutrient availability. The curve fits of the sampled data indicate that the maximum metal removal typically occurred on day 2 in both mono-metal systems for cobalt and nickel (**Error! Reference source not found.**). N utrient deficient di-metal systems exhibited similar trends to the mono-metal systems (**Error! Reference source not found.**). However, the measured metal concentration in nutrient enriched di-metal systems indicated the maximum metal removal occurred at day 3 (**Error! Reference s ource not found.**). Additional sampling points between day 2 and day 4 would provide greater resolution in assessing the maximum metal removal by *S. leopoliensis* for both mono-metal and di-metal systems. The simulated curves from the measured nickel and cobalt concentrations indicate the potential variability in the concentrations, which would be impacted by the rates of metal sorption and desorption (**Figure 2.13, Figure 2.14**). The boundaries in the simulated cobalt curves suggest slightly greater variability compared to the simulated nickel curves (**Figure 2.13, Figure 2.14**).

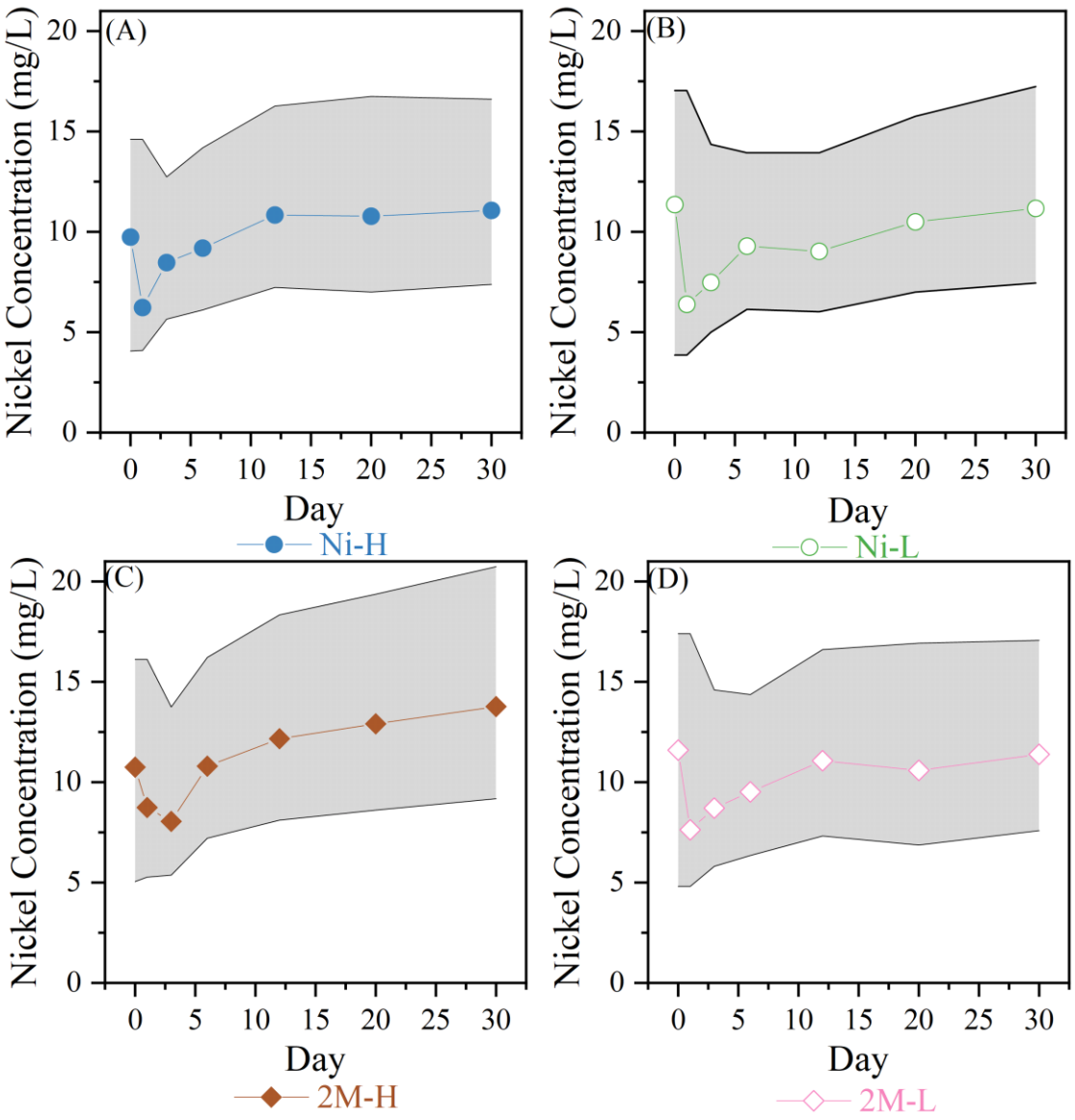


Figure 2.13. Plots showing 30 simulated curves compiled with the maximum metal removal and maximum metal release on a given day based on the measured concentration of nickel in mono-metal nutrient enriched (A) and nutrient deficient (B) systems, and di-metal nutrient enriched (C) and nutrient deficient (D) systems.

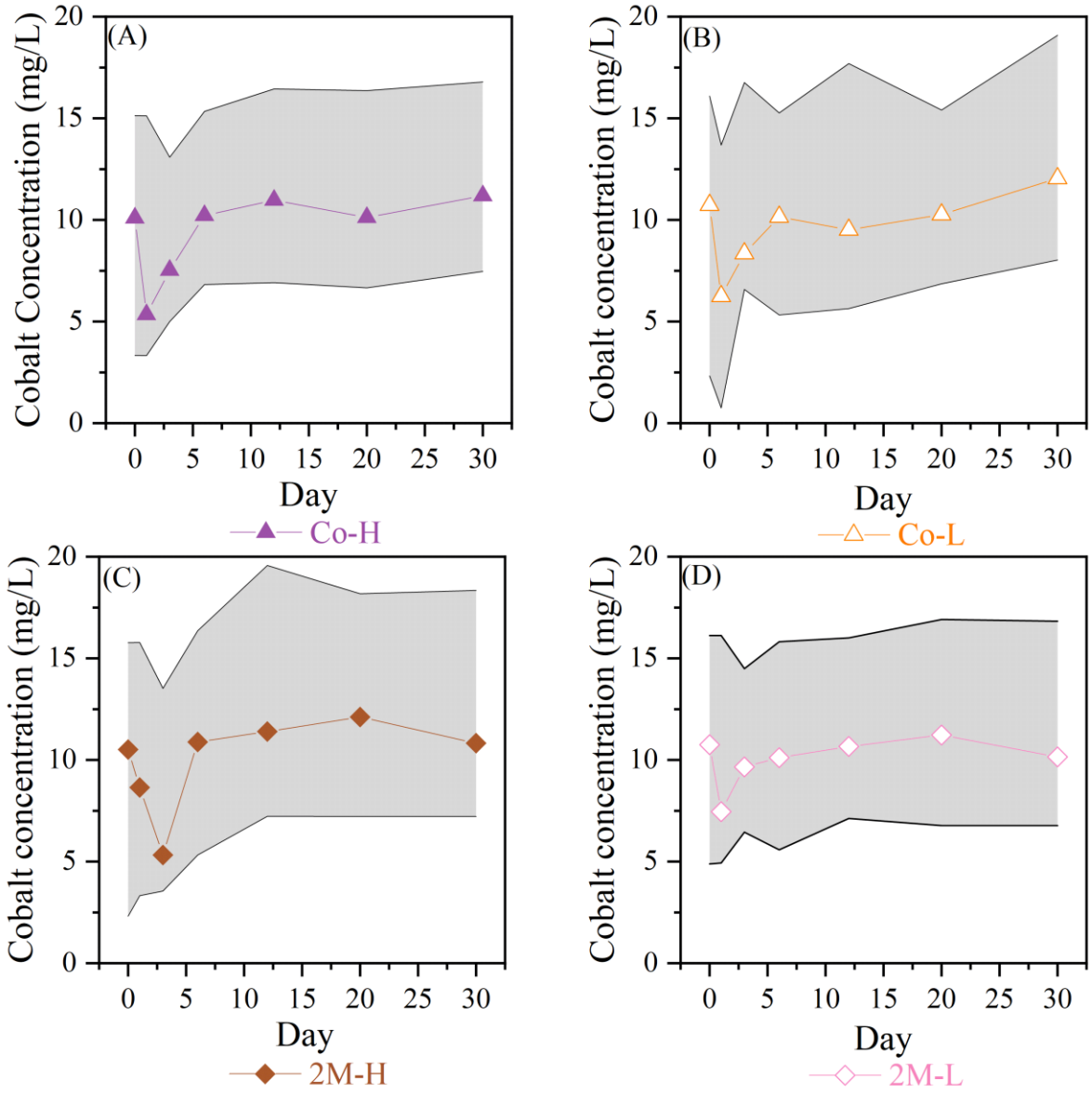


Figure 2.14. Plots showing 30 simulated curves compiled with its maximum metal removal and maximum metal release as boundaries based on measured cobalt concentrations. The filled areas indicate the potential concentration in mono-metal nutrient enriched (A), mono metal and nutrient deficient (B) systems, and di-metal nutrient enriched (C) and nutrient deficient (D) systems.

The impact of nickel and cobalt on cyanobacterial strains is well documented as elevated concentrations can exhibit different sensitivity that can impair cellular functions (Azeez and Banerjee 1991; Muyseen et al. 2004; Balaji et al. 2014; Martinez-Ruis and Martinez Jeronimo 2015; Martinez-Ruis and Martinez Jeronimo 2016, Bishop et al. 2019, Fawzy et al 2020; Facey et al.2022). The decrease in the dissolved oxygen, pH and cell density suggests a portion of the

cyanobacteria may have exhibited cellular death. In addition, the observed increase in nitrate and phosphate concentrations in the solution over the course of the experiment can be attributed to the gradual decomposition of cyanobacterial cells. The toxicity of Ni^{2+} and Co^{2+} at a concentration of 10 mg/L has been documented as harmful to cyanobacteria (Selim & Haffner 2020; Fawzy et al. 2022), resulting in the release of nutrients such as nitrate and phosphate into solution (Chuai et al. 2011; Zhang et al. 2020). The decomposition and the death of cyanobacterial cells would impact the cell density, which was observed in decreasing after reaching results in a reduction in cell density, which directly impacts in the decline observed in both pH and D.O. after the maximum biosorption was achieved. However, this study did not conduct trypan blue staining to determine the ratio of dead to live cells (Cheng et al. 2019). Therefore, the limitation of the study exists and will need further investigation kinetics and specific interactions of the cyanobacteria in the elevated metal environment.

2.4.2 Impact of low nutrient environments

Cyanobacteria in nutrient deficient environments can adapt cell structures (e.g., phospholipid membranes) to scavenge for phosphorus to maintain growth (Van Mooy et al. 2009). Cyanobacteria grown in nitrogen limited environments often exhibit higher concentrations of EPS compared to nitrogen-rich environments (Qian et al. 2022), which was observed by SEM in the present study. Studies have also shown a greater amount of EPS being produced by cyanobacteria during the stationary phase of growth, which was likely achieved partway through this study (Otero and Vincenzini 2003; Qian et al. 2022). Inducing nutrient limitations can aid cells in reducing the potential toxic effects of the metals in solution (Duan et al. 2023). Inducing nutrient limitations increased nickel removal compared to the nutrient enriched conditions. By comparing the results of the mono-metal and di-metal systems suggests that adding multiple metal species can induce additional stress into the system, causing an increase in the production of EPS, and therefore allowing more ligands (e.g., carboxyl) to be available to bind metals (Ozturk et al. 2014; Bishop et al. 2019).

The production of EPS, as described above, can impact nutrient cycling, with EPS providing a means of accumulating phosphorus from solution. The retention of phosphorus could be achieved by being bound to functional groups in the EPS (Konhausser 2007; Zhou et al. 2017; Duan et al. 2022). Furthermore, phosphorus concentrations could potentially increase as a result of polyphosphate found within the cyanobacteria. Previous studies have shown that nutrient

deficient environments or the presence of metals can enhance extracellular polyphosphate (Jensen et al. 1982; Singh et al 1992; Duan et al. 2023). Raman spectroscopy results showed peaks present around 1234 cm^{-1} and 1415 cm^{-1} in both the 2-M and Ni-doped samples, which indicate the vibrations of νP=O bonds. As a result, biosorption throughout the experiment may have been impacted by metal-polyphosphate complexes forming in the EPS.

2.4.3 Implication for ultramafic mine operations

Cyanobacteria are prevalent within ultramafic mine sites (Koner 2017, Lu et al. 2017), with potential applications as a bioremediation tool (McCutcheon et al. 2017). The industrial application of photobioreactors in ultramafic mine sites still require further development (McCutcheon et al. 2019; Jones et al. 2023b), and this study demonstrates the possible applications to metal recovery in addition to the carbon sequestration purposes previously studied. A two-stage bioreactor using leached material containing *S. leopoliensis* could remove metals from solution, and release the metals of interest within 24 hours in a multi-metal environment. Therefore, *S. leopoliensis* can act as a cation trap for metals of interest (Baselga-Cervera et al. 2018). The addition of BG-11 to a photobioreactor would be necessary as ultramafic mine sites exhibit low nitrate and phosphate concentrations (McCutcheon et al. 2017; Paulo et al. 2023). Therefore, utilizing native strains of cyanobacteria may be better suited to adapting to the low nutrient environment and yield greater metal removal from solution. This can be an attractive solution for passive recovery of metals of interest while lowering the operation cost compared to traditional remediation methods. This study showed *S. leopoliensis* can still remove up to 30.6% and 34.2% for Co and Ni, respectively, in nutrient depleted environments. Further optimization may enhance the recovery of metals (e.g., Ni^{2+}) by modifying the pH or temperature. Therefore, further optimization of a photobioreactor would be of interest, including identifying optimal cyanobacteria strains to target the immobilization of different metals of interest.

2.5 Conclusions

Biosorption of cobalt and nickel remains of interest as a tool for concentrating metals from mine waste waters, as biotechnology can be a sustainable, low-cost method enhancing for metal recovery. In this study, the removal of nickel and cobalt within solution was typically achieved within the first 72 hours of the experiment. However, the concentration of nickel and cobalt at 10 mg/L may have impeded the growth and became toxic to S. *leopoliensis*, which

hindered metal removal in solution. Imposing the nutrient limitation and adding additional metals can enhance the removal of a targeted metal from the solution. Additional research will be necessary for large scale implementation of microbially metal recovery as a technology for use at sustainable mining operations.

Chapter 3 Preliminary Investigation of Critical Metal Incorporation during Biotic Carbonate Mineral Precipitation

3.1 Introduction:

Atmospheric CO_2 is an environmental concern that is contributing to climate change, which in turn is resulting in an increased frequency of forest fires, and biodiversity and habitat loss (IPCC 2018; IPCC 2021). Typically, natural CO_2 sequestration in soils, forests, and oceans offsets CO_2 emissions, but these processes are slow compared to the current increase in atmospheric CO_2 concentrations caused by anthropogenic emissions (Smith et al. 2016, Bowman et al. 2020). This growing concern has led multiple nations and governmental agencies to focus on developing carbon capture technology to lower net global carbon emissions and temperature (IPCC 2022; Natural Resources Canada 2023).

Geological carbon sequestration (GCS) is a method of storing CO_2 in geological reservoirs, including deep saline aquifers, ultramafic subsurface lithologies, and mining waste (Leung et al. 2014; Dai et al. 2020). Many GCS processes produce carbonate mineral precipitates from solution as a stable form of long-term carbon storage, referred to as enhanced weathering and mineralization (EWM) (Wilson et al. 2009; McCutcheon et al. 2016; Power et al. 2024). The selection of suitable sites for carbonate mineral precipitation for GCS involves identifying sites with cations and carbon sources available in high abundances (Dai et al. 2020; Jones et al. 2023b). Nations such as Iceland, Oman, Australia, and Canada all host locations suitable for GCS, with Iceland being home to successful, large-scale CGS implementation (Alfredsson et al. 2013; Gras et al. 2020, Al-kindi 2024).

Geological carbon sequestration sites are typically hosted in ultramafic to mafic terranes because these lithologies weather to produce alkaline leachates rich in divalent cations that can participate in carbonate mineral precipitation reactions (Stanfield et al. 2024). Typically, waters in mafic mine environments have elevated dissolved Ca^{2+}concentrations, with leachates containing 10 to 1000 mg/L calcium (Power et al. 2009; Muhammed et al. 2010; Gras et al. 2020, Wang et al. 2024). Carbon sequestration can occur in both in-situ and ex-situ geological settings where the physiochemical parameters of the environment dictate the mineral formation products (Diloreto et al. 2023). For example, formation of Ca-carbonate minerals (calcite ($CaCO_3$), aragonite ($CaCO_3$), vaterite ($CaCO_3$)) or Mg-carbonate minerals (magnesite ($MgCO_3$), hydromagnesite ($Mg_5(CO_3)_4(OH)_2 \cdot 4H_2O$), dypingite ($Mg_5(CO_3)_4(OH)_2 \cdot 5H_2O$), nesquehonite

($MgCO_3 \cdot 3H_2O$)) are determined by temperature, pH, alkalinity, and the respective availability of Ca^{2+} and Mg^{2+} cations (Blue et al. 2017; Chang et al. 2017, Turvey et al. 2018; McCutcheon et al. 2019; Khajani et al. 2021; Cheng et al. 2024). When dissolved in water, CO_2 forms carbonic acid (H_2CO_3) that can be used to generate alkalinity as bicarbonate (HCO_3^-) and carbonate (CO_3^{2-}) anions (Liu et al. 2013; Dai et al. 2020). The generated alkalinity can be used in carbonate mineralization reactions depending on kinetics and the abundance of divalent cations (Dai et al. 2020).

During the process of EWM, the dissolution products of enhanced mineral weathering react with atmospheric CO_2 to form secondary carbonate minerals (Power et al. 2024). The enhanced weathering of minerals is of interest because it reduces net CO_2 emissions naturally with no need of subsurface injection (Alfredsson et al. 2013; Gras et al.2020; Power et al. 2021). It is possible to use ultramafic and mafic mine tailings, residues, and mineral wastes as carbonate sinks through abiotic mineral weathering reactions that consume CO_2 from the atmosphere (Power et al. 2014, Turvey et al. 2018; Gras et al. 2020; Jones et al. 2023b). Extensive research has shown that historic mines and current mine operations are suitable sites for GCS via EWM and provide secondary value by being used for carbon sequestration projects (McCutcheon et al. 2016; Hamilton et al. 2018; Jones et al. 2023a).

In addition to the divalent cations required for carbonation reactions, alkaline mine waste materials contain recoverable trace concentrations of critical metals (Hamilton et al. 2016; Hamilton et al. 2018; Gras et al. 2020; Khudhur et al. 2022; Zeyen et al. 2022; Wang et al. 2024). The trace concentrations of these metals can become precious over time as the number of high-grade ore deposits is decreasing (Mudd and Jolwitt 2014; Wilson and Hamilton 2022). Currently, mining waste rock and tailings is challenging because it is not economically viable to extract trace metals from these materials using traditional methods (Hamilton et al. 2018; Henne et al. 2020). However, metal recovery can be paired with mineral carbonation through sequential precipitation using the pH swing method (Hamilton et al. 2020; Wilson and Hamilton 2022). In this process, leachates produced during enhanced weathering of ultramafic and mafic waste materials are used to first precipitate the metals (e.g., nickel) as sulfide minerals, followed by secondary carbonate mineral precipitation (Wang et al. 2021; Wang and Dreisinger 2022). Therefore, mine operations are incentivized to implement carbon sequestration, with the aim of becoming more environmentally sustainable.

Biotic and abiotic processes can impact metal mobility by accelerating the weathering of primary minerals to form secondary minerals (Gillispie et al. 2017; Hamilton et al. 2018; Henne et al. 2018). Previous research indicates critical metal enrichment can occur by ionic exchange between minerals (carbonate and hematite) and the aqueous solution (Drake et al. 2018; Scullet-Dean et al. 2023). At historic mine sites in ultramafic and mafic terranes, transition metals including nickel, cobalt, and chromium, are passively attenuated into Mg-carbonate minerals (Hamilton et al. 2016; Hamilton et al. 2018). While this provides a method of concentrating metals and limiting metal mobility from mine sites, metal recovery would require dissolving the carbonate minerals, thereby re-emitting the captured CO_2 (McCutcheon et al. 2017). As such, a better understanding of transition metal incorporation into the secondary minerals that form at mine sites is needed.

Microorganisms can accelerate mineral weathering and induce mineral precipitation reactions in both natural and anthropogenic environments (Jansson and Norhten 2010; McCutcheon et al. 2014; McCutcheon et al. 2016; Dong et al. 2022; Jones et al. 2023a). Extensive research has shown that cyanobacteria can precipitate Ca- and Mg-carbonate minerals on their cell exteriors and extracellular polymeric substances (EPS) (Obst et al. 2005; Obst et al. 2009a; Obst et al. 2009b; McCutcheon et al. 2014, Shiraishi et al. 2020). Nucleation occurs when Ca^{2+} bound to ligands, either on the cellular wall or in the EPS, results in supersaturation conditions and nucleation of calcite crystals (Dittrich and Sibler 2006; Obst et al. 2009b; Shiraishi 2012; Gérard et al. 2013). Typically, calcite crystals start forming after 24 hours on the surface of the cell and the excreted EPS (Obst et al. 2009b).

Cyanobacteria are abundant in ultramafic and mafic mine settings and their abundance depends on in the depth of the tailing profile (Koner et al. 2022; Lu et al. 2022). Cyanobacteria can contribute to carbonate mineral precipitation and cementation of mineral grains in mine tailings, thereby solidifying and stabilizing the tailings (McCutcheon et al. 2016; McCutcheon et al. 2017). *S. leopoliensis* is a cyanobacterium that has been well-studied to unravel the mechanisms and kinetics involved in carbonate mineral precipitation (Dittrich and Sibler 2006; Obst et al. 2009a, Obst et al. 2009b; Bundeleva et al. 2014). However, investigation of microbial carbonate mineral precipitation in relation to transition metals has been limited. Whether cyanobacterial strains can immobilize metals with site-specific metal incorporation during carbonate precipitation, similar to what has been observed in abiotic processes, is still in need of investigation

(Elzinga and Reeder 2002). Thus, understanding how the cyanobacteria strains that facilitate carbonate mineral nucleation and possible co-precipitation of metals is important for future application to EWM and potential metal recovery from mine tailings.

3.2 Research objective

The aim of this chapter is to conduct a preliminary experiment to explore the fate of cobalt and nickel during microbially induced carbonate mineral precipitation by S. *leopoliensis.* The biomass and mineral precipitates will be characterized using scanning electron microscopy and Raman spectroscopy. The expectation is that microbially induced carbonate mineral precipitation will occur, with trace concentrations of critical metals being incorporated into calcite produced. The preliminary findings will be used to assess the suitability of S. *leopoliensis* for use in microbially mediated EWM and metal recovery.

3.3 Methods:

3.3.1 Bacterial Strain and culture conditions:

The same strain of cyanobacteria, *S. leopoliensis* (CPCC-102), used in the experiment presented in Chapter 2 was used for the experiment presented in this chapter. This experiment consisted of growing the cyanobacteria and inducing biogenic calcium carbon mineral precipitation in 125 mL Erlenmeyer flasks. The total solution volume of each flask was to be 65 mL. This experiment used Rippka et al. (1979)'s BG–11 medium recipe presented in Chapter 2, with modifications to reflect nutrient and calcium concentrations representative of mafic mine environments (**Table *3.1***). Nutrient concentrations were representative of mine environments: 1.65 mg/L of phosphate and 13.2 mg/L of nitrate (Nawab et al. 2017; McCutcheon et al. 2017, Paulo et al. 2023). Like the first experiment, a trace metal solution that contained HBO_3, $MnCl_2{\cdot}4H_2O$, $ZnSO_4{\cdot}7H_2O$, $Na_2MoO_4{\cdot}2H_2O$, Na_2CO_3, $CuSO_4{\cdot}5H_2O$, was added (Rippka et al. 1979). However, the addition of $CoNO_3{\cdot}6H_2O$ was excluded from the trace metal mix because it contained both cobalt and nitrate that would impact the experiment. Ni and Co were added to the experiment at concentrations of 10 mg/L, added as $NiCl_2{\cdot}6H_2O$ and $CoCl_2{\cdot}6H_2O$, respectively. Metals were added to the flasks 48 hours into the experiment, in which calcium carbonate mineral nucleation was expected to have begun nucleating (Obst et al. 2009b).

To ensure precipitation of calcite, a suitable concentration of calcium was determined based on saturation indices predicted using the PHREEQC interactive version 3.7.3.15968 (Parkhurst and Appelo 2013). Using the minteq.v4 database and the water chemistry data from the

first experiment to determine possible precipitates, a calcium concentration of 720 mg/L was selected (Parkhurst and Appelo 2013; Obst et al 2009b). The solution was prepared to account for the necessary dilution that would occur with the addition of the metal and inoculum solutions. Therefore, the BG-11 concentration was increased by a factor of 1.3, to yield a higher Ca^{2+} concentration of approximately 750 mg/L. However, a volume to volume transfer error must have occurred, resulting in a higher concentration of Ca^{2+}. A further experimental error did occur during preparation of one of the 2 L of BG–11, resulting in the cobalt and di-metal system day 3 flasks, nickel day 2 flasks, and all the abiotic control containing less calcium than intended.

Table 3.1. Quantities of ingredients in the BG-11 growth medium used in the biogenic calcite precipitation experiment. Flasks were prepared by combining 5 mL of the metal solution, 10–15 mL of cyanobacteria inoculum, and 45–50 mL BG-11 medium for the total final volume of 65 mL per flask. BG-11 medium and trace metal mix recipe from Rippka et al. 1979

Ingredient	**Quantity**
$NaNO_3$	0.0235 g
K_2HPO_4	0.0039 g
$MgSO_4 \cdot 6H_2O$	0.0975 g
$CaCl_2 \cdot 2H_2O$	3.4440 g
citric acid	0.0078 g
ferric ammonium citrate	0.0078 g
EDTA	0.0013 g
Na_2CO_3	0.026 g
Trace metal mix	1.3 mL
$CoCl_2$-$6H_2O$ (10 mg/L)	5.0 mL
$NiCl_2$-$6H_2O$ (10 mg/L)	5.0 mL
Milli-Q water	1L

The cyanobacteria were grown for 35 days in standard BG-11 medium prior to the start of the experiment. The $CaCO_3$ precipitation experiment was housed inside a Conviron GEN1000 growth chamber at a light intensity of 400-500 lux in a 12-hr day/night cycle. Sampling occurred on days 0, 1, 2, and 3, with one flask per treatment sampled on each day for water chemistry analyses.

3.3.2 Water Chemistry analyses:

Water chemistry analyses followed the procedures in Section 2.4.3. Experiment solution pH, conductivity, and DO were monitored using a the Thermo Scientific Orion Star A 329 Multiparameter Meter. Dissolved anion concentrations were measured using the Dionex 600-IC-

CO_3 system, while concentrations of dissolved cations, including Ca^{2+}, Ni^{2+} and Co^{2+} along with other metals were measured by Inductively coupled plasma-mass spectrometry (ICP-MS) following the sample preparation procedure described in Section 2.5. Total alkalinity was determined using the titration method with sulfuric acid (Hach Method 8203). The aliquot of 10 mL was filtered through a 0.45 µm polyether sulfone (PES) syringe filter before undergoing titration.

3.3.3 Scanning Electron microscopy (SEM):

Sample preparation and scanning electron microscopy were conducted as described in Section 2.4.5. SE-SEM was used to observe the experiment cultures and mineral precipitates, and EDS as used to determine the elemental composition of the precipitates.

3.3.4 Raman spectroscopy:

Raman spectroscopy followed Section 2.4.6. This method monitored the changes in functional groups, possible incorporation of the transition metals into mineral precipitates, and metal biosorption onto bacterial cell EPS' functional groups. The grating was changed to 1800 lines/mm diffraction grating to increase the spectral window (100–2000 cm^{-1}).

3.3.5 Data analysis:

Data analysis was conducted similar to the method described in Section 2.5. Raman spectra were compared to reference spectra collected from abiotic calcite, vaterite, and aragonite samples. Additional functional groups and peaks present in the Raman spectra were compared to abiotic control group spectra collected in the preliminary experiment.

3.4 Results:

3.4.1 Water Chemistry analyses:

Bulk water chemistry was monitored throughout the experiment. The pH increased and then steadily decreased amongst all the different treatments throughout the duration of the experiment (**Figure 3.1A**). The pH of the abiotic control fluctuated between 7.75 and 9.5 throughout the experiment. Di-metal, cobalt, and nickel systems exhibited similar trends in the biotic control, with an increase in the first days of the experiment to pH 9.5–10, followed by a

gradual decrease to pH 7.75–8.5 (**Figure 3.1A**). The highest recorded pH value during the experiment was 9.92 in the cobalt flask on Day 2.

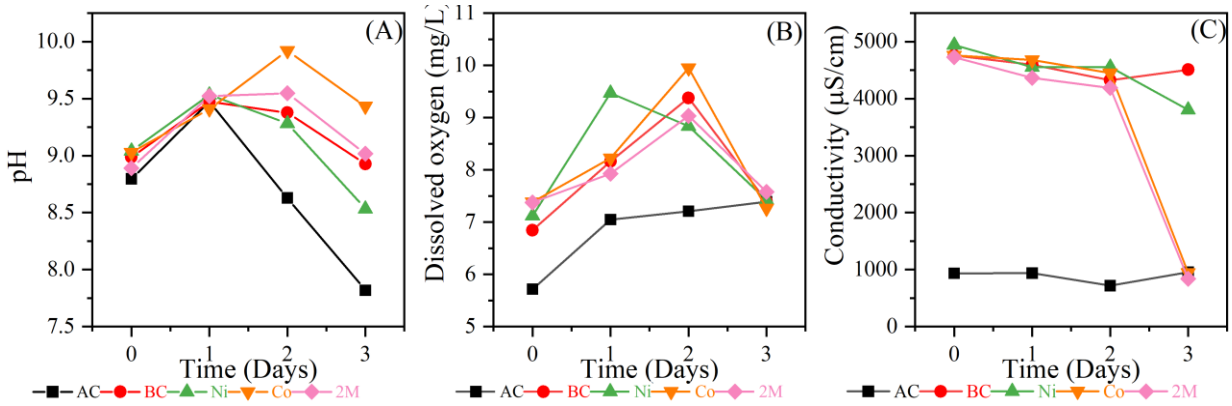


Figure 3.1. Evolution of pH (A), dissolved oxygen (B), and conductivity (C) throughout the 3 day experiment. Each enviorment condition include abiotic control (AC), biotic control (BC),Ni-doped system, Co-doped systsem (Co), and di-metal system(2M).

The DO in the abiotic control showed a gradual increase from below 6 mg/L to a final concentration of approximately 7.5 mg/L on day 3 (**Figure 3.1B**). In all biotic flasks, the DO increased from ~7 mg/L to 9-10 mg/L in the first 2 days, followed by a decrease to 7.5 mg/L on day 3. The DO in the nickel flasks exhibited this increase and decrease slightly earlier than the other flasks inoculated with *S. leopoliensis*. Of the peak DO concentrations measured on day 2, cobalt exhibited the highest DO, while the di-metal system was the lowest (**Figure 3.1B**).

The conductivity measurements were impacted by the incorrect amount of calcium added to some of the flasks during setup of the experiment, specifically, in all abiotic control flasks and the cobalt and di-metal flasks day 3 (**Figure 3.1C**). The conductivity in the biotic control remained relatively stable throughout the experiment, while the conductivity in the nickel flask decreased and then remained relatively stable for the rest of the experiment.

The measured nitrate concentration decreased over time until an eventual plateau was reached in most flasks (**Figure 3.2A**). The nitrate concentration in the abiotic control remained consistently low. The nitrate concentration in flasks containing *S. leopoliensis*, including the biotic control, decreased by approximately 30% during on the first 2 days of the experiment. After the initial decline, the nitrate concentration in the biotic control, cobalt, and di-metal systems plateaued (**Figure 3.2A**).

Dissolved phosphorus was measured as both phosphate and total dissolved elemental phosphorus concentrations; however, the measured phosphate was mostly < 0.4 mg/L throughout the experiment and therefore was not quantified or included in the figure below. The phosphorus concentration decreased in all flasks by Day 1 of the experiment and remained below 1 mg/L in all systems (**Figure 3.2B**).

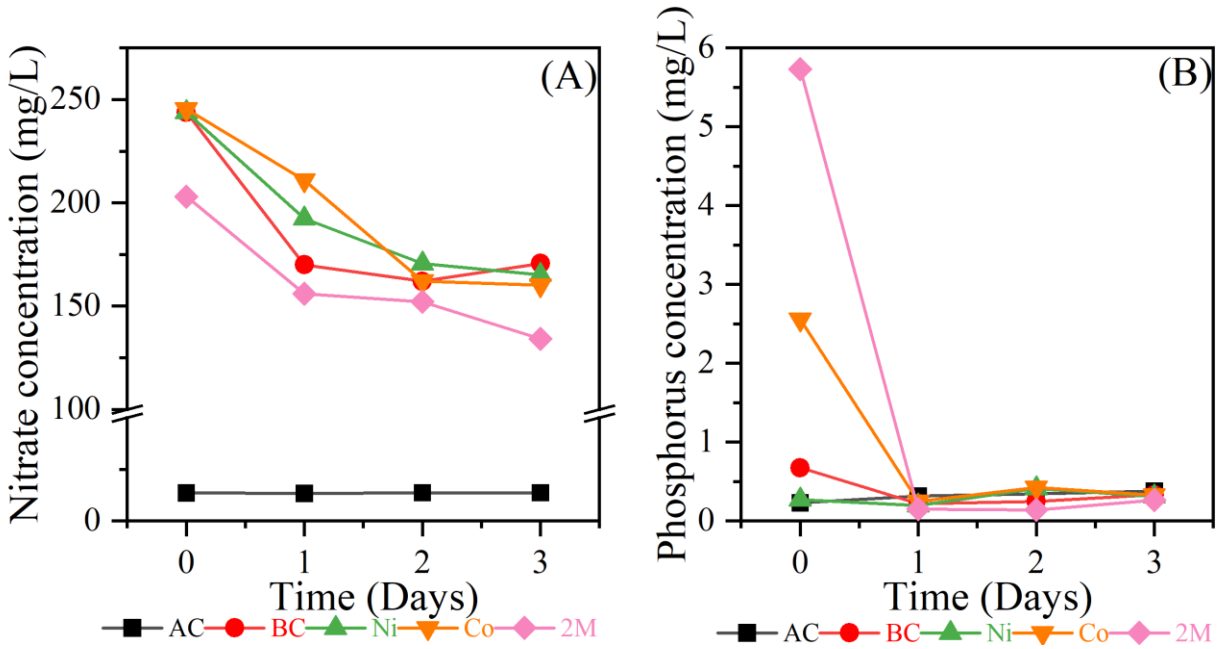


Figure 3.2. Nitrate (A) and Phosphorus (B) concentrations measured in mg/L throughout the experiment.

The measured alkalinity increased throughout the experiment in all biotic flasks, while the alkalinity in the abiotic control group was lower than the biotic flasks, with alkalinity as $CaCO_3$ increasing up to 43 mg/L by the end of the experiment (**Figure 3.3A**). Similarly, the alkalinity gradually increased up to 100 mg/L of $CaCO_3$ by the end of the experiment in the biotic control (**Figure 3.3B**). The alkalinity in the nickel, cobalt and di-metal system increased in most of the flasks (**Figure 3.3C-D**).

With respect to the concentration of calcium, the data for the abiotic, nickel, cobalt, and di-metal flasks were impacted by the incorrect concentration of calcium added to certain flasks. The reduced calcium concentrations in the abiotic flasks showed little change except for a decrease on day 2, followed by an increase on day 3 (**Figure 3.3A**). The concentration of calcium in the biotic control decreased between day 0 and 3 (**Figure 3.3B**). The calcium concentration in the nickel flasks decreased slightly over time (**Figure 3.3C**). The cobalt flask

indicated a decline in calcium decrease over the 48 hours of the experiment (**Figure 3.3D**). The di-metal system showed a steady decrease in calcium in the first 48 hours (**Figure 3.3E).** The anomalously low concentrations of calcium in the nickel (day 2) and cobalt and di-metal (day 3) systems were due to the incorrect concentration of calcium being added to the flasks and should be disregarded (**Figure 3.3C-E**).

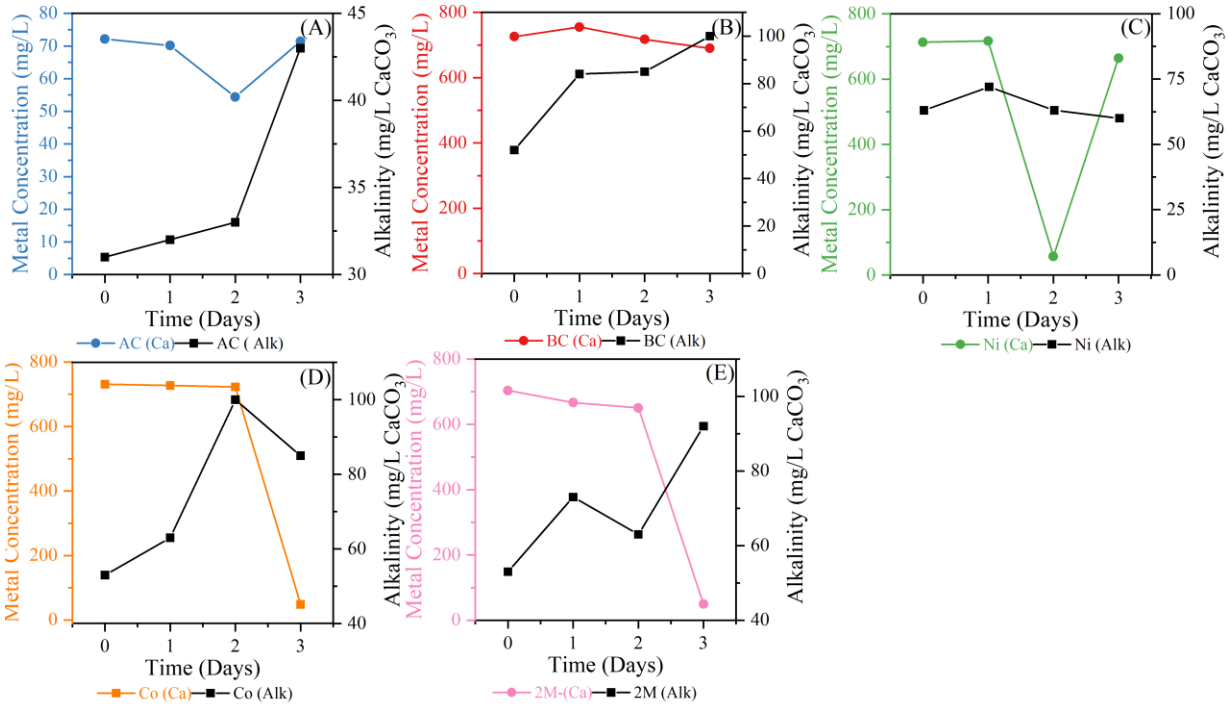


Figure 3.3. Alkalinity concentrations reported as mg/L $CaCO_3$, and Ca concentrations (mg/L) over the 3-day experiment in the abiotic (A), biotic (B), nickel (C), cobalt (D), and di-metal systems (E).

After 24 hours of the metals being introduced, the nickel concentration in both the mono-metal and di-metal systems decreased. The initial metal concentrations were not measured; however, nickel and cobalt were added to achieve starting concentrations of 10 mg/L. The amount of nickel remaining in the mono-metal and di-metal systems after 24 hours differed from each other (**Table 3.2**). With the assumption that 10 mg/L was introduced into each system, the di-metal system showed over 94.5% nickel removal after 24 hours. Meanwhile, the mono-metal system achieved 17.4% nickel removal in the same timeframe. The cobalt mono-metal and di-

metal systems exhibited 81.9% and 89.5% cobalt removal after 24 hours, respectively (**Table 3.2**).

Table 3.2. Co and Ni removal efficiency in the 24 hours after metal addition. Metals were added on day 2 of the experiment, with the dissolved metal concentrations measured on day 3 used to calculate removal (%).

Sample	**System** =	Metal Removal (%)
Co	Mono-metal	81.2
Co	Di-metal	89.5
Ni	Mono-metal	17.4
Ni	Di-metal	94.5

3.5 Scanning electron microscopy-energy dispersive spectroscopy:

The abiotic flasks precipitated a crystalline mineral phase within the first 24 hours of the experiment (**Figure 3.4A)**. In the biotic flasks with and without metals, the amount of EPS produced by *S. leopoliensis* increased with time. Trace amounts of calcium was detected by EDS (**Error! Reference source not found.**). On the first day, the amorphous calcite carbonate (ACC) n anoparticles began surrounding *S. leopoliensis* in all flasks, which can be confirmed by the presence of calcium ions (**Table 3.3, Figure 3.4A, C,E,G,I**). Trace amounts of Ni and Co were detected by EDS in all the metal-doped flasks. It is important to note that the di-metal system had relative similar concentrations of Ni and Co compared to the mono-metal systems.

Table 3.3. The average elemental composition (atomic%) of samples observed using SE-SEM, as measured using EDS.

		Atomic (%)						
	Day	C	N	O	Si	Ca	Co	Ni
AC (n=4)	1	53.0		39.3		7.7		
BC (n=5)	1	66.7	14.7	17.4	0.4	0.7		
Ni (n=8)	1	67.3	12.7	17.1	2.0	0.9		

Co (n=2)	1	66.8	12.4	18.5	1.8	0.5		
2M (n=9)	1	62.4	7.5	23.3	5.9	1.7		
AC (n=2)	3	85		14.2		0.8		
BC (n=11)	3	73.8	16.7	15.5	0.8	0.4		
Ni (n=3)	3	59.3	13.4	22.9	3.8	0.4		0.1
Co (n=2)	3	72.5	12.6	13.7	0.4	0.5	0.2	
2M (n=15)	3	68.1	14.8	15.8	0.6	0.5	0.1	0.1

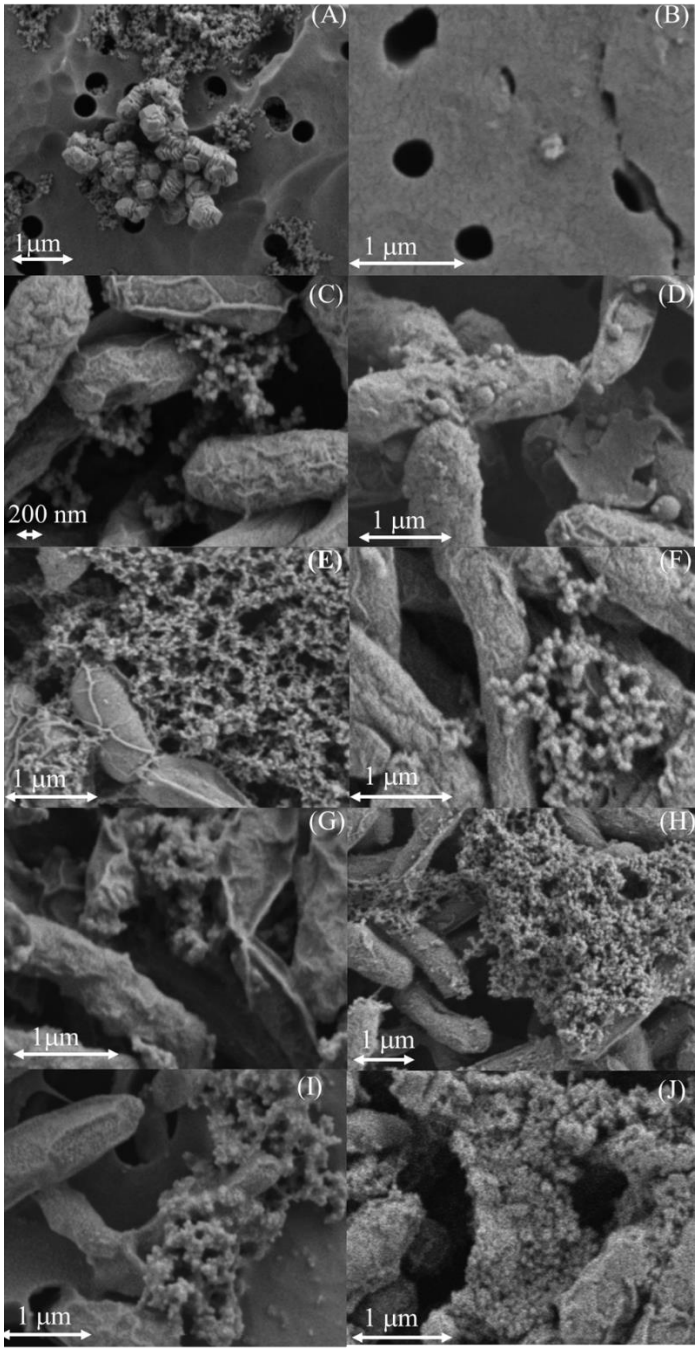


Figure 3.4. SEM micrographs of precipitation products in each condition including abiotic control group (A,B), biotic control group (C,D), nickel (E,F), cobalt (G,H) and both metals present (I,J). For each treatment, the displayed micrographs show samples collected on day 1(A, C, E, G, I), and day 3 (B, D, F, H).

3.5.1 Raman Spectroscopy:

Raman data was measured on cyanobacteria samples from day 1 and day 3 to observe any vibrations, including functional groups and signs of calcite and its polymorphs. The biotic control and abiotic control exhibited identical characteristic peaks (**Figure 3.5**). There are distinct peaks at 1075 cm-1 and 1090 cm-1 in the biotic control group, which are indicative of vaterite (Behrens et al. 1995, Wehrmeister et al. 2010). A distinct peak was present around 1086 cm^{-1}in the biotic control group on day 1 but was absent on day 3 (**Figure 3.6**). Functional groups that were present in the biotic control groups on both days included amide (I) and amide (III) bands (Yee et al.2003; Dittrich and Sibbler 2006; Liu et al. 2015). Carboxyl vibration was also present on day 3 in the biotic control group (Yee et al.2003; Dittrich and Sibbler 2006; Liu et al. 2015) (**Figure 3.7**).

The added transition metals can cause shifts in the vaterite peaks (**Figure 3.7**). The exposure of nickel shifted the vaterite peaks to 1080 cm^{-1}, 1088 cm^{-1} and 1092 cm^{-1}compared to the typical vaterite peaks at 1075 cm^{-1}, 1085 cm^{-1}, and 1090 cm^{-1} (Behrens et al. 1995, Wehrmeister et al. 2010). Cobalt doped samples similarly showed peak shifts, with peaks at 1088 $cm^{-1}$and 1093 cm^{-1}. The di-metal system showed a peak shift to 1095 cm^{-1}, however, the peak at 1075 $cm^{-1}$was not present at all. In addition, different functional groups vibrated because of the added transition metals. The di-metal doped samples vibrated a peak at 1555 cm^{-1}, which was assigned to an amide (II) vibration that was absent in both the biotic control group and the mono-metal systems (Yee et al.2003; Dittrich and Sibbler 2006; Liu et al. 2015). The presence of cobalt resulted in carboxyl vibrations in both mono-metal and di-metal system in 1739 cm^{-1} and 1738 cm^{-1}, respectively (Yee et al.2003; Dittrich and Sibbler 2006; Liu et al. 2015). Similarly, both mono-metal and di-metal systems containing nickel showed an amide (I) band at 1653 $cm^{-1}$and 1650 cm^{-1}, respectively (Yee et al.2003; Dittrich and Sibbler 2006; Liu et al. 2015).

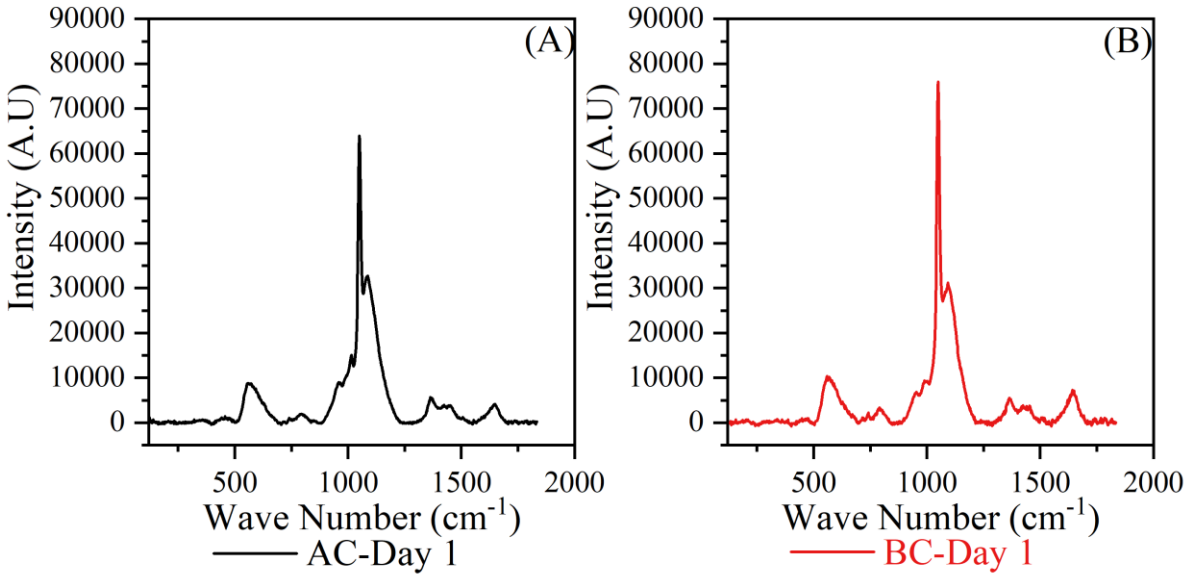


Figure 3.5. Raman spectroscopy spectra of precipitates in the abiotic (A) and biotic (B) control groups on day 1 of the experiment. Both the abiotic and biotic control group exhibit similar spectra shape to one another.

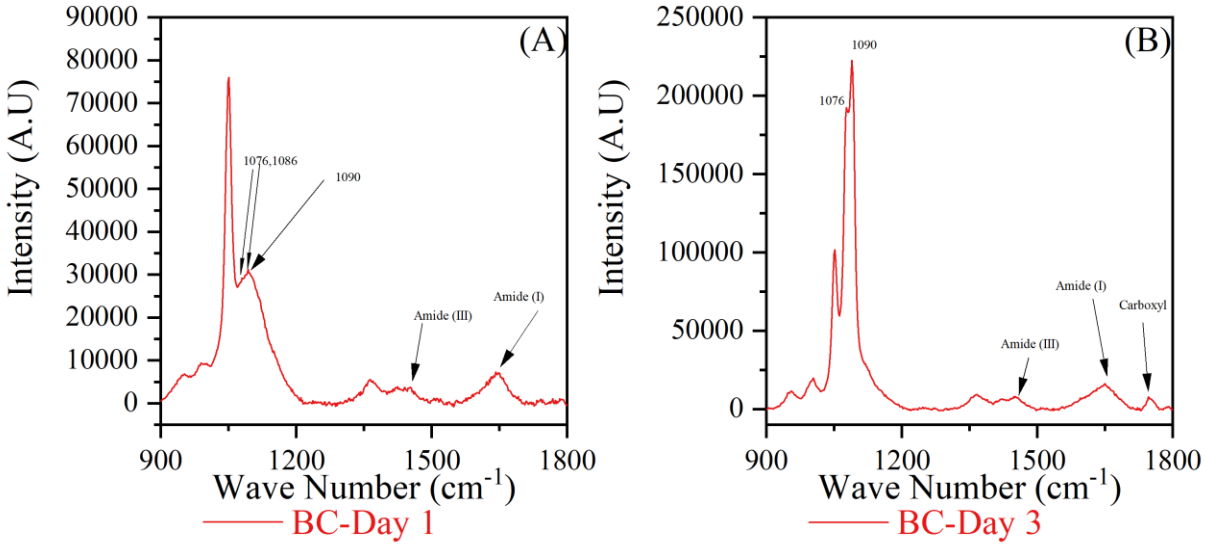


Figure 3.6. Raman spectra of the biotic control samples comprising cells, EPS, and associated precipitates on day 1 (A) and day 3 (B).

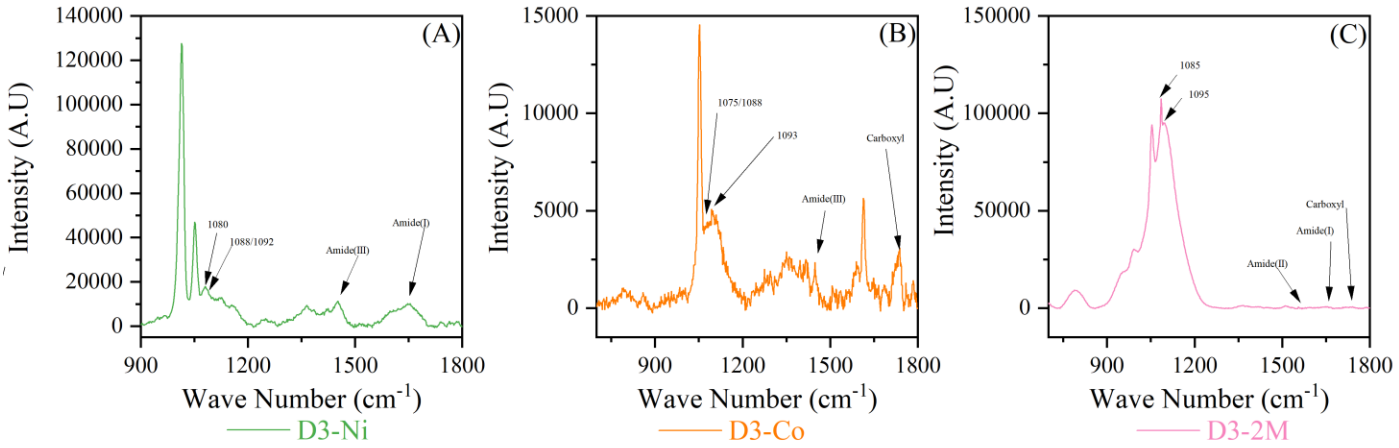


Figure 3.7 Raman spectra collected on day 3 in the Ni (A), Co (B) and di-metal (C) samples that contain cells, EPS and the precipitates. Peaks are labeled to indicate vaterite peaks and notable functional groups identified in the spectra.

3.6 Discussion

3.6.1 Biogenic calcium carbonate mineral precipitation:

Cyanobacteria photosynthesis can induce carbonate precipitation by generating alkalinity during photosynthesis (Thompson and Ferris 1988; Obst et al. 2009b). This 72-hour long study showed successful precipitation of amorphous calcium carbonates (ACC) based on the SEM results, despite being in a nutrient limited environment (**Figure 3.4**C-D). This study did not show any precipitation of crystalline biogenic calcite, such as has been observed in previous studies (Obst et al. 2009b; Shiraishi et al. 2020). It would be beneficial to conduct a long-term study, to fully understand the growth of calcium carbonate minerals under the influence of a nutrient limited environment.

The addition of metals may have induced additional excretion of EPS from the cells, which could provide additional nucleation sites for ACC to form (Pereira et al. 2011, Obst et al. 2009a; Shiraishi et al. 2020). Although Raman spectroscopy indicated some calcium carbonate being present, these preliminary results showed vaterite. Since no crystalline calcium carbonate precipitates were observed in the SEM samples, the formation of vaterite may have been because of sample drying prior to conducting the Raman measurements. This suggests that the precipitates observed were most likely not precipitated by *S. leopoliensis*. To overcome this challenge, a combination of cell washing, filtering and vacuum drying may reduce unintentional precipitation from the bulk solution (Zhu et al 2018; Yu et al. 2020).

The nickel and cobalt were metals of interest in this study for their economic value and presence in ultramafic and mafic mine sites. The nickel and cobalt concentrations were not measured during the initial nucleation of experiment on day 2, which would provide a starting concentration of both metals before the decrease observed in the metal. This was followed by a proportion of both metals being released into solution, with some retention of the both nickel and cobalt by the biomass in both the mono-metal and di-metal systems. This retention of the metals likely occurred in the EPS produced by *S. leopoliensis*, which likely included the functional groups identified in the Raman spectroscopy (Pereira et al. 2021). Besides binding of metals to the EPS material, the metals removed from solution may have been incorporated into the ACC precipitates that were observed, (Lakshtanov and Stipp 2007; Katsikopoulos et al. 2008) or bound through surface complexation to these precipitates (González -López et al. 2017; Castillo Alvarez et al. 2020). The small ACC precipitates may have contained trace amounts of transition metals (**Figure 3.4**). Further studies and additional analysis will be necessary to better understand how transition metals in solution influence the structure of carbonate mineral precipitates formed biologically.

3.6.2 Implications of ultramafic mine environment:

Previous studies have used different cyanobacteria strains and mine site starting materials to test enhanced weathering for possible CO_2 storage in Ca-carbonate or Mg-carbonate minerals (McCutcheon et al. 2016; Jones et al. 2023a). This study only showed the precipitation of ACC in the first 72 hours, instead of crystalline carbonate phases. A longer-term experiment would enable a better characterization of the kinetics and possible involvement by cyanobacteria in the precipitation of carbonate minerals under nutrient limited conditions. Identification of specific cyanobacteria strains that can precipitate stable carbonate phases under nutrient limited conditions would have application to sequestering atmospheric CO_2 in photobioreactors. This is essential to transition from laboratory studies to application in industry.

This study showed potential applications to metal remediation through the successful immobilization of cobalt and nickel from solution. Previous studies have predominantly focused on ureolytic bacteria to immobilize metals (Qiao et al. 2021; Bai et al. 2021), however, these studies showed similar result using photosynthetic bacteria such as *S. leopoliensis*. *S. leopoliensis* indicating these microbes immobilize Co^{2+} and Ni^{2+} within the first 24 hours (Table 3.2). Ureolytic bacteria exhibited similar functionality with various degrees of success, ranging

from 59.46–99.99% metal removal within the first 12 hours of metals added into their respective environments (Qiao et al. 2021; Zhang et al. 2019). While significant retention and immobilization by ureolytic bacteria has been observed in calcium-rich environment, the studies have also shown the eventual re-release of metals (Zeng et al. 2021). For this purpose, further investigation using cyanobacteria to determine any possible re-release of transition metals over an extended period will be vital for future application in the mining industry.

Optimizing carbonate mineral precipitation and the incorporation of metals has applications as an additional carbonation step after acid leaching of ultramafic mine tailings would be a possible method for rapid removal and retention of metals from the waste material (Hamilton and Wilson 2020; Wang et al. 2023). This could be achieved using a multi-stage bioreactor where, after acid leaching, mineral carbonation is used to immobilize the critical metals and allow metal enrichment over an extended period by abiotic (Hamilton et al. 2018; Zhang et al. 2020) or biotic incorporation into carbonates (He et al.2022; Zhao et al. 2023) by constant dissolution and reprecipitation in an engineered environment. Using microbial carbonation in this manner may be a cost-effective solution while addressing multiple environmental challenges including offsetting CO_2 and potential sinks of hazardous materials.

3.7 Conclusion:

The measured nickel and cobalt concentrations over the duration of the study suggest immobilization through biosorption to EPS. SEM-EDS indicated precipitation of ACC by *S. leopoliensis* in the presence of cobalt and nickel. The nucleated precipitates were nanometer-scale in size, and were largely amorphous. Immobilization of cobalt and nickel was observed, with up to 89.5% and 94.5% removed by some combination of co-precipitation, biosorption, and surface complexation. This study provides preliminary insights into transition metal incorporation into biogenic ACC and is a step towards creating new methods to remediate and recover metals from mafic and ultramafic mine environments.

Chapter 4 Conclusion:

4.1 Summary of Findings:

The mining industry has an opportunity to become more environmentally sustainable as the global reliance on critical metals continues to increase. Previous research has explored a variety of ways to implement carbon capture technologies in different mine waste materials. Specifically, there is growing interest in the utilization of mine waste materials to reduce emissions from mine sites through the drawdown of atmospheric carbon dioxide (Power et al. 2014; McCutcheon and Power 2023). Additionally, mine waste materials typically contain trace concentrations of metals (Hamilton et al. 2018), and mineral carbonation has been proposed as a potential tool to recover and immobilize metals of interest (Wilson and Hamilton 2020). Bioremediation can serve as a tool for immobilization of metals through biosorption and could be used for the recovery of metals in later stages of processing. Results from this thesis contribute to the understanding of biosorption of nickel and cobalt by *S. leopoliensis*, and the fate of metals during biogenic carbonate precipitation, which have applications to metal recovery from ultramafic mine materials.

Chapter 2, Biosorption of Critical Metals in a Simulated Ultramafic Mine Site, investigated a lab grown strain of cyanobacteria, *S. leopoliensis*, and its ability to adsorb nickel and cobalt from solution in a simulated ultramafic mine solution. *S. leopoliensis* was grown in nutrient deficient and enriched solutions with the addition of 10 mg/L of Ni and Co, added as individual metals or both metals together. Aqueous samples were filtered and collected to determine the concentration of cations (Co^2, Ni^{2+}) and anions (NO_3^-, PO_4^-) of interest for 30 days. Imposing nutrient limitation to the cyanobacteria, to increase EPS production, resulted in enhanced metal removal. The increased production of EPS was observed using microscopy, and the aqueous geochemistry measurements indicated an extent of cobalt and nickel removal reaching up to 30% under nutrient deficient conditions. Raman spectroscopy measurements of the experimental cultures identified both Ni-O and Co-O bonds. This suggests the presence of metal-oxygen complexes, which may have formed by metals being bound to functional groups in the cellular wall and surrounding EPS. These metal-oxygen complexes may have contributed to the reduced dissolved metal concentrations measured in the experimental solutions. *S. leopoliensis* removed metals from solution within 72 hours in the nutrient limited environment (e.g. ultramafic mine sites), indicating this process is rapid in reducing aqueous metal

concentrations. However, consideration needs to be given to the stability of the bound metals, because the observed desorption would impede any meaningful remediation. Further investigation will be necessary to optimize this biosorption process for industrial applications in ultramafic and mafic mining operations.

The aim of Chapter 3, Immobilization of Critical Metals during Biotic Mineral Precipitation, was to conduct a preliminary study targeting the incorporation of critical metals into biogenic calcium carbonate minerals. *S. leopoliensis* was grown in nutrient deficient conditions for 48 hours, after which 10 mg/L of Co^{2+} and Ni^{2+} were added as individual metals or both metals together. Alkalinity was generated in all flasks containing the cyanobacteria due to photosynthesis. SEM results showed *S. leopoliensis* cells produced EPS to which nanometer-sized ACC particles were bound. EDS of the cell exteriors and ACC bound to the EPS identified trace amounts of calcium, nickel, or cobalt, or all three elements. The metal removal from solution for both cobalt and nickel was approximately 90%, which is substantially higher than observed in Chapter 2. Surface complexation and co-precipitation likely contributed to the removal of nickel and cobalt from solution. Further investigation and analysis is necessary to better understand transition metal incorporation into ACC particles before implementation at ultramafic and mafic mine operations for bioremediation purposes. Future directions:

Pure culture cyanobacteria can be ideal in understanding the possibility of utilizing cyanobacteria in an ultramafic mine site as a tool for bioremediation and enhancing recovery of metals. Further optimization and understanding of limitations, including environmental conditions such as fluctuating temperature and pH in the mine environment, would aid in the development of a bioremediation solution using cyanobacteria in mine site operations. The demonstrated ability of *S. leopoliensis* to remove metals within 72 hours indicate that this process can quickly concentrate metal out of solution. However, consideration needs to be given to the stability of the bound metals, because the observed desorption would impede any meaningful remediation. In addition, the ability of cyanobacteria to incorporate transition metals into carbonate precipitates is not well characterized, and further studies of other cyanobacteria strains would be of interest. To further understand the potential recovery of metals from ultramafic mining operations, it would be necessary to compare different types of waste and the corresponding mobilization of metals by native cyanobacteria. Future studies should focus on optimization mineral carbonation by native cyanobacteria in ultramafic mine sites, paired with

long-term studies of the incorporation of transition metals into biogenic carbonates. The development of a photobioreactor using multiple stages from bioleaching to carbonation and bio-recovery of critical metals would be a great step towards sustainable mining and net-neutral mining.

4.2 Summary of Findings:

Laboratory studies can be ideal for understanding the possibility of utilizing cyanobacteria as tools for bioremediation and enhanced recovery of metals at mine sites. However, engineered environments, such as tailings storage facilities, experience fluctuating temperature, pH, and other physicochemical conditions that can affect the mobility of metals, the suitability of certain cyanobacteria, and the stability of biomineralization products. Therefore, continuous research in understanding the kinetics and incorporation of metals is necessary for the development of a bioremediation solution using cyanobacteria. In addition, the ability of cyanobacteria to incorporate transition metals into ACC nano precipitates is still not well characterized. Further characterization will be necessary to understand both the kinetics and possible incorporation of these metals into the structure of the ACC and eventual calcium carbonate minerals. To further understand the potential recovery of metals from ultramafic mining operations, it would be necessary to examine the impact of different concentrations of transition metals and possible incorporation into Ca-rich carbonate minerals by native cyanobacteria. Future studies should focus on optimization of mineral carbonation by native cyanobacteria in ultramafic and mafic mine sites, paired with long-term studies of transition metal immobilization into biogenic carbonate phases. Through this future work, it may be possible to develop a photobioreactor that uses multiple stages to achieve: 1) bioleaching, 2) carbonation, and 3) bio-recovery of critical metals. Development of such technology would be a great step towards sustainable mining and net-neutral mining.

References:

Al-Amin, A., Parvin, F., Chakraborty, J., and Kim, Y.-I. 2021. Cyanobacteria mediated heavy metal removal: a review on mechanism, biosynthesis, and removal capability. Environmental Technology Reviews, **10**: 44–57. Taylor & Francis. doi:10.1080/21622515.2020.1869323.

Alfredsson, H.A., Oelkers, E.H., Hardarsson, B.S., Franzson, H., Gunnlaugsson, E., and Gislason, S.R. 2013. The geology and water chemistry of the Hellisheidi, SW-Iceland carbon storage site. International Journal of Greenhouse Gas Control, **12**: 399–418. doi:10.1016/j.ijggc.2012.11.019.

Al-Kindi, M. 2024. Overview of the carbon capture and storage opportunities in Oman. Geological Society, London, Special Publications, **550**: SP550-2024–7. doi:10.1144/SP550-2024-7.

Alsaç, E.P., Boke, M., Bissonnette, J.R., and Smith, R.D.L. 2024. Interplay between element-specific distortions and electrocatalytic oxygen evolution for cobalt–iron hydroxides. Chemical Science, **15**: 15339–15351. doi:10.1039/D4SC01841A.

Alsaç, E.P., Zhou, K., Rong, W., Salamon, S., Landers, J., Wende, H., and Smith, R.D.L. 2022. Identification of non-traditional coordination environments for iron ions in nickel hydroxide lattices. Energy & Environmental Science, **15**: 2638–2652. doi:10.1039/D2EE00396A.

Asghari, I., Mousavi, S.M., Amiri, F., and Tavassoli, S. 2013. Bioleaching of spent refinery catalysts: A review. Journal of Industrial and Engineering Chemistry, **19**: 1069–1081. doi:10.1016/j.jiec.2012.12.005.

Azeez, P.A., and Banerjee, D.K. 1991. Nickel uptake and toxicity in cyanobacteria. Toxicological & Environmental Chemistry, **30**: 43–50. doi:10.1080/02772249109357639.

Bai, H., Liu, D., Zheng, W., Ma, L., Yang, S., Cao, J., Lu, X., Wang, H., and Mehta, N. 2021. Microbially-induced calcium carbonate precipitation by a halophilic ureolytic bacterium and its potential for remediation of heavy metal-contaminated saline environments. International Biodeterioration & Biodegradation, **165**: 105311. doi:10.1016/j.ibiod.2021.105311.

Balaji, S., Kalaivani, T., and Rajasekaran, C. 2014. Biosorption of zinc and nickel and Its Effect on growth of different *Spirulina* strains. Clean– Soil, Air, Water, **42**: 507–512. doi:10.1002/clen.201200340.

Baselga-Cervera, B., Romero-López, J., García-Balboa, C., Costas, E., and López-Rodas, V. 2018. Improvement of the uranium sequestration ability of a *Chlamydomonas sp*. (ChlSP Strain) isolated from extreme uranium mine tailings through selection for potential bioremediation application. Frontiers in Microbiology, **9**: 523. doi:10.3389/fmicb.2018.00523.

Begum, W., Rai, S., Banerjee, S., Bhattacharjee, S., Hossain Mondal, M., Bhattarai, A., and Saha, B. 2022. A comprehensive review on the sources, essentiality and toxicological profile of nickel. RSC Advances, **12**: 9139–9153. doi:10.1039/D2RA00378C.

Behrens, G., Kuhn, L.T., Ubic, R., and Heuer, A.H. 1995. Raman spectra of vateritic Calcium carbonate. Spectroscopy Letters, **28**: 983–995. doi:10.1080/00387019508009934.

Bell, S., Crayston, J.A., Dines, T.J., Ellahi, S.B., and Smith, C.I. 2003. A resonance raman, surface-enhanced resonance raman, IR, and ab initio vibrational spectroscopic study of nickel(II) tetraazaannulene Complexes. Inorganic Chemistry, **42**: 3565–3575. doi:10.1021/ic026216e.

Benning, L.G., Phoenix, V.R., Yee, N., and Tobin, M.J. 2004. Molecular characterization of cyanobacterial silicification using synchrotron infrared micro-spectroscopy1. Geochimica et Cosmochimica Acta, **68**: 729–741. doi:10.1016/S0016-7037(03)00489-7.

Bishop, B.A., Flynn, S.L., Warchola, T.J., Alam, M.S., Robbins, L.J., Liu, Y., Owttrim, G.W., Alessi, D.S., and Konhauser, K.O. 2019. Adsorption of biologically critical trace elements to the marine cyanobacterium *Synechococcus sp*. PCC 7002: Implications for marine trace metal cycling. Chemical Geology, **525**: 28–36. doi:10.1016/j.chemgeo.2019.05.021.

Blanco-Vieites, M., Suárez-Montes, D., Hernández Battez, A., and Rodríguez, E. 2023. Enhancement of *Arthrospira* sp. culturing for sulfate removal and mining wastewater bioremediation. International Journal of Phytoremediation, **25**: 1116–1126. doi:10.1080/15226514.2022.2135680.

Blue, C.R., Giuffre, A., Mergelsberg, S., Han, N., De Yoreo, J.J., and Dove, P.M. 2017. Chemical and physical controls on the transformation of amorphous calcium carbonate

into crystalline CaCO polymorphs. Geochimica et Cosmochimica Acta, **196**: 179–196. doi:10.1016/j.gca.2016.09.004.

Boisvert, S., Joly, D., Leclerc, S., Govindachary, S., Harnois, J., and Carpentier, R. 2007. Inhibition of the oxygen-evolving complex of photosystem II and depletion of extrinsic polypeptides by nickel. BioMetals, **20**: 879–889. doi:10.1007/s10534-007-9081-z.

Bowman, D.M.J.S., Kolden, C.A., Abatzoglou, J.T., Johnston, F.H., van der Werf, G.R., and Flannigan, M. 2020. Vegetation fires in the Anthropocene. Nature Reviews Earth & Environment, **1**: 500–515. doi:10.1038/s43017-020-0085-3.

Braissant, O., Decho, A.W., Przekop, K.M., Gallagher, K.L., Glunk, C., Dupraz, C., and Visscher, P.T. 2009. Characteristics and turnover of exopolymeric substances in a hypersaline microbial mat. FEMS Microbiology Ecology, **67**: 293–307. doi:10.1111/j.1574-6941.2008.00614.x.

Bullock, L.A., James, R.H., Matter, J., Renforth, P., and Teagle, D.A.H. 2021. Global carbon dioxide removal potential of waste materials from metal and diamond mining. Frontiers in Climate, **3**. doi:10.3389/fclim.2021.694175.

Bullock, L.A., Yang, A., and Darton, R.C. 2022. Kinetics-informed global assessment of mine tailings for CO2 removal. Science of The Total Environment, **808**: 152111. doi:10.1016/j.scitotenv.2021.152111.

Bundeleva, I.A., Ménez, B., Augé, T., Bodénan, F., Recham, N., and Guyot, F. 2014. Effect of cyanobacteria *Synechococcus* PCC 7942 on carbonation kinetics of olivine at 20°C. Minerals Engineering, **59**: 2–11. doi:10.1016/j.mineng.2014.01.019.

Buxton, S., Garman, E., Heim, K.E., Lyons-Darden, T., Schlekat, C.E., Taylor, M.D., and Oller, A.R. 2019. Concise review of nickel human health toxicology and ecotoxicology. Inorganics, **7**: 89. doi:10.3390/inorganics7070089.

Carreira, A.R.F., Veloso, T., Macário, I.P.E., Pereira, J.L., Ventura, S.P.M., Passos, H., and Coutinho, J.A.P. 2023. The role of biomass elemental composition and ion-exchange in metal sorption by algae. Chemosphere, **314**: 137675. doi:10.1016/j.chemosphere.2022.137675.

Castenholz, R.W. 1989. Oxygenic Photosynthetic Bacteria (sect. 19). Group l. Cyanobacteria. Bergey's Manual of Systematic Bacteriology, **3**: 1710–1799. Williams and Wiikins Co.

Castillo Alvarez, C., Quitté, G., Schott, J., and Oelkers, E.H. 2020. Experimental determination of Ni isotope fractionation during Ni adsorption from an aqueous fluid onto calcite surfaces. Geochimica et Cosmochimica Acta, **273**: 26–36. doi:10.1016/j.gca.2020.01.010.

Chang, R., Kim, S., Lee, S., Choi, S., Kim, M., and Park, Y. 2017. Calcium carbonate precipitation for CO_2 storage and utilization: A review of the carbonate crystallization and polymorphism. Frontiers in Energy Research, **5**. Available from https://www.frontiersin.org/articles/10.3389/fenrg.2017.00017.

Chen, M., Zeng, H., Larkum, A.W.D., and Cai, Z.-L. 2004. Raman properties of chlorophyll *d*, the major pigment of *Acaryochloris marina*: studies using both Raman spectroscopy and density functional theory. Spectrochimica Acta Part A: Molecular and Biomolecular Spectroscopy, **60**: 527–534. doi:10.1016/S1386-1425(03)00258-0.

Cheng, J., Raudsepp, M.J., Wilson, S., and Alessi, D.S. 2024. Amorphous-to-crystalline transition of Ca–Mg-carbonates as a function of composition, time, and temperature. Crystal Growth & Design, **24**: 2349–2361. doi:10.1021/acs.cgd.3c01232.

Cheng, Q., Zhou, Q., Jin, Z., Jiang, Y., Xu, L., Jiang, H., and Zhao, Y. 2019. Bioaccumulation, growth performance, and transcriptomic response of Dictyosphaerium sp. after exposure to nonylphenol. Science of The Total Environment, **687**: 416–422. doi:10.1016/j.scitotenv.2019.06.136.

Chuai, X., Ding, W., Chen, X., Wang, X., Miao, A., Xi, B., He, L., and Yang, L. 2011. Phosphorus release from cyanobacterial blooms in Meiliang Bay of Lake Taihu, China. Ecological Engineering, **37**: 842–849. doi:10.1016/j.ecoleng.2011.01.001.

Costa, O.Y.A., Raaijmakers, J.M., and Kuramae, E.E. 2018. Microbial extracellular polymeric substances: Ecological function and impact on soil aggregation. Frontiers in Microbiology, **9**. Available from https://www.frontiersin.org/articles/10.3389/fmicb.2018.01636.

Dai, Z., Xu, L., Xiao, T., McPherson, B., Zhang, X., Zheng, L., Dong, S., Yang, Z., Soltanian, M.R., Yang, C., Ampomah, W., Jia, W., Yin, S., Xu, T., Bacon, D., and Viswanathan, H. 2020. Reactive chemical transport simulations of geologic carbon sequestration: Methods and applications. Earth-Science Reviews, **208**: 103265. doi:10.1016/j.earscirev.2020.103265.

Diloreto, Z., Ahmad, M.S., Al Saad Al-Kuwari, H., Sadooni, F., Bontognali, T.R.R., and Dittrich, M. 2023. Raman spectroscopic and microbial study of biofilms hosted gypsum deposits in the hypersaline wetlands: Astrobiological perspective. Astrobiology, **23**: 991–1005. doi:10.1089/ast.2023.0003.

Dittrich, M., and Obst, M. 2004. Are picoplankton responsible for calcite precipitation in lakes? AMBIO: A Journal of the Human Environment, **33**: 559–564. doi:10.1579/0044-7447-33.8.559.

Dittrich, M., and Sibler, S. 2006. Influence of H^+ and calcium ions on surface functional groups of *Synechococcus* PCC 7942 Cells. Langmuir, **22**: 5435–5442. doi:10.1021/la0531143.

Dixit, S., and Singh, D.P. 2013. Phycoremediation of lead and cadmium by employing *Nostoc muscorum* as biosorbent and optimization of its biosorption potential. International Journal of Phytoremediation, **15**: 801–813. Taylor & Francis. doi:10.1080/15226514.2012.735290.

Dong, H., Huang, L., Zhao, L., Zeng, Q., Liu, X., Sheng, Y., Shi, L., Wu, G., Jiang, H., Li, F., Zhang, L., Guo, D., Li, G., Hou, W., and Chen, H. 2022. A critical review of mineral–microbe interaction and co-evolution: mechanisms and applications. National Science Review, **9**: nwac128. doi:10.1093/nsr/nwac128.

Drake, H., Mathurin, F.A., Zack, T., Schäfer, T., Roberts, N.M., Whitehouse, M., Karlsson, A., Broman, C., and Åström, M.E. 2018. Incorporation of metals into calcite in a deep anoxic granite aquifer. Environmental Science & Technology, **52**: 493–502. doi:10.1021/acs.est.7b05258.

Duan, Z., Tan, X., Shi, L., Zeng, Q., Ali, I., Zhu, R., Chen, H., and Parajuli, K. 2023. Phosphorus accumulation in extracellular polymeric substances (EPS) of colony-forming cyanobacteria challenges imbalanced nutrient reduction strategies in eutrophic lakes. Environmental Science & Technology, **57**: 1600–1612. doi:10.1021/acs.est.2c04398.

Elzinga, E.J., and Reeder, R.J. 2002. X-ray absorption spectroscopy study of Cu^{2+} and Zn^{2+} adsorption complexes at the calcite surface: Implications for site-specific metal incorporation preferences during calcite crystal growth. Geochimica et Cosmochimica Acta, **66**: 3943–3954. doi:10.1016/S0016-7037(02)00971-7.

Engel, A., Thoms, S., Riebesell, U., Rochelle-Newall, E., and Zondervan, I. 2004. Polysaccharide aggregation as a potential sink of marine dissolved organic carbon. Nature, **428**: 929–932. doi:10.1038/nature02453.

Facey, J.A., King, J.J., Apte, S.C., and Mitrovic, S.M. 2022. Assessing the importance of cobalt as a micronutrient for freshwater cyanobacteria. Journal of Phycology, **58**: 71–79. doi:10.1111/jpy.13216.

Fallowfield, H.J., and Daft, M.J. 1988. The extracellular release of dissolved organic carbon by freshwater cyanobacteria and algae and the interaction with *Lysobacter* CP-1. British Phycological Journal, **23**: 317–326. doi:10.1080/00071618800650351.

Fan, X., Ding, S., Gao, S., Chen, M., Fu, Z., Gong, M., Wang, Y., and Tsang, D.C.W. 2021. A holistic understanding of cobalt cycling and limiting roles in the eutrophic Lake Taihu. Chemosphere, **277**: 130234. doi:10.1016/j.chemosphere.2021.130234.

Fawzy, M.A., Hifney, A.F., Adam, M.S., and Al-Badaani, A.A. 2020. Biosorption of cobalt and its effect on growth and metabolites of *Synechocystis pevalekii* and *Scenedesmus bernardii*: Isothermal analysis. Environmental Technology & Innovation, **19**: 100953. doi:10.1016/j.eti.2020.100953.

Gao, S., Lin, Y., Jiao, X., Sun, Y., Luo, Q., Zhang, W., Li, D., Yang, J., and Xie, Y. 2016. Partially oxidized atomic cobalt layers for carbon dioxide electroreduction to liquid fuel. Nature, **529**: 68–71. doi:10.1038/nature16455.

Gardea-Torresdey, J.L., Arenas, J.L., Francisco, N.M.C., Tiemann, K.J., and Webb, R. 1998. Ability of immobilized cyanobacteria to remove metal ions from solution and demonstration of the presence of metallothionein genes in various strains. Journal of Hazardous Substance Research, **1**. Kansas State University Libraries. doi:10.4148/1090-7025.1001.

Gavrilescu, M. 2022. Microbial recovery of critical metals from secondary sources. Bioresource Technology, **344**: 126208. doi:10.1016/j.biortech.2021.126208.

Gérard, E., Ménez, B., Couradeau, E., Moreira, D., Benzerara, K., Tavera, R., and López-García, P. 2013. Specific carbonate–microbe interactions in the modern microbialites of Lake Alchichica (Mexico). The ISME Journal, **7**: 1997–2009. doi:10.1038/ismej.2013.81.

Gillispie, E.C., Austin, R.E., Rivera, N.A., Bolich, R., Duckworth, O.W., Bradley, P., Amoozegar, A., Hesterberg, D., and Polizzotto, M.L. 2016. Soil weathering as an engine for manganese contamination of well water. Environmental Science & Technology, **50**: 9963–9971. doi:10.1021/acs.est.6b01686.

González-Dávila, M. 1995. The role of phytoplankton cells on the control of heavy metal concentration in seawater. Marine Chemistry, **48**: 215–236. doi:10.1016/0304-4203(94)00045-F.

González-López, J., Fernández-González, Á., Jiménez, A., Godelitsas, A., Ladas, S., Provatas, G., Lagogiannis, A., Pasias, I.N., Thomaidis, N.S., and Prieto, M. 2017. Dissolution and sorption processes on the surface of calcite in the presence of high Co^{2+} concentration. Minerals, **7**: 23. doi:10.3390/min7020023.

Gras, A., Beaudoin, G., Molson, J., and Plante, B. 2020. Atmospheric carbon sequestration in ultramafic mining residues and impacts on leachate water chemistry at the Dumont Nickel Project, Quebec, Canada. Chemical Geology, **546**: 119661. doi:10.1016/j.chemgeo.2020.119661.

Gupta, P., and Diwan, B. 2017. Bacterial exopolysaccharide mediated heavy metal removal: A Review on biosynthesis, mechanism and remediation strategies. Biotechnology Reports, **13**: 58–71. doi:10.1016/j.btre.2016.12.006.

Hamilton, J.L., Wilson, S., Morgan, B., Harrison, A.L., Turvey, C.C., Paterson, D.J., Dipple, G.M., and Southam, G. 2020. Accelerating mineral carbonation in ultramafic Mine tailings via direct CO_2 reaction and heap leaching with potential for base metal Enrichment and Recovery. Economic Geology, **115**: 303–323. doi:10.5382/econgeo.4710.

Hamilton, J.L., Wilson, S., Morgan, B., Turvey, C.C., Paterson, D.J., MacRae, C., McCutcheon, J., and Southam, G. 2016. Nesquehonite sequesters transition metals and CO_2 during accelerated carbon mineralisation. International Journal of Greenhouse Gas Control, **55**: 73–81. doi:10.1016/j.ijggc.2016.11.006.

Hamilton, J.L., Wilson, S.A., Morgan, B., Turvey, C.C., Paterson, D.J., Jowitt, S.M., McCutcheon, J., and Southam, G. 2018. Fate of transition metals during passive carbonation of ultramafic mine tailings via air capture with potential for metal resource

recovery. International Journal of Greenhouse Gas Control, **71**: 155–167. doi:10.1016/j.ijggc.2018.02.008.

Hausladen, D.M., Alexander-Ozinskas, A., McClain, C., and Fendorf, S. 2018. Hexavalent chromium sources and distribution in California groundwater. Environmental Science & Technology, **52**: 8242–8251. doi:10.1021/acs.est.7b06627.

He, Z., Xu, Y., Yang, X., Shi, J., Wang, X., Jin, Z., Zhang, D., and Pan, X. 2022. Passivation of heavy metals in copper–nickel tailings by *in-situ* bio-mineralization: A pilot trial and mechanistic analysis. Science of The Total Environment, **838**: 156504. doi:10.1016/j.scitotenv.2022.156504.

Henne, A., Craw, D., Vasconcelos, P., and Southam, G. 2018. Bioleaching of waste material from the Salobo mine, Brazil: Recovery of refractory copper from Cu hosted in silicate minerals. Chemical Geology, **498**: 72–82. doi:10.1016/j.chemgeo.2018.08.029.

Huang, L., Jin, Y., Zhou, D., Liu, L., Huang, S., Zhao, Y., and Chen, Y. 2022a. A review of the role of extracellular polymeric substances (EPS) in wastewater treatment systems. International Journal of Environmental Research and Public Health, **19**. doi:10.3390/ijerph191912191.

Huang, L., Jin, Y., Zhou, D., Liu, L., Huang, S., Zhao, Y., and Chen, Y. 2022b. A review of the role of extracellular polymeric Substances (EPS) in wastewater treatment systems. International Journal of Environmental Research and Public Health, **19**: 12191. doi:10.3390/ijerph191912191.

IPCC, 2018: Summary for Policymakers. In: *Global warming of 1.5°C. An IPCC Special Report on the impacts of global warming of 1.5°C above pre-industrial levels and related global greenhouse gas emission pathways, in the context of strengthening the global response to the threat of climate change, sustainable development, and efforts to eradicate poverty* [Masson-Delmotte, V., P. Zhai, H.-O. Pörtner, D. Roberts, J. Skea, P.R. Shukla, A. Pirani, W. Moufouma-Okia, C. Péan, R. Pidcock, S. Connors, J.B.R. Matthews, Y. Chen, X. Zhou, M.I. Gomis, E. Lonnoy, T. Maycock, M. Tignor, and T. Waterfield (eds.)]. Cambridge University Press, Cambridge, UK and New York, NY, USA, pp. 3-24, doi:10.1017/9781009157940.001.

IPCC, 2021: Climate Change 2021: The physical science basis. Contribution of working group I to the sixth assessment report of the Intergovernmental Panel on Climate

Change[Masson-Delmotte, V., P. Zhai, A. Pirani, S.L. Connors, C. Péan, S. Berger, N. Caud, Y. Chen, L. Goldfarb, M.I. Gomis, M. Huang, K. Leitzell, E. Lonnoy, J.B.R. Matthews, T.K. Maycock, T. Waterfield, O. Yelekçi, R. Yu, and B. Zhou (eds.)]. Cambridge University Press, Cambridge, United Kingdom and New York, NY, USA, In press, doi:10.1017/9781009157896.

IPCC, 2022: *Climate Change 2022: Impacts, Adaptation, and Vulnerability.* contribution of working group II to the sixth assessment report of the Intergovernmental Panel on Climate Change [H.-O. Pörtner, D.C. Roberts, M. Tignor, E.S. Poloczanska, K. Mintenbeck, A. Alegría, M. Craig, S. Langsdorf, S. Löschke, V. Möller, A. Okem, B. Rama (eds.)]. Cambridge University Press. Cambridge University Press, Cambridge, UK and New York, NY, USA, 3056 pp., doi:10.1017/9781009325844.

Jansson, C., and Northen, T. 2010. Calcifying cyanobacteria—the potential of biomineralization for carbon capture and storage. Current Opinion in Biotechnology, **21**: 365–371. doi:10.1016/j.copbio.2010.03.017.

Jehlička, J., Edwards, H.G.M., Němec, I., and Oren, A. 2015. Raman spectroscopic study of the *Chromobacterium violaceum* pigment violacein using multiwavelength excitation and DFT calculations. Spectrochimica Acta Part A: Molecular and Biomolecular Spectroscopy, **151**: 459–467. doi:10.1016/j.saa.2015.06.051.

Jensen, T.E., Baxter, M., Rachlin, J.W., and Jani, V. 1982. Uptake of heavy metals by *Plectonema boryanum* (cyanophyceae) into cellular components, especially polyphosphate bodies: An X-ray energy dispersive study. Environmental Pollution Series A, Ecological and Biological, **27**: 119–127. doi:10.1016/0143-1471(82)90104-0.

Jones, T.R., Poitras, J., Levett, A., Langendam, A., Vietti, A., and Southam, G. 2023a. Accelerated carbonate biomineralisation of Venetia diamond mine coarse residue deposit (CRD) material – A field trial study. Science of The Total Environment, **893**: 164853. doi:10.1016/j.scitotenv.2023.164853.

Jones, T.R., Poitras, J., Paterson, D., and Southam, G. 2023b. Historical diamond mine waste reveals carbon sequestration resource in kimberlite residue. Chemical Geology, **617**: 121270. doi:10.1016/j.chemgeo.2022.121270.

Kamennaya, N.A., Ajo-Franklin, C.M., Northen, T., and Jansson, C. 2012. Cyanobacteria as biocatalysts for carbonate mineralization. Minerals, **2**: 338–364. doi:10.3390/min2040338.

Kandji, E.H.B., Plante, B., Bussière, B., Beaudoin, G., and Dupont, P.-P. 2017. Kinetic testing to evaluate the mineral carbonation and metal leaching potential of ultramafic tailings: Case study of the Dumont Nickel Project, Amos, Québec. Applied Geochemistry, **84**: 262–276. doi:10.1016/j.apgeochem.2017.07.005.

Karaca, O., Cameselle, C., and Reddy, K.R. 2018. Mine tailing disposal sites: contamination problems, remedial options and phytocaps for sustainable remediation. Reviews in Environmental Science and Bio/Technology, **17**: 205–228. doi:10.1007/s11157-017-9453-y.

Katsikopoulos, D., Fernández-González, Á., Prieto, A.C., and Prieto, M. 2008. Co-crystallization of Co(II) with calcite: Implications for the mobility of cobalt in aqueous environments. Chemical Geology, **254**: 87–100. doi:10.1016/j.chemgeo.2008.06.003.

Khanjani, M., Westenberg, D.J., Kumar, A., and Ma, H. 2021. Tuning polymorphs and morphology of microbially induced calcium carbonate: Controlling factors and underlying mechanisms. ACS Omega, **6**: 11988–12003. doi:10.1021/acsomega.1c00559.

Khudhur, F.W.K., MacDonald, J.M., Macente, A., and Daly, L. 2022. The utilization of alkaline wastes in passive carbon capture and sequestration: Promises, challenges and environmental aspects. Science of The Total Environment, **823**: 153553. doi:10.1016/j.scitotenv.2022.153553.

Kierczak, J., Pietranik, A., and Pędziwiatr, A. 2021. Ultramafic geoecosystems as a natural source of Ni, Cr, and Co to the environment: A review. Science of The Total Environment, **755**: 142620. doi:10.1016/j.scitotenv.2020.142620.

Koner, S., Tsai, H.-C., Chen, J.-S., Hussain, B., Rajendran, S.K., and Hsu, B.-M. 2022. Exploration of pristine plate-tectonic plains and mining exposure areas for indigenous microbial communities and its impact on the mineral-microbial geochemical weathering process in ultramafic setting. Environmental Research, **214**: 113802. doi:10.1016/j.envres.2022.113802.

Konhauser, K. 2007. Introduction of Geomicrobiology. Blackwell Publishing Company.

Lakshtanov, L.Z., and Stipp, S.L.S. 2007. Experimental study of nickel (II) interaction with calcite: Adsorption and coprecipitation. Geochimica et Cosmochimica Acta, **71**: 3686–3697. doi:10.1016/j.gca.2007.04.006.

Leung, D.Y.C., Caramanna, G., and Maroto-Valer, M.M. 2014. An overview of current status of carbon dioxide capture and storage technologies. Renewable and Sustainable Energy Reviews, **39**: 426–443. doi:10.1016/j.rser.2014.07.093.

Leyssens, L., Vinck, B., Van Der Straeten, C., Wuyts, F., and Maes, L. 2017. Cobalt toxicity in humans—A review of the potential sources and systemic health effects. Toxicology, **387**: 43–56. doi:10.1016/j.tox.2017.05.015.

QiLiu, H.-H., Zhang, G., Yi, Z., and Wang, Y. 2013. A permeability-change relationship in the dryout zone for CO_2 injection into saline aquifers. International Journal of Greenhouse Gas Control, **15**: 42–47. doi:10.1016/j.ijggc.2013.01.034.

Liu, Y., Alessi, D.S., Owttrim, G.W., Kenney, J.P.L., Zhou, Q., Lalonde, S.V., and Konhauser, K.O. 2016. Cell surface acid-base properties of the cyanobacterium *Synechococcus*: Influences of nitrogen source, growth phase and N:P ratios. Geochimica et Cosmochimica Acta, **187**: 179–194. doi:10.1016/j.gca.2016.05.023.

Liu, Y., Alessi, D.S., Owttrim, G.W., Petrash, D.A., Mloszewska, A.M., Lalonde, S.V., Martinez, R.E., Zhou, Q., and Konhauser, K.O. 2015. Cell surface reactivity of *Synechococcus* sp. PCC 7002: Implications for metal sorption from seawater. Geochimica et Cosmochimica Acta, **169**: 30–44. doi:10.1016/j.gca.2015.07.033.

Loudermilk, A., and Dixon, D.A. 2024. Prediction of the pK_a 's of hydrated metal carbonates and bicarbonates for Mg, Ca, Mn, Fe, Co, Ni, Cu, and Zn Dications. The Journal of Physical Chemistry A, **128**: 5331–5343. doi:10.1021/acs.jpca.4c02879.

Lu, M., Wang, X., Li, Y., Liu, H., An, X., and Lian, B. 2022. Soil microbial community structure and environmental effects of serpentine weathering under different vegetative covers in the serpentine mining area of Donghai County, China. Science of The Total Environment, **835**: 155452. doi:10.1016/j.scitotenv.2022.155452.

Ma, X., Coleman, M.L., and Waldbauer, J.R. 2018. Distinct molecular signatures in dissolved organic matter produced by viral lysis of marine cyanobacteria. Environmental Microbiology, **20**: 3001–3011. doi:10.1111/1462-2920.14338.

Mani, D., and Kumar, C. 2014. Biotechnological advances in bioremediation of heavy metals contaminated ecosystems: an overview with special reference to phytoremediation. International Journal of Environmental Science and Technology, **11**: 843–872. doi:10.1007/s13762-013-0299-8.

Martínez-Ruiz, E.B., and Martínez-Jerónimo, F. 2015. Nickel has biochemical, physiological, and structural effects on the green microalga *Ankistrodesmus falcatus*: An integrative study. Aquatic Toxicology, **169**: 27–36. doi:10.1016/j.aquatox.2015.10.007.

Martínez-Ruiz, E.B., and Martínez-Jerónimo, F. 2016. How do toxic metals affect harmful cyanobacteria? An integrative study with a toxigenic strain of *Microcystis aeruginosa* exposed to nickel stress. Ecotoxicology and Environmental Safety, **133**: 36–46. doi:10.1016/j.ecoenv.2016.06.040.

Mathivanan, K., Chandirika, J.U., Mathimani, T., Rajaram, R., Annadurai, G., and Yin, H. 2021. Production and functionality of exopolysaccharides in bacteria exposed to a toxic metal environment. Ecotoxicology and Environmental Safety, **208**: 111567. doi:10.1016/j.ecoenv.2020.111567.

McCutcheon, J., and Power, I.M. 2023. Microbially mediated carbon dioxide removal for sustainable mining. PLOS Biology, **21**: e3002026. Public Library of Science.

McCutcheon, J., Power, I.M., Harrison, A.L., Dipple, G.M., and Southam, G. 2014. A greenhouse-scale photosynthetic microbial bioreactor for carbon sequestration in magnesium carbonate minerals. Environmental Science & Technology, **48**: 9142–9151. American Chemical Society. doi:10.1021/es500344s.

McCutcheon, J., Power, I.M., Shuster, J., Harrison, A.L., Dipple, G.M., and Southam, G. 2019. Carbon sequestration in biogenic magnesite and other magnesium carbonate minerals. Environmental Science & Technology, **53**: 3225–3237. doi:10.1021/acs.est.8b07055.

McCutcheon, J., and Southam, G. 2018. Advanced biofilm staining techniques for TEM and SEM in geomicrobiology: Implications for visualizing EPS architecture, mineral nucleation, and microfossil generation. Chemical Geology, **498**: 115–127. doi:10.1016/j.chemgeo.2018.09.016.

McCutcheon, J., Turvey, C.C., Wilson, S.A., Hamilton, J.L., and Southam, G. 2017. Experimental deployment of microbial mineral carbonation at an asbestos mine:

Potential applications to carbon storage and tailings stabilization. Minerals, **7**. doi:10.3390/min7100191.

McCutcheon, J., Wilson, S.A., and Southam, G. 2016. Microbially accelerated carbonate mineral precipitation as a strategy for in situ carbon sequestration and rehabilitation of Asbestos Mine Sites. Environmental Science & Technology, **50**: 1419–1427. American Chemical Society. doi:10.1021/acs.est.5b04293.

Micheletti, E., Colica, G., Viti, C., Tamagnini, P., and De Philippis, R. 2008. Selectivity in the heavy metal removal by exopolysaccharide-producing cyanobacteria. Journal of Applied Microbiology, **105**: 88–94. doi:10.1111/j.1365-2672.2008.03728.x.

Ministry of Natural Resources, and Ministry of innovation, science and industry. 2023. The Canadian critical minerals strategy. *In* Government of Canada. Critical Minerals in Canada. Available from https://www.canada.ca/en/campaign/critical-minerals-in-canada/canadian-critical-minerals-strategy.html.

Mota, R., Pereira, S.B., Meazzini, M., Fernandes, R., Santos, A., Evans, C.A., De Philippis, R., Wright, P.C., and Tamagnini, P. 2015. Effects of heavy metals on *Cyanothece sp.* CCY 0110 growth, extracellular polymeric substances (EPS) production, ultrastructure and protein profiles. Journal of Proteomics, **120**: 75–94. doi:10.1016/j.jprot.2015.03.004.

Mudd, G.M., and Jowitt, S.M. 2014. A Detailed Assessment of Global nickel resource trends and endowments. Economic Geology, **109**: 1813–1841. doi:10.2113/econgeo.109.7.1813.

Muhammad, S., Tahir Shah, M., and Khan, S. 2010. Arsenic health risk assessment in drinking water and source apportionment using multivariate statistical techniques in Kohistan region, northern Pakistan. Food and Chemical Toxicology, **48**: 2855–2864. doi:10.1016/j.fct.2010.07.018.

Muyssen, B.T.A., Brix, K.V., DeForest, D.K., and Janssen, C.R. 2004. Nickel essentiality and homeostasis in aquatic organisms. Environmental Reviews, **12**: 113–131. doi:10.1139/a04-004.

Nawab, J., Khan, S., Khan, M.A., Sher, H., Rehamn, U.U., Ali, S., and Shah, S.M. 2017. Potentially toxic metals and biological contamination in drinking water sources in chromite mining-impacted areas of Pakistan: A comparative study. Exposure and Health, **9**: 275–287. doi:10.1007/s12403-016-0240-8.

Natural Resources Canada. 2023. Capturing the opportunity: A carbon management strategy for Canada. Natural Resources Canada. Available from https://natural-resources.canada.ca/climate-change/canadas-green-future/capturing-the-opportunity-carbon-management-strategy-for-canada/canadas-carbon-management-strategy/25337.

Nejidat, A., Meshulam, M., Diaz-Reck, D., and Ronen, Z. 2023. Emergence of hydrocarbon-degrading bacteria in crude oil-contaminated soil in a hyperarid ecosystem: Effect of phosphate addition and augmentation with nitrogen-fixing cyanobacteria on oil bioremediation. International Biodeterioration & Biodegradation, **178**: 105556. doi:10.1016/j.ibiod.2022.105556.

Nicolaus, B., Panico, A., Lama, L., Romano, I., Manca, M.C., De Giulio, A., and Gambacorta, A. 1999. Chemical composition and production of exopolysaccharides from representative members of heterocystous and non-heterocystous cyanobacteria. Phytochemistry, **52**: 639–647. doi:10.1016/S0031-9422(99)00202-2.

Obst, M., and Dittrich, M. 2005. Living under an atomic force microscope: An optimized approach for *in vivo* investigations on surface alterations towards biomineral nucleation on cyanobacterial cells. Geobiology, **3**: 179–193. doi:10.1111/j.1472-4669.2005.00054.x.

Obst, M., Dynes, J.J., Lawrence, J.R., Swerhone, G.D.W., Benzerara, K., Karunakaran, C., Kaznatcheev, K., Tyliszczak, T., and Hitchcock, A.P. 2009a. Precipitation of amorphous $CaCO_3$ (aragonite-like) by cyanobacteria: A STXM study of the influence of EPS on the nucleation process. Geochimica et Cosmochimica Acta, **73**: 4180–4198. doi:10.1016/j.gca.2009.04.013.

Obst, M., Wehrli, B., and Dittrich, M. 2009b. $CaCO_3$ nucleation by cyanobacteria: laboratory evidence for a passive, surface-induced mechanism. Geobiology, **7**: 324–347. doi:10.1111/j.1472-4669.2009.00200.x.

Otero, A., and Vincenzini, M. 2003. Extracellular polysaccharide synthesis by *Nostoc* strains as affected by N source and light intensity. Journal of Biotechnology, **102**: 143–152. doi:10.1016/S0168-1656(03)00022-1.

Ozturk, S., Aslim, B., Suludere, Z., and Tan, S. 2014. Metal removal of cyanobacterial exopolysaccharides by uronic acid content and monosaccharide composition. Carbohydrate Polymers, **101**: 265–271. doi:10.1016/j.carbpol.2013.09.040.

Paulo, C., Kenney, J.P.L., Persson, P., and Dittrich, M. 2018. Effects of phosphorus in growth media on biomineralization and cell surface properties of marine cyanobacteria *Synechococcus*. Geosciences, **8**. doi:10.3390/geosciences8120471.

Paulo, C., Power, I.M., Zeyen, N., Wang, B., and Wilson, S. 2023. Geochemical modeling of CO_2 sequestration in ultramafic mine wastes from Australia, Canada, and South Africa: Implications for carbon accounting and monitoring. Applied Geochemistry, **152**: 105630. doi:10.1016/j.apgeochem.2023.105630.

Parkhurst, D.L., and Appelo, C.A.J., 2013, Description of input and examples for PHREEQC version 3—A computer program for speciation, batch-reaction, one-dimensional transport, and inverse geochemical calculations: U.S. Geological Survey Techniques and Methods, book 6, chap. A43, 497 p., https://doi.org/10.3133/tm6A43

Pereira, S., Micheletti, E., Zille, A., Santos, A., Moradas-Ferreira, P., Tamagnini, P., and De Philippis, R. 2011. Using extracellular polymeric substances (EPS)-producing cyanobacteria for the bioremediation of heavy metals: do cations compete for the EPS functional groups and also accumulate inside the cell? Microbiology, **157**: 451–458. doi:10.1099/mic.0.041038-0.

Power, I.M., Dipple, G.M., and Southam, G. 2010. Bioleaching of ultramafic tailings by *Acidithiobacillus* spp. for CO_2 sequestration. Environmental Science & Technology, **44**: 456–462. doi:10.1021/es900986n.

Power, I.M., Harrison, A.L., Dipple, G.M., Wilson, S., Kelemen, P.B., Hitch, M., and Southam, G. 2013. Carbon mineralization: From natural analogues to engineered systems. Reviews in Mineralogy and Geochemistry, **77**: 305–360. doi:10.2138/rmg.2013.77.9.

Power, I.M., McCutcheon, J., Harrison, A.L., Wilson, S., Dipple, G.M., Kelly, S., Southam, C., and Southam, G. 2014. Strategizing carbon-neutral mines: A case for pilot projects. Minerals, **4**: 399–436. doi:10.3390/min4020399.

Power, I.M., Paulo, C., Long, H., Lockhart, J.A., Stubbs, A.R., French, D., and Caldwell, R. 2021. Carbonation, cementation, and stabilization of ultramafic mine tailings. Environmental Science & Technology, **55**: 10056–10066. doi:10.1021/acs.est.1c01570.

Power, I.M., Paulo, C., and Rausis, K. 2024. The mining industry's role in enhanced weathering and mineralization for CO_2 removal. Environmental Science & Technology, **58**: 43–53. doi:10.1021/acs.est.3c05081.

Qian, L., Ye, X., Xiao, J., Lin, S., Wang, H., Liu, Z., Ma, Y., Yang, L., Zhang, Z., and Wu, L. 2022. Nitrogen concentration acting as an environmental signal regulates cyanobacterial EPS excretion. Chemosphere, **291**: 132878. doi:10.1016/j.chemosphere.2021.132878.

Qiao, S., Zeng, G., Wang, X., Dai, C., Sheng, M., Chen, Q., Xu, F., and Xu, H. 2021. Multiple heavy metals immobilization based on microbially induced carbonate precipitation by ureolytic bacteria and the precipitation patterns exploration. Chemosphere, **274**: 129661. doi:10.1016/j.chemosphere.2021.129661.

Rezaei, M., Pourang, N., and Moradi, A.M. 2022. Removal of lead from aqueous solutions using three biosorbents of aquatic origin with the emphasis on the affective factors. Scientific Reports, **12**: 751. doi:10.1038/s41598-021-04744-0.

Rippka, R., Deruelles, J., Waterbury, J.B., Herdman, M., and Stanier, R.Y. 1979. Generic assignments, strain Histories and properties of pure cultures of cyanobacteria. Microbiology, **111**: 1–61. doi:10.1099/00221287-111-1-1.

Rueda, E., García-Galán, M.J., Ortiz, A., Uggetti, E., Carretero, J., García, J., and Díez-Montero, R. 2020. Bioremediation of agricultural runoff and biopolymers production from cyanobacteria cultured in demonstrative full-scale photobioreactors. Process Safety and Environmental Protection, **139**: 241–250. doi:10.1016/j.psep.2020.03.035.

Scullett-Dean, G., Hamilton, J.L., Repina, O., Brand, H.E.A., Burton, E.D., Saunders, M., and Santini, T.C. 2023. Uptake and incorporation of Al, Cr, V, Zn and Mo in hematite: Competition, synergies and influence on structural properties. Journal of Hazardous Materials, **445**: 130630. doi:10.1016/j.jhazmat.2022.130630.

Selim, K.A., and Haffner, M. 2020. Heavy metal stress alters the response of the unicellular cyanobacterium *Synechococcus elongatus* PCC 7942 to mitrogen starvation. Life, **10**. doi:10.3390/life10110275.

Shiraishi, F. 2012. Chemical conditions favoring photosynthesis-induced $CaCO_3$ precipitation and implications for microbial carbonate formation in the ancient ocean. Geochimica et Cosmochimica Acta, **77**: 157–174. doi:10.1016/j.gca.2011.11.004.

Shiraishi, F., Omori, T., Tomioka, N., Motai, S., Suga, H., and Takahashi, Y. 2020. Characteristics of $CaCO_3$ nucleated around cyanobacteria: Implications for calcification process. Geochimica et Cosmochimica Acta, **285**: 55–69. doi:10.1016/j.gca.2020.06.033.

Singh, A.L., Asthana, R.K., Srivastava, S.C., and Singh, S.P. 1992. Nickel uptake and its localization in a cyanobacterium. FEMS Microbiology Letters, **99**: 165–168. doi:10.1111/j.1574-6968.1992.tb05560.x.

Smith, P., Davis, S.J., Creutzig, F., Fuss, S., Minx, J., Gabrielle, B., Kato, E., Jackson, R.B., Cowie, A., Kriegler, E., van Vuuren, D.P., Rogelj, J., Ciais, P., Milne, J., Canadell, J.G., McCollum, D., Peters, G., Andrew, R., Krey, V., Shrestha, G., Friedlingstein, P., Gasser, T., Grübler, A., Heidug, W.K., Jonas, M., Jones, C.D., Kraxner, F., Littleton, E., Lowe, J., Moreira, J.R., Nakicenovic, N., Obersteiner, M., Patwardhan, A., Rogner, M., Rubin, E., Sharifi, A., Torvanger, A., Yamagata, Y., Edmonds, J., and Yongsung, C. 2016. Biophysical and economic limits to negative CO_2 emissions. Nature Climate Change, **6**: 42–50. doi:10.1038/nclimate2870.

Smječanin, N., Nuhanović, M., Sulejmanović, J., Mašić, E., and Sher, F. 2023. Highly effective sustainable membrane-based cyanobacteria for uranium uptake from aqueous environment. Chemosphere, **313**: 137488. doi:10.1016/j.chemosphere.2022.137488.

Stanfield, C.H., Miller, Q.R.S., Battu, A.K., Lahiri, N., Nagurney, A.B., Cao, R., Nienhuis, E.T., DePaolo, D.J., Latta, D.E., and Schaef, H.T. 2024. Carbon mineralization and critical mineral resource evaluation pathways for mafic–ultramafic assets. ACS Earth and Space Chemistry, **8**: 1204–1213. doi:10.1021/acsearthspacechem.4c00005.

Thompson, J.B., and Ferris, F.G. 1990. Cyanobacterial precipitation of gypsum, calcite, and magnesite from natural alkaline lake water. Geology, **18**: 995. doi:10.1130/0091-7613(1990)018<0995:CPOGCA>2.3.CO;2.

Turvey, C.C., Wilson, S., Hamilton, J.L., Tait, A.W., McCutcheon, J., Beinlich, A., Fallon, S.J., Dipple, G.M., and Southam, G. 2018. Hydrotalcites and hydrated Mg-carbonates as carbon sinks in serpentinite mineral wastes from the Woodsreef chrysotile mine, New South Wales, Australia: Controls on carbonate mineralogy and efficiency of CO_2 air capture in mine tailings. International Journal of Greenhouse Gas Control, **79**: 38–60. doi:10.1016/j.ijggc.2018.09.015.

Van Mooy, B.A.S., Fredricks, H.F., Pedler, B.E., Dyhrman, S.T., Karl, D.M., Koblížek, M., Lomas, M.W., Mincer, T.J., Moore, L.R., Moutin, T., Rappé, M.S., and Webb, E.A. 2009. Phytoplankton in the ocean use non-phosphorus lipids in response to phosphorus scarcity. Nature, **458**: 69–72. doi:10.1038/nature07659.

Wang, B., Zeyen, N., Wilson, S., Honda-McNeil, M.J., Hamilton, J.L., Von Gunten, K., Alessi, D.S., Jones, T.R., Paterson, D.J., and Southam, G. 2024. Migration of transition metals and potential for carbon mineralization during acid leaching of processed kimberlite from Venetia diamond mine, South Africa. Applied Geochemistry, **166**: 105986. doi:10.1016/j.apgeochem.2024.105986.

Wang, F., and Dreisinger, D. 2022. Carbon mineralization with concurrent critical metal recovery from olivine. Proceedings of the National Academy of Sciences, **119**: e2203937119. doi:10.1073/pnas.2203937119.

Wang, F., Dreisinger, D., Jarvis, M., Hitchins, T., and Trytten, L. 2021. CO_2 mineralization and concurrent utilization for nickel conversion from nickel silicates to nickel sulfides. Chemical Engineering Journal, **406**: 126761. doi:10.1016/j.cej.2020.126761.

Wehrmeister, U., Soldati, A.L., Jacob, D.E., Häger, T., and Hofmeister, W. 2010. Raman spectroscopy of synthetic, geological and biological vaterite: A Raman spectroscopic study. Journal of Raman Spectroscopy, **41**: 193–201. doi:10.1002/jrs.2438.

Wilson, S., Dipple, G.M., Power, I.M., Thom, J.M., Anderson, R.G., Raudsepp, M., Gabites, J.E., and Southam, G. 2009. Carbon dioxide fixation within mine wastes of ultramafic-hosted ore deposits: Examples from the Clinton Creek and Cassiar Chrysotile Deposits, Canada. Economic Geology, **104**: 95–112. doi:10.2113/gsecongeo.104.1.95.

Wilson, S., and Hamilton, J.L. 2022. Fizzy ore processing sequesters CO_2 while supplying critical metals. Proceedings of the National Academy of Sciences, **119**: e2212424119. doi:10.1073/pnas.2212424119.

Yee, N., Benning, L.G., Phoenix, V.R., and Ferris, F.G. 2004. Characterization of metal−cyanobacteria sorption reactions: A combined macroscopic and infrared spectroscopic investigation. Environmental Science & Technology, **38**: 775–782. doi:10.1021/es0346680.

Yu, R., Chai, H., Yu, Z., Wu, X., Liu, Y., Shen, L., Li, J., Ye, J., Liu, D., Ma, T., Gao, F., and Zeng, W. 2020a. Behavior and mechanism of cesium biosorption from aqueous solution by living *Synechococcu*s PCC7002. Microorganisms, **8**. doi:10.3390/microorganisms8040491.

Zeng, W., Li, F., Wu, C., Yu, R., Wu, X., Shen, L., Liu, Y., Qiu, G., and Li, J. 2020a. Role of extracellular polymeric substance (EPS) in toxicity response of soil bacteria *Bacillus sp.*

S3 to multiple heavy metals. Bioprocess and Biosystems Engineering, **43**: 153–167. doi:10.1007/s00449-019-02213-7.

Zeng, W., Zhang, S., Xia, M., Wu, X., Qiu, G., and Shen, L. 2020b. Insights into the production of extracellular polymeric substances of *Cupriavidus pauculus* 1490 under the stimulation of heavy metal ions. RSC Advances, **10**: 20385–20394. The Royal Society of Chemistry. doi:10.1039/C9RA10560C.

Zeng, Y., Chen, Z., Du, Y., Lyu, Q., Yang, Z., Liu, Y., and Yan, Z. 2021. Microbiologically induced calcite precipitation technology for mineralizing lead and cadmium in landfill leachate. Journal of Environmental Management, **296**: 113199. doi:10.1016/j.jenvman.2021.113199.

Zerkle, A.L., House, C.H., Cox, R.P., and Canfield, D.E. 2006. Metal limitation of cyanobacterial N_2 fixation and implications for the Precambrian nitrogen cycle. Geobiology, **4**: 285–297. doi:10.1111/j.1472-4669.2006.00082.x.

Zeyen, N., Wang, B., Wilson, S.A., Paulo, C., Stubbs, A.R., Power, I.M., Steele-Maclnnis, M., Lanzirotti, A., Newville, M., Paterson, D.J., Hamilton, J.L., Jones, T.R., Turvey, C.C., Dipple, G.M., and Southam, G. 2022. Cation exchange in smectites as a new Approach to mineral carbonation. Frontiers in Climate, **4**. Available from https://www.frontiersin.org/articles/10.3389/fclim.2022.913632.

Zhang, J., Kumari, D., Fang, C., and Achal, V. 2019. Combining the microbial calcite precipitation process with biochar in order to improve nickel remediation. Applied Geochemistry, **103**: 68–71. doi:10.1016/j.apgeochem.2019.02.011.

Zhang, L., Wang, W., Yue, C., and Si, Y. 2024. Biogenic calcium improved Cd^{2+} and Pb^{2+} immobilization in soil using the ureolytic bacteria *Bacillus pasteurii*. Science of The Total Environment, **921**: 171060. doi:10.1016/j.scitotenv.2024.171060.

Zhang, X., Guo, J., Wu, S., Chen, F., and Yang, Y. 2020. Divalent heavy metals and uranyl cations incorporated in calcite change its dissolution process. Scientific Reports, **10**: 16864. doi:10.1038/s41598-020-73555-6.

Zhao, H., Han, Y., Liang, M., Han, Z., Woo, J., Meng, L., Chi, X., Tucker, M.E., Han, C., Zhao, Y., Zhao, Y., and Yan, H. 2023. Effect of magnesium and ferric ions on the biomineralization of calcium carbonate induced by *Synechocystis sp*. PCC 6803. Minerals, **13**: 1486. doi:10.3390/min13121486.

Zhou, Y., Nguyen, B.T., Zhou, C., Straka, L., Lai, Y.S., Xia, S., and Rittmann, B.E. 2017. The distribution of phosphorus and its transformations during batch growth *of Synechocystis*. Water Research, **122**: 355–362. doi:10.1016/j.watres.2017.06.017.

Zhu, T., Lin, Y., Lu, X., and Dittrich, M. 2018. Assessment of cyanobacterial species for carbonate precipitation on mortar surface under different conditions. Ecological Engineering, **120**: 154–163. doi:10.1016/j.ecoleng.2018.05.038.

Appendix:

Appendix A: Supplementary Information

Table A-1: Raw data from IC measuring anions of interest and organic compounds over the 30-day experiments. All anions of interest were reported as mg/L Note: if value was below the detection limit was reported as <0.5.

Sample	Fluoride	Lactate	Acetate	Propionate	Formate	Chloride	Nitrite	Bromide	Nitrate	Sulfate	Phosphate	Thiosulfate
D0-CG-H-IC	< 0.5	< 0.5	0.7	< 0.5	1.7	16.4	< 0.5	< 0.5	1396.6	38.2	16.5	< 0.5
D0-CG-L-IC	< 0.5	0.4	0.8	< 0.5	1.6	13.7	< 0.5	< 0.5	192.3	37.4	0.7	< 0.5
D0-Co-H-IC	< 0.5	< 0.5	0.9	< 0.5	1.4	29.5	< 0.5	< 0.5	1276.2	32.6	16.4	< 0.5
D0-Co-L-IC	< 0.5	< 0.5	4.3	< 0.5	n.a.	25.4	< 0.5	< 0.5	173.9	34.1	2.6	< 0.5
D0-Ni-H-IC	< 0.5	< 0.5	n.a.	< 0.5	n.a.	26.8	< 0.5	< 0.5	1283.0	28.9	12.3	< 0.5
D0-Ni-L-IC	< 0.5	< 0.5	7.1	< 0.5	n.a.	24.2	< 0.5	< 0.5	173.7	30.3	1.7	< 0.5
D0-2M-H-IC	< 0.5	< 0.5	0.2	< 0.5	n.a.	37.3	< 0.5	< 0.5	1069.2	22.7	11.4	< 0.5
D0-2M-L-IC	< 0.5	< 0.5	0.1	< 0.5	0.2	40.9	< 0.5	< 0.5	167.1	25.2	2.2	< 0.5
D1-CG-H-IC	< 0.5	< 0.5	0.3	< 0.5	1.3	13.4	< 0.5	< 0.5	1313.5	29.6	12.6	< 0.5
D1-CG-L-IC	< 0.5	< 0.5	0.7	< 0.5	0.3	11.8	< 0.5	< 0.5	162.9	32.2	1.9	< 0.5
D1-Co-H-IC	< 0.5	< 0.5	0.6	< 0.5	1.5	28.0	< 0.5	< 0.5	1171.0	28.0	9.1	< 0.5
D1-Co-L-IC	< 0.5	< 0.5	0.6	< 0.5	1.5	30.3	< 0.5	< 0.5	159.9	28.2	< 0.5	< 0.5
D1-Ni-H-IC	< 0.5	< 0.5	1.0	< 0.5	1.0	28.9	< 0.5	< 0.5	1174.0	29.6	10.3	< 0.5
D1-Ni-L-IC	< 0.5	< 0.5	0.7	< 0.5	1.3	31.3	< 0.5	< 0.5	160.4	30.2	1.0	< 0.5
D1-2M-H-IC	< 0.5	< 0.5	0.8	< 0.5	1.3	42.7	< 0.5	< 0.5	1050.4	24.9	7.2	< 0.5
D1-2M-L-IC	< 0.5	< 0.5	0.6	< 0.5	1.3	42.3	< 0.5	< 0.5	157.4	26.8	0.8	< 0.5
D3-CG-H-IC	< 0.5	< 0.5	1.1	< 0.5	1.9	13.9	< 0.5	< 0.5	1299.1	32.2	13.7	< 0.5
D3-CG-L-IC	< 0.5	< 0.5	0.9	< 0.5	1.8	11.6	< 0.5	< 0.5	160.1	31.6	2.0	< 0.5
D3-Co-H-IC	< 0.5	< 0.5	0.7	< 0.5	1.3	27.5	< 0.5	< 0.5	1168.7	27.9	9.6	< 0.5
D3-Co-L-IC	< 0.5	< 0.5	0.6	< 0.5	1.4	30.3	< 0.5	< 0.5	159.6	33.5	1.4	< 0.5
D3-Ni-H-IC	< 0.5	< 0.5	0.6	< 0.5	1.3	28.6	< 0.5	< 0.5	1184.3	29.7	11.2	< 0.5
D3-Ni-L-IC	< 0.5	< 0.5	0.6	< 0.5	1.3	31.0	< 0.5	< 0.5	158.4	28.8	1.9	< 0.5
D3-2M-H-IC	< 0.5	< 0.5	0.8	< 0.5	1.8	38.0	< 0.5	< 0.5	1058.6	26.1	5.3	< 0.5
D3-2M-L-IC	< 0.5	< 0.5	0.6	< 0.5	1.5	42.4	< 0.5	< 0.5	157.5	25.3	0.9	< 0.5
D6-CG-H-IC	< 0.5	< 0.5	2.1	< 0.5	1.8	11.8	< 0.5	< 0.5	1314.0	31.7	0.7	< 0.5
D6-CG-L-IC	< 0.5	< 0.5	1.5	< 0.5	1.3	14.7	< 0.5	< 0.5	150.8	32.1	12.8	< 0.5
D6-Co-H-IC	< 0.5	< 0.5	0.7	< 0.5	1.3	27.6	< 0.5	< 0.5	1173.2	26.2	12.8	< 0.5
D6-Co-L-IC	< 0.5	< 0.5	0.5	< 0.5	1.2	30.4	< 0.5	< 0.5	159.6	28.3	3.1	< 0.5
D6-Ni-H-IC	< 0.5	< 0.5	0.7	< 0.5	1.3	27.7	< 0.5	< 0.5	1192.3	29.5	18.0	< 0.5
D6-Ni-L-IC	< 0.5	< 0.5	0.6	< 0.5	1.4	30.8	< 0.5	< 0.5	158.0	28.3	1.6	< 0.5
D6-2M-H-IC	< 0.5	< 0.5	0.5	< 0.5	1.2	40.6	< 0.5	< 0.5	1079.1	24.7	11.0	< 0.5
D6-2M-L-IC	< 0.5	< 0.5	1.9	< 0.5	0.7	42.6	< 0.5	< 0.5	158.3	24.0	0.8	< 0.5
D12-CG-H-IC	< 0.5	< 0.5	120.6	< 0.5	< 0.5	14.6	< 0.5	< 0.5	1326.9	30.0	13.5	< 0.5
D12-CG-L-IC	< 0.5	< 0.5	78.5	< 0.5	< 0.5	12.0	< 0.5	< 0.5	103.9	30.0	< 0.5	< 0.5
D6-Co-H-IC	< 0.5	< 0.5	0.9	< 0.5	1.3	28.2	< 0.5	< 0.5	1200.0	27.0	13.9	< 0.5
D12-Co-L-IC	< 0.5	< 0.5	0.6	< 0.5	1.4	29.3	< 0.5	< 0.5	154.4	27.4	1.2	< 0.5
D12-Ni-H-IC	< 0.5	< 0.5	1.2	< 0.5	1.4	28.6	< 0.5	< 0.5	1177.5	27.2	17.3	< 0.5
D12-Ni-L-IC	< 0.5	< 0.5	1.2	< 0.5	1.6	30.9	< 0.5	< 0.5	164.9	28.9	3.5	< 0.5
D12-2M-H-IC	< 0.5	< 0.5	0.6	< 0.5	1.4	41.4	< 0.5	< 0.5	1087.3	23.7	10.1	< 0.5
D12-2M-L-IC	< 0.5	< 0.5	1.3	< 0.5	1.4	43.8	< 0.5	< 0.5	160.3	25.5	1.3	< 0.5

D20-CG-H-IC	< 0.5	< 0.5	174.6	< 0.5	< 0.5	14.5	1.6	< 0.5	1339.7	31.5	13.3	< 0.5
D20-CG-L-IC	< 0.5	< 0.5	108.57	< 0.5	< 0.5	12.25	< 0.5	< 0.5	158.04	31.07	0.48	< 0.5
D20-Co-H-IC	< 0.5	< 0.5	0.76	< 0.5	1.15	26.98	< 0.5	< 0.5	1170.61	26.45	12.75	< 0.5
D20-Co-L-IC	< 0.5	< 0.5	0.53	< 0.5	1.20	31.17	< 0.5	< 0.5	161.87	29.42	3.16	< 0.5
D20-Ni-H-IC	< 0.5	< 0.5	1.36	< 0.5	1.43	29.40	< 0.5	< 0.5	1205.43	28.85	16.97	< 0.5
D20-Ni-L-IC	< 0.5	< 0.5	1.15	< 0.5	1.50	31.78	< 0.5	< 0.5	160.05	27.65	0.71	< 0.5
D20-2M-H-IC	< 0.5	< 0.5	0.80	< 0.5	1.30	42.55	< 0.5	< 0.5	1129.77	25.65	11.48	< 0.5
D20-2M-L-IC	< 0.5	< 0.5	0.64	< 0.5	1.28	45.33	< 0.5	< 0.5	164.43	25.62	1.20	< 0.5
D30-CG-H-IC	< 0.5	< 0.5	146.99	< 0.5	0.25	14.69	< 0.5	< 0.5	1400.73	30.82	12.55	< 0.5
D30-CG-L-IC	< 0.5	< 0.5	203.77	< 0.5	0.29	12.49	0.11	< 0.5	104.64	33.66	n.a.	< 0.5
D30-Co-H-IC	< 0.5	< 0.5	1.03	< 0.5	1.53	29.82	< 0.5	< 0.5	1276.16	28.61	13.28	< 0.5
D03-Co-L-IC	< 0.5	< 0.5	0.78	< 0.5	1.24	33.80	< 0.5	< 0.5	173.92	31.37	3.31	< 0.5
D30-Ni-H-IC	< 0.5	< 0.5	2.20	< 0.5	1.32	30.48	< 0.5	< 0.5	1264.86	28.68	20.52	< 0.5
D30-Ni-L-IC	< 0.5	< 0.5	0.99	< 0.5	1.27	33.50	< 0.5	< 0.5	168.94	30.70	3.56	< 0.5
D30-2M-H-IC	< 0.5	< 0.5	0.98	< 0.5	1.42	42.07	< 0.5	< 0.5	1150.38	26.33	12.37	< 0.5
D30-2M-L-IC	< 0.5	< 0.5	1.00	< 0.5	1.09	44.16	< 0.5	< 0.5	167.17	26.25	1.31	< 0.5

Table A-2: Measured ICP-MS data based on cations in the BG-11 recipe reported as μg/L over the duration of the 30 days of the experiment in chapter 2.

Sample Name	Na	Mg	Al	P	K	Ca	Ti	V	Cr	Mn	Fe	Co	Ni	Cu	Zn	Sr	Zr	Ba
D0-CG-H-IC	536133.0	8469.0	17.1	6810.0	19904.0	5125.0	8.3	0.2	0.1	116.0	39.5	0.3	0.5	11.9	8.6	1.9	0.1	0.4
D0-CG-L-IC	99751.0	9344.0	27.1	1329.0	4089.0	5958.0	1.7	0.2	0.2	199.0	72.0	0.4	1.0	17.9	39.8	2.9	BDL	0.4
D0-Co-H-IC	485547.0	8141.0	10.9	6973.0	18471.0	6621.0	8.6	0.3	0.2	219.0	123.0	10091.0	3.8	22.2	17.3	3.5	0.2	0.7
D0-Co-L-IC	78751.0	8490.0	14.9	1216.0	3419.0	5706.0	1.7	0.2	0.4	223.0	13.0	10732.0	5.0	17.1	20.6	2.5	BDL	0.5
D0-Ni-H-IC	491942.0	8168.0	4.6	6458.0	18715.0	5058.0	8.0	0.2	0.2	121.0	28.2	2.4	9737.0	13.4	8.5	2.6	0.1	0.5
D0-Ni-L-IC	82152.0	8676.0	17.0	1276.0	3529.0	5750.0	1.6	0.2	0.5	209.0	11.9	0.6	11364.0	18.2	35.8	2.6	BDL	0.5
D0-2M-H-IC	433971.0	7430.0	4.7	6598.0	16681.0	6107.0	8.6	0.3	0.5	231.0	106.0	10516.0	10754.0	17.0	18.1	2.7	0.2	0.7
D0-2M-L-IC	80478.0	7835.0	18.4	1292.0	3511.0	8522.0	1.8	0.2	0.5	171.0	11.6	10750.0	11600.0	25.2	19.9	4.0	BDL	1.4
D1-CG-H-IC	539734.0	8202.0	17.0	7473.0	19627.0	4773.0	9.2	0.2	2.0	67.9	1.8	2.7	3.5	10.4	6.6	1.6	*0.0*	1.4
D1-CG-L-IC	85841.0	9057.0	25.1	1475.0	3378.0	6105.0	1.9	0.2	3.2	148.0	9.8	0.8	1.2	12.7	32.7	2.3	BDL	0.3

D1-Co-L-IC	84017.0	8126.0	BDL	692.0	3569.0	8944.0	1.2	0.1	5.0	48.3	BDL	6246.0	3.0	12.6	1.3	3.7	BDL	1.0
D1-Ni-H-IC	487001.0	7569.0	BDL	6568.0	17696.0	5792.0	8.1	0.2	2.9	56.9	3.5	1.7	6233.0	4.5	4.9	2.3	BDL	0.3
D1-Ni-L-IC	82597.0	8482.0	BDL	906.0	3591.0	9063.0	1.4	0.0	2.4	45.5	BDL	1.1	6388.0	3.9	1.8	3.9	BDL	1.0
D1-2M-H-IC	439102.0	6873.0	BDL	3884.0	16405.0	5007.0	5.3	0.2	1.2	39.1	BDL	8651.0	8743.0	4.9	*0.7*	2.1	BDL	0.5
D1-2M-L-IC	80084.0	7601.0	BDL	463.0	3660.0	8272.0	0.9	0.1	2.0	51.1	BDL	7461.0	7631.0	4.5	*0.8*	3.7	BDL	1.3
D3-CG-H-IC	536464.0	8545.0	13.6	9155.0	19938.0	5373.0	11.7	0.2	3.9	96.7	21.2	4.7	3.5	10.3	8.0	1.6	BDL	0.5
D3-CG-L-IC	86375.0	8876.0	22.8	1560.0	3432.0	6141.0	2.3	0.2	4.3	107.0	BDL	1.1	6.5	12.2	29.7	2.3	BDL	0.2
D3-Co-H-IC	490765.0	7417.0	BDL	6864.0	18020.0	5676.0	8.9	0.2	4.0	47.9	BDL	7526.0	4.8	9.4	2.2	2.0	BDL	0.2
D3-Co-L-IC	85268.0	8232.0	BDL	1073.0	3725.0	9145.0	1.6	0.1	3.3	57.1	BDL	8348.0	3.2	13.0	1.4	3.9	BDL	1.1
D3-Ni-H-IC	496108.0	7915.0	BDL	6919.0	18348.0	6122.0	8.8	0.1	2.2	73.8	BDL	1.4	8474.0	4.8	2.1	2.4	BDL	0.4
D3-Ni-L-IC	84087.0	8755.0	BDL	1248.0	3792.0	9678.0	1.8	0.0	2.4	58.0	BDL	2.2	7484.0	4.4	*0.3*	4.2	BDL	1.1
D3-2M-H-IC	452034.0	6764.0	BDL	5376.0	16236.0	5431.0	7.2	0.2	4.6	26.3	BDL	5322.0	8051.0	4.2	*0.8*	1.9	BDL	0.3
D3-2M-L-IC	83463.0	7835.0	BDL	959.0	3802.0	8584.0	1.4	0.1	1.6	62.8	BDL	9655.0	8709.0	6.6	2.7	3.7	BDL	1.3
D6-CG-H-IC	88055.0	9394.0	23.2	1307.0	3165.0	6696.0	1.9	0.2	2.4	163.0	BDL	0.4	0.6	11.0	37.6	2.6	BDL	0.3
D6-CG-L-IC	562316.0	8608.0	16.0	6819.0	20106.0	5130.0	8.0	0.2	1.0	105.0	1.5	0.4	0.5	8.3	8.7	1.9	BDL	0.6
D6-Co-H-IC	495946.0	7883.0	BDL	9007.0	18533.0	6817.0	11.0	0.3	3.7	235.0	30.2	10220.0	4.7	8.5	4.5	2.6	BDL	0.4
D6-Co-L-IC	85879.0	8436.0	BDL	1679.0	3894.0	9547.0	2.5	0.2	3.1	103.0	BDL	10153.0	3.4	12.1	5.0	4.1	BDL	1.2
D6-Ni-H-IC	501697.0	8821.0	BDL	11198.0	18301.0	8821.0	14.2	0.1	3.0	305.0	2.0	0.4	9188.0	5.3	2.0	3.7	BDL	0.7
D6-Ni-L-IC	86092.0	8590.0	BDL	1962.0	3845.0	10054.0	3.0	0.1	4.3	154.0	BDL	0.3	9292.0	6.1	1.5	4.4	BDL	1.4
D6-2M-H-IC	455526.0	6998.0	BDL	7064.0	16847.0	5857.0	9.6	0.2	3.0	111.0	*0.6*	10882.0	10805.0	6.0	4.6	2.3	BDL	0.4
D6-2M-L-IC	83760.0	7744.0	BDL	1467.0	3742.0	8924.0	2.4	0.1	3.1	110.0	BDL	10119.0	9518.0	6.6	1.9	4.0	BDL	1.4
D12-CG-H-IC	572920.0	8674.0	10.4	8202.0	20453.0	6038.0	10.5	0.2	2.8	266.0	178.0	1.2	1.3	7.7	30.9	2.3	0.1	1.2

D12-CG-L-IC	90918.0	9354.0	19.2	36.0	1506.0	6333.0	0.3	0.1	1.3	304.0	BDL	0.6	0.9	10.9	49.7	2.8	0.1	0.7
D12-Co-H-IC*	501288.0	7516.0	BDL	9206.0	18384.0	6621.0	12.0	0.3	5.1	189.0	14.9	10968.0	4.0	8.6	4.7	2.4	*0.0*	0.3
D12-Co-L-IC	82396.0	8131.0	BDL	2045.0	3808.0	9584.0	3.2	0.2	6.3	164.0	4.1	9512.0	7.0	13.1	5.6	4.2	BDL	1.2
D12-Ni-H-IC	495703.0	8388.0	BDL	12093.0	18598.0	8447.0	15.5	0.1	5.2	420.0	BDL	0.4	10842.0	5.6	2.1	3.6	BDL	0.5
D12-Ni-L-IC	87925.0	9061.0	BDL	2213.0	4103.0	11091.0	3.2	0.1	2.8	229.0	BDL	0.8	9029.0	6.6	1.0	5.2	BDL	1.5
D12-2M-H-IC	458910.0	7215.0	BDL	6857.0	17662.0	5841.0	9.1	0.2	2.3	149.0	*1.2*	11403.0	12166.0	6.7	4.5	2.5	BDL	0.5
D12-2M-L-IC	85567.0	7884.0	BDL	1447.0	3952.0	8830.0	2.2	0.1	2.6	113.0	BDL	10670.0	11073.0	6.6	2.4	4.0	BDL	1.4
D20-CG-H-IC	591386.0	9017.0	11.4	7266.0	22377.0	5664.0	9.0	0.2	1.8	245.0	175.0	1.4	1.8	6.1	27.2	2.3	*0.0*	1.4
D20-CG-L-IC	89571.0	9554.0	14.1	1591.0	3890.0	6876.0	2.3	0.2	4.4	707.0	312.0	1.4	2.0	11.0	79.5	2.9	0.1	0.9
D20-Co-H-IC	495929.0	7929.0	BDL	9615.0	18600.0	7039.0	12.3	0.3	4.4	282.0	41.7	10123.0	3.7	8.4	5.0	2.6	*0.0*	0.3
D20-Co-L-IC	85858.0	8856.0	BDL	1865.0	4099.0	10036.0	2.7	0.1	3.1	245.0	19.8	10263.0	3.2	13.3	5.4	4.4	BDL	1.1
D20-Ni-H-IC	505632.0	8613.0	BDL	10884.0	18843.0	8517.0	13.7	0.1	3.4	460.0	12.8	0.4	10776.0	6.1	2.5	3.7	BDL	0.5
D20-Ni-L-IC	86752.0	8832.0	BDL	1839.0	4054.0	9948.0	2.7	0.1	2.9	269.0	BDL	0.4	10498.0	5.9	1.1	4.6	BDL	1.4
D20-2M-H-IC	481617.0	7570.0	BDL	7087.0	18452.0	6130.0	9.1	0.2	2.0	177.0	12.1	12115.0	12913.0	6.2	4.4	2.7	BDL	0.6
D20-2M-L-IC	88249.0	8260.0	BDL	1565.0	4070.0	9421.0	2.3	0.1	3.0	242.0	BDL	11225.0	10590.0	6.5	2.4	4.3	BDL	1.5
D30-CG-H-IC	603927.0	9272.0	20.7	8664.0	22882.0	5946.0	10.6	0.2	2.9	215.0	127.0	2.1	3.0	9.5	28.4	2.4	*0.0*	1.4
D30-CG-L-IC	95366.0	10269.0	19.9	591.0	4321.0	6873.0	1.1	0.1	2.1	609.0	274.0	0.4	0.8	9.5	69.6	3.0	0.1	1.0

D30-Co-H-IC	532734.0	8820.0	BDL	8693.0	20882.0	7341.0	10.5	0.3	2.0	319.0	88.8	11194.0	3.9	9.6	7.5	3.0	*0.0*	0.5
D03-Co-L-IC	92591.0	9331.0	BDL	1859.0	4405.0	10268.0	2.7	0.2	3.0	150.0	*0.1*	12047.0	3.8	12.4	5.1	4.5	BDL	1.3
D30-Ni-H-IC	536362.0	10013.0	BDL	12070.0	20481.0	10041.0	14.7	0.1	2.0	531.0	*0.5*	1.5	11068.0	6.1	1.6	4.4	BDL	0.4
D30-Ni-L-IC	92318.0	9677.0	BDL	1827.0	4418.0	10735.0	2.6	0.1	1.9	328.0	BDL	2.2	11172.0	6.0	*0.7*	4.9	BDL	1.6
D30-2M-H-IC	497617.0	7839.0	BDL	7803.0	18824.0	6650.0	10.2	0.2	2.4	209.0	12.7	10829.0	13772.0	5.9	3.2	2.8	BDL	0.5
D30-2M-L-IC	91208.0	8412.0	BDL	1619.0	4192.0	9509.0	2.5	0.1	2.5	201.0	64.6	10149.0	11390.0	8.8	6.7	4.3	*0.0*	1.9
D1-Co-H-IC	492339.0	7219.0	BDL	6088.0	17900.0	5570.0	8.2	0.2	4.4	31.6	BDL	5346.0	2.7	9.1	1.4	2.0	BDL	0.3

Table A- 3: Recorded pH probe measurements in the both nutrient enriched and nutrient deficient systems throughout the 30-day experiment

Time	CG-H	CG-L	NI-H	NI-L	Co-H	Co-L	2M-H	2M-L
Day 0	8.89	9.17	8.69	7.92	8.30	7.91	7.84	7.66
Day1	9.55	9.51	8.44	8.36	8.59	8.56	8.79	8.23
Day 3	8.34	9.24	8.11	8.05	8.19	8.07	7.80	8.16
Day 6	9.54	9.04	7.80	7.89	7.69	7.80	7.72	7.74
Day 12	4.96	9.37	7.78	7.88	7.74	7.77	7.79	7.78
Day 20	5.01	4.98	7.87	7.88	7.85	7.95	7.85	7.81
Day 30	4.86	4.94	7.87	7.92	7.87	7.94	7.87	7.82

Table A- 4: Recorded conductivity reported as μS/cm through out the 30-day experiment in the both nutrient enriched and nutrient deficient systems

Time	CG-H	CG-L	NI-H	NI-L	Co-H	Co-L	2M-H	2M-L
Day 0	2758.0	590.1	2565.0	577.5	2572.0	563.8	2348.0	603.0
Day1	2727.0	544.1	2531.0	578.6	2419.0	568.0	2176.0	589.1
Day 3	2735.0	548.7	2535.0	575.3	2474.0	573.1	2250.7	594.2
Day 6	2910.0	569.6	2624.0	618.9	2624.0	599.7	2416.0	639.4
Day 12	2857.7	528.3	2599.0	616.5	2560.3	554.5	2451.0	660.5
Day 20	3075.0	648.0	2706.0	689.2	2583.7	649.3	2598.7	672.1
Day 30	3153.7	627.6	2887.0	706.7	2883.7	682.4	2668.3	692.6

Table A- 5: Recorded D.O in solution reported as mg/L during the 30-day experiment in the both nutrient enriched and nutrient deficient systems

Time	CG-H	CG-L	NI-H	NI-L	Co-H	Co-L	2M-H	2M-L
Day 0	8.01	8.09	7.59	7.89	7.91	7.76	7.43	7.67
Day1	8.01	7.94	7.95	8.11	7.91	7.99	7.70	7.88
Day 3	7.70	7.90	7.56	7.65	7.73	7.76	7.58	7.67
Day 6	8.32	8.08	7.52	7.56	7.66	7.72	7.47	7.51

Day 12	7.41	7.64	7.39	7.32	7.59	7.52	7.31	7.81
Day 20	7.62	7.33	7.69	7.55	7.54	7.51	7.64	7.69
Day 30	7.61	7.39	7.54	7.56	7.51	7.41	7.39	7.63

Table A- 6: Measured IC data from Chapter 3 experiment

	Fluoride	**Lactate**	**Acetate**	**Propionate**	**Formate**	**Chloride**	**Nitrite**	**Bromide**	**Nitrate**	**Sulfate**	**phosphate**	**Thiosulfate**
D0-AC--IC	< 0.4	< 0.4	0.3	< 0.4	< 0.4	133.3	< 0.4	< 0.4	13.5	30.4	< 0.4	< 0.4
D0-BC-IC	< 0.4	0.2	1.2	< 0.4	6.9	1299.5	< 0.4	< 0.4	243.8	28.9	< 0.4	< 0.4
D0-Co-IC	< 0.4	0.2	1.3	< 0.4	7.1	1313.5	< 0.4	< 0.4	245.4	28.5	< 0.4	< 0.4
D0-Ni-IC	< 0.4	0.2	1.3	< 0.4	7.1	1293.8	< 0.4	< 0.4	243.9	28.8	< 0.4	< 0.4
D0-2M-IC	< 0.4	1.2	3.9	< 0.4	24.8	1306.0	< 0.4	< 0.4	203.0	26.9	< 0.4	< 0.4
D1-AC--IC	< 0.4	0.1	0.2	< 0.4	< 0.4	132.3	< 0.4	< 0.4	13.3	31.6	< 0.4	< 0.4
D1-BC-IC	< 0.4	1.2	3.0	< 0.4	22.4	1308.6	< 0.4	< 0.4	170.0	25.6	< 0.4	< 0.4
D1-Co-IC	< 0.4	2.2	4.7	< 0.4	41.5	1268.4	< 0.4	< 0.4	210.8	24.4	< 0.4	< 0.4
D1-Ni-IC	< 0.4	2.2	4.5	< 0.4	37.9	1291.4	< 0.4	< 0.4	192.5	25.0	< 0.4	< 0.4
D1-2M-IC	< 0.4	0.1	1.0	< 0.4	5.6	1288.4	< 0.4	< 0.4	156.0	26.7	< 0.4	< 0.4
D2-AC--IC	< 0.4	< 0.4	0.2	< 0.4	< 0.4	135.3	< 0.4	< 0.4	13.6	32.3	0.4	< 0.4
D2-BC-IC	< 0.4	1.1	3.1	< 0.4	21.5	1306.5	< 0.4	< 0.4	162.1	26.3	< 0.4	< 0.4
D2-Co-IC	< 0.4	2.0	4.5	< 0.4	35.9	1312.8	< 0.4	< 0.4	182.7	25.6	< 0.4	< 0.4
D2-Ni-IC	< 0.4	1.8	6.4	< 0.4	28.5	109.7	< 0.4	< 0.4	170.6	27.0	0.3	< 0.4
D2-2M-IC	< 0.4	< 0.4	2.3	< 0.4	5.7	1251.6	< 0.4	< 0.4	152.1	25.1	< 0.4	< 0.4
D3-AC--IC	< 0.4	< 0.4	0.3	< 0.4	< 0.4	133.9	< 0.4	< 0.4	13.6	32.1	0.4	< 0.4
D3-BC-IC	< 0.4	1.2	3.5	< 0.4	23.0	1294.9	< 0.4	< 0.4	170.7	25.3	< 0.4	< 0.4
D3-Co-IC	< 0.4	1.6	6.7	< 0.4	28.1	109.5	< 0.4	< 0.4	162.2	22.5	< 0.4	< 0.4

D3-Ni-IC	< 0.4	1.9	4.6	< 0.4	32.4	1167.1	< 0.4	< 0.4	165.2	22.2	< 0.4	< 0.4
D3-2M-IC	< 0.4	< 0.4	2.3	< 0.4	5.2	111.7	< 0.4	< 0.4	134.1	22.1	< 0.4	< 0.4

Table A- 7*:* Measured ICP-MS data accounted for dilution factor of 1000 from Chapter 3 experiment

	Na	Mg	A	P	K	Ca	Ti	V	Cr	Mn	Fe	Co	Ni	Cu	Zn	Sr	Zr	Ba
D0-2M	360.1	17.1	0.1	5.7	18.6	703.7	0.0	0.0	0.0	0.2	BDL	0.0	0.0	0.4	0.2	0.3	*0.0*	0.0
D1-2M	116.0	9.0	0.1	0.2	5.7	666.6	BDL	0.0	0.0	0.0	0.4	0.0	0.0	0.2	0.1	0.3	BDL	0.0
D2-2M	114.7	8.8	0.1	0.1	5.8	650.4	BDL	0.0	0.0	0.0	0.5	0.0	0.0	0.2	0.1	0.3	BDL	0.0
D3-2M	105.4	7.6	0.0	0.3	5.5	49.6	BDL	BDL	0.0	0.0	0.4	1.0	0.6	0.2	0.1	0.0	BDL	0.0
D0-AC	19.7	10.3	0.1	0.2	2.0	72.2	BDL	0.0	0.0	0.3	0.2	BDL	0.0	0.3	0.1	0.0	BDL	0.0
D1-AC	20.8	10.2	0.1	0.3	2.0	70.2	BDL	0.0	0.0	0.3	0.3	0.0	0.0	0.6	0.1	0.0	BDL	0.0
D2-AC	14.7	7.8	0.1	0.3	1.6	54.4	BDL	0.0	BDL	0.2	0.1	BDL	0.0	0.7	0.1	0.0	BDL	0.0
D3-AC	19.4	10.3	0.1	0.4	1.9	71.5	BDL	0.0	BDL	0.4	0.1	BDL	0.0	0.3	0.1	0.0	BDL	0.0
D0-Co	209.8	12.8	0.1	2.6	11.5	730.9	0.0	0.0	0.0	0.2	2.2	0.0	0.0	0.3	0.1	0.3	BDL	0.0
D1-Co	146.0	9.8	0.1	0.2	5.9	727.1	BDL	0.0	0.0	0.2	0.3	0.0	0.0	0.2	0.1	0.3	BDL	0.0
D2-Co	173.9	9.6	0.1	0.4	6.3	722.8	BDL	0.0	0.0	0.1	0.9	0.0	0.0	0.2	0.1	0.3	BDL	0.0
D3-Co	117.5	7.9	0.0	0.3	5.5	48.2	BDL	BDL	0.0	0.0	0.3	1.8	0.0	0.2	0.1	0.0	BDL	0.0
D0-BC	131.6	9.6	0.1	0.7	5.6	725.7	BDL	0.0	0.0	0.3	0.5	0.0	0.0	0.2	0.1	0.3	*0.0*	0.0
D1-BC	134.2	9.8	0.1	0.2	5.9	755.1	BDL	0.0	0.0	0.1	0.3	0.0	0.0	0.2	0.1	0.3	BDL	0.0
D2-BC	120.3	9.2	0.1	0.2	5.5	717.1	BDL	0.0	0.0	0.1	0.3	BDL	0.0	0.2	0.1	0.3	BDL	0.0
D3-BC	124.5	9.0	0.1	0.3	5.7	689.7	BDL	0.0	0.0	0.1	0.3	BDL	0.0	0.2	0.1	0.3	BDL	0.0
DO-Ni	127.1	9.3	0.1	0.3	5.5	713.2	BDL	0.0	0.0	0.2	0.3	0.0	0.0	0.3	0.1	0.3	BDL	0.0
D1-Ni	129.4	9.2	0.1	0.2	5.4	716.8	0.0	0.0	0.0	0.1	0.3	0.0	0.0	0.2	0.1	0.3	BDL	0.0
D2-Ni	134.7	9.6	0.1	0.4	5.9	57.0	0.0	0.0	0.0	0.0	0.2	BDL	0.0	0.2	0.1	0.0	BDL	0.0
D3-Ni	115.0	8.4	0.0	0.3	5.2	664.6	0.0	0.0	0.0	0.1	0.2	0.0	8.3	0.2	0.1	0.3	BDL	0.0

Table A- 8: Recorded pH measurements from Chapter 3 experiment

	AC	BC	NI	Co	2M
Day 0	8.80	8.99	9.04	9.03	8.89
Day1	9.47	9.47	9.53	9.41	9.52
Day 2	8.63	9.38	9.28	9.92	9.55
Day 3	7.82	8.93	8.53	9.43	9.02

Table A- 9: Recorded conductivity measurements reported as mS/cm from Chapter 3 experiment

	AC	BC	NI	Co	2M
Day 0	935.9	4758	4940	4757	4726
Day1	938.2	4598	4551	4677	4365
Day 2	717.2	4323	4554	4446	4189
Day 3	956.2	4506	3804	945.2	839.1

Table A- 10: Recorded Alkalinity measurements reported as mg/L of $CaCO_3$ from Chapter 3 experiment

	AC	BC	NI	Co	2M
Day 0	31	52	63	53	31
Day1	32	84	72	63	32
Day 2	33	85	63	100	33
Day 3	43	100	60	85	43

Table A- 11: Recorded Alkalinity reported as mg/L measurements over the72 hours

Time	AC	BC	Ni	Co	2M
Day 0	5.72	6.85	7.12	7.39	7.38

Day1	7.05	8.16	9.47	8.22	7.93
Day 2	7.21	9.38	8.84	9.95	9.04
Day 3	7.39	7.39	7.43	7.27	7.58